

ABSTRACT

Title of Dissertation: FRACTURE OF BRITTLE LAYERS JOINED WITH HIGH ELASTIC MODULUS COMPOSITE

James Jin-Wu Lee, Doctorate of Philosophy 2007

Dissertation Directed by: Associate Professor Isabel K. Lloyd
Department of Materials Science and Engineering

Dr. Brian R. Lawn
National Institute of Standards and Technology

Ceramic properties such as biocompatibility and inertness have secured their use in biomedical prosthetics. The brittle nature of ceramics governs their application in any design and fabrication technique. Current all-ceramic dental crowns have a reported failure rate of approximately 3% a year. An investigation into a possible improved design over current all-ceramic dental crowns is performed. Current methods of fabricating all-ceramic dental crowns involve laborious and time consuming application of porcelain veneer layers onto a core material. The proposed design is to join independently fabricated veneer and core layers together using a high elastic modulus composite.

Fracture behavior of brittle layers joined by a high elastic modulus composite is studied in this dissertation. There are two dominant fracture mechanisms of

concern for dental crowns when joining brittle layers with a more compliant interlayer; the formation of radial cracks in the veneer or core and the propagation of cracks between brittle layers. The occlusal loading on dental crowns can be simulated with the use of Hertzian contact testing on flat brittle laminates, which allow for the study of radial cracks in the veneer. It is shown for the first time that bottom-surface radial cracks in the veneer due to flexure can be suppressed using a high elastic modulus joining interlayer. The relationship between the critical loads for radial crack formation, P_{cr} and the interlayer modulus and thickness is elucidated. Furthermore, using the high modulus composite as an interlayer increases the long term cyclic loading lifetime over joins with similar moduli to currently available dental adhesives. The propagation of cracks between adjacent brittle layers is shown to be controlled by a reinitiation mechanism and not penetration through the adhesive. Cracks that traverse the layer of origin arrest at the join interface in brittle laminates. Reinitiation loads are dictated by strength of the adjacent brittle layer and modulus of adhesive. This study shows that it is possible to use a high modulus composite as a joining material in the fabrication of dental crowns, while suppressing the formation of radial cracks in the veneer and limiting the propagation of cracks between adjacent brittle layers.

FRACTURE OF BRITTLE LAYERS JOINED WITH HIGH ELASTIC MODULUS COMPOSITE

By

James Jin-Wu Lee

Dissertation submitted to the Faculty of the Graduate School of the
University of Maryland, College Park in partial fulfillment
of the requirements for the degree of
Doctor of Philosophy
2007

Advisory Committee:

Associate Professor Isabel K. Lloyd, Chair/Advisor
Dr. Brian R. Lawn, Co-advisor
Professor Lourdes Salamanca-Riba
Professor Manfred Wuttig
Associate Professor David Bigio

©Copyright by
James Jin-Wu Lee
2007

Dedication

To my beloved wife Jessica,
my father Hong Koo Lee and my mother Young Ja Lee.

Acknowledgements

I am eternally grateful and indebted to both Dr. Isabel K. Lloyd and Dr. Brian R. Lawn for their never ending help and guidance on the work presented within this dissertation. Dr. Lloyd has always treated me with great favor and patience in regards to research and my studies. Her willingness to yield her time and resources to further my career, ambitions and to instruct me in the matters of life cannot be repaid. Above all what distinguish Dr. Lloyd is that she does this for all of her students, a testimony to her beautiful spirit. From the first time I entered the Dr. Lawn's laboratory at NIST, he has given me a deep appreciation for science. Dr. Lawn's profound patience, instruction and candid discussions have been an extraordinarily productive resource for me. Words come short in expressing my gratitude for him. The deep loyalty and friendship from all of his former students is evidence of his great character.

I would also like to thank my colleague Mr. Yijun Wang. His help, discussions, collaboration and friendship have been a great source of encouragement. I must also thank Dr. Herzl Chai. Dr. Chai's instructions about experimental technique and FEM work was a wonderful resource. I would as well like to thank Dr. Sanjit Bhowmick for his discussion, assistance and wisdom regarding mechanical testing and sample preparation. I would like to acknowledge Dr. Yeon-Gil Jung, from the Changwon National University South Korea, for his aide in specimen fabrication and insightful discussions.

So many people have directly assisted me in my research and I am thankful for all of their contributions. I would like to acknowledge Dr. Srinivasa R. Raghavan and Mr. Bani Cipriano for the use of their laboratory and assistance with the rheology measurements. Help with SEM images came from Dr. Tim Zhang and is greatly appreciated. I would also like to thank Ms. Mey Saied for her insight during group meetings and assistance in the laboratory. The shared knowledge and discussions with Dr. Otto C. Wilson from Catholic University of America is greatly appreciated.

I would like to acknowledge all the wonderful people at New York University College of Dentistry for their aide in my work. Dr. Dianne Rekow and Dr. Van P. Thompson were instrumental in the advancement of my research. Their suggestions and discussions were a key to many issues regarding clinical relevance. Also from NYUCD, Dr. Yu Zhang whose freely given encouragement and knowledge helped my work.

Financial support is thankfully acknowledged from NIDCR Research Supplement/Underrepresented Minorities for the Parent grant PO1 DE10976.

With deep gratitude and joy I would like to thank my parents who supported my education for so many years. Finally to my wife Jessica, whose love and encouragement made all of this possible.

Table of Contents

List of Tables	vii
List of Figures	viii
Chapter 1: Introduction	1
Chapter 2: Background	4
2.1 Introduction	4
2.2 Dental Crowns	6
2.2.1 Current All-ceramic Crown Fabrication	6
2.2.2 Freeform Fabrication	10
2.3 Flat Model Testing	16
2.3.1 Testing of Brittle Laminates	16
2.3.2 Current Dental Adhesives as an Interlayer	19
2.4 High Modulus Composite Joins	23
2.5 Summary	24
Chapter 3: Composite Processing and Specimen Preparation	25
3.1 Introduction	25
3.2 Materials and Methods: Bulk Composite Fabrication	26
3.3 Composite Properties	34
3.3.1 Mixing and Viscosity	34
3.3.1 Microstructure and Bulk Density	36
3.4 Join Fabrication For Hertzian Contact Testing	40
3.5 Aesthetic Properties of Bulk and Joins	41
3.6 Composite Novelty	42
3.7 Summary	49
Chapter 4: Hertzian Loading of Layered Structures and the Effect of Join Elastic Modulus	50
4.1 Introduction	50
4.2 Experimental Setup: In Situ Hertzian Contact Testing	50
4.3 Radial Crack Testing in Single Cycle Loading	53
4.4 Radial Crack Testing in Multi Cycle Loading	62
4.5 Summary	65

Chapter 5: Crack Containment Between Layers Joined with Composite/Epoxy Interlayer	66
5.1 Introduction.....	66
5.2 Experimental Set-up.....	66
5.3 Hertzian Contact Radial Crack Growth: Core/Join/Veneer	67
5.4 Plane Strain Driven Cracks: 4 Point Bend Bar	85
5.4.1 Bend Bar: Experimental Setup.....	85
5.4.2 Bend Bar: Experimental Results	88
5.5 Two-Dimensional Transverse Cracks: Line Load via Knife Indenter	100
5.5.1 Knife Indenter: Experimental Setup.....	100
5.5.2 Knife-Indenter Experimental Results.....	102
5.6 Summary	107
Chapter 6: Conclusions	108
Chapter 7: Future Work	111
Appendix: Fracture Mechanics of Line Load Indentation	112
A.1 General Mechanics.....	112
A.2 Crack penetration	113
A.3 Crack Reinitiation	116
References:.....	122
Curriculum Vitae	

List of Tables

Table 3.1: Materials list.	28
Table 3.2: Weight Percents of matrix, alumina filler and any surfactant additions	31
Table 3.3: Perceived and Measured Viscosity	35

List of Figures

Figure 2.1: A schematic of the basic natural tooth design. The enamel is the contact bearing surface supported by bone-like dentin. The contact of opposing teeth during chewing causes point contact loading on the occlusal surface of the enamel. 5

Figure 2.4: A cross section view of the layers of a all ceramic dental crown. Generally total crown thickness is approximately 1.5 mm with a variable cement thickness of 20 – 200 μm 12

Figure 2.5: A failure of an all ceramic crown presented in a patient from of Ken Malament DDS 13

Figure 2.6: An assortment of different ceramic products fabricated by direct writing techniques from Dr. Jim Smay (Oklahoma State University). 14

Figure 2.7: The proposed CAD/CAM dental crown design with independently fabricated veneers and cores that would have to be joined and placed in the mouth. On the right, is the relevant flat layered structure for mechanical testing. (Left figure from Dr. Guangming Zhang)..... 15

Figure 2.8: Critical Load, P_{rad} vs adhesive thickness for different overlayer thicknesses d (inset in the top right is the experimental schematic). 18

Figure 2.9: Point loads can cause radial fracture in the top layer of glass. Critical load dependence (Radial Crack) on modulus of support material, E_i . A total of 9 adhesives are studied. Black bars: good bond after testing; Gray bars: delamination after testing; White bars: delamination prior to testing..... 21

Figure 2.10: Critical Load Dependence (Radial Crack) on thickness of adhesive interlayer. 22

Figure 3.1: Flow chart of composite processing29

Figure 3.2: Mixing apparatus. A) PTFE coated spatula. B) Spatula with drill mount. C) Mixing cup mounted onto vibration platform..... 30

Figure 3.3: Relative Viscosity vs. Frequency 32

Figure 3.4: ESEM of 80 wt.% loaded composite..... 37

Figure 3.5: Density of Crosslinked samples versus Filler Weight percent. 38

Figure 3.6: Porosity of Crosslinked samples versus Filler Weight percent. 39

Figure 3.7: Flat laminates placed over type. Note the change in translucency as the thickness of the composite (72wt% alumina, 28wt% BisGMA/TEDGMA) interlayer is increased. a) no composite b) 50 μm join thickness c) 100 μm join thickness d) 250 μm join thickness	43
Figure 3.8: Bulk composite specimens (72wt% alumina, 28wt% BisGMA/TEDGMA)	44
Figure 3.9: Indentation obtained elastic moduli versus the amount of nano alumina filler additions to polymeric matrix	48
Figure 4.1: Specimen schematic for flat model testing with Hertzian contact	52
Figure 4.2: Image sequence of single cycle Hertzian contact taken from video. Radial crack initiation is apparent in veneer layers. No delamination is present between the composite join and the glass layers.....	54
Figure 4.3: Plotted P_{cr} for epoxy and composite joined specimens (veneer thickness = 1mm).....	57
Figure 4.4: P_{cr} versus join elastic modulus for different adhesive thicknesses (veneer thickness = 1mm).....	59
Figure 4.5: Effect of veneer thickness on P_{cr} for all join moduli.....	61
Figure 4.6: Indentation load vs the number of cycles required to generate a radial crack in a 1 mm glass veneer layer. Both epoxy ($E = 2.3$ GPa) and composite joins ($E = 22$ GPa) have join thickness $h = 80$ μm	64
Figure 5.1: Etched, unabraded or abraded glass layer mounted onto polycarbonate substrate. Vickers indent bottom of lower layer. No delamination observed.	70
Figure 5.2: - Video sequence of Hertzian Contact experiment. Bottom surface of top glass is left unabraded. Catastrophic failure at high loads. No delamination is apparent.....	72
Figure 5.3: - Video sequence of Hertzian Contact experiment. Bottom surface of top glass abraded. Catastrophic failure at high loads. No delamination observed.	75
Figure 5.4: Fractured Specimen, renucleation is concluded. No apparent delamination. Cracks planes in lower & upper layers similar. Joins are translucent.	76

Figure 5.5: Vickers Microhardness. Cross sections of laminate joined structure. Crack propagation is observed between layers. Glass surfaces etched. Composite Layer, 72 wt% nano alumina, $E = 22$ GPa.....	79
Figure 5.6: 30 N Vickers indent close to interface. Crack arrests in composite, no delamination.....	80
Figure 5.7: 90 N close to interface. Crack arrests in composite, no delamination.	81
Figure 5.8: 90 N close to interface. Spurious chipping causes the crack tip to arrest inside the composite layer.	83
Figure 5.9: Maximum load of 200 N. Crack arrests in composite, no delamination. Crack cannot be driven into opposite glass layer using Vickers indentations.	84
Figure 5.10: Beam Test, place lower surface under tension and drive cracks from Vickers indent into opposite interfaces.....	87
Figure 5.11: Video sequence of cracks reaching join interfaces for a sample made with 2 μm thick epoxy joints.....	90
Figure 5.12: Crack length plotted against applied strain. Abrasion of glass surfaces reduces the loads at which reinitiation take place. A = abraded reinitiation and U = unabraded reinitiation of cracks in outer layer.....	94
Figure 5.13: Level of strain needed to reinitiate cracks into the outer glass layer for a variety of different thicknesses. Even at thin joints cracks arrest in the join interface.....	95
Figure 5.14: Micrographs of sample made with epoxy and abraded glass surfaces 2 μm joints.	98
Figure 5.15: Micrographs of sample made with epoxy and unabraded glass surfaces 2 μm joints.	99
Figure 5.16: Experimental schematic of Knife indenter experiment. A line load is placed on the top glass layer and a crack is driven toward the interface. Top surface of the lower glass layer is either abraded or unabraded	101
Figure 5.17: $h = 2$ μm , $d = 1$ mm, Reinitiation Mechanism is observed in the lower glass.....	103
Figure 5.18: Plots of the line load Pl in N/mm as a function of crack length. The less stiff epoxy requires a higher line load to reinitiate cracks into the lower glass than the samples made composite joins..	104

Figure 5.19: Plot of the effect of the epoxy join thickness on the reinitiation of crack in the lower glass. It is experimentally observed that crack arrest at the interface even for thin joins prior to cracks entering the lower glass layer 106

Figure A.1: Schematic of line force crack configuration in layer system consisting of two brittle plates bonded by a polymer-based adhesive. Crack can propagate into lower brittle layer either by continuous penetration or reinitiation from a surface flaw ahead of an arrested primary crack tip. 118

Figure A.2: Plot of function $\Phi(c/d)$ for brittle plates bonded with adhesives of relative thickness $h/d = 0.05$ and modulus $E_2/E_1 = 0.04$ and 0.22 119

Figure A.3: Plot of $\chi_e P_1^P / Td^{1/2}$ versus c/d for given h/d and E_2/E_1 120

Figure A.4: Plot of $\chi_e P_1^I / S_1 d$ versus c/d for given h/d 121

Chapter 1: Introduction

The benefits of all-ceramic crowns over the traditional porcelain-fused-to-metal (PFM) are increasing their clinical use. All-ceramic crowns offer superior aesthetics and are free of metals that can lower biocompatibility and cause discoloration of soft tissue near the gum line. However failure rates of all-ceramic crowns are significant, motivating their manufacturers and clinicians to seek improvements in design and fabrication techniques. Indeed current methods used by dentist and prosthodontist to prepare a dental crown for implantation may be a source of many clinical failures [1]. The sandblasting of the undersurface of ceramic layers that are intended to improve bonding to a prepared tooth structure introduces a flaw population that reduces the strength of the crown [1-4]. Current manufacturing methods of all-ceramic crowns are labor intensive and require highly trained artisans to make some layers of the crown by hand.

The separate and independent fabrication of individual layers of the all-ceramic crown may introduce a level of automation and reduce fabrication variances associated with hand craftsmanship. These layers could then be joined to produce a laminar composite. The parent grant is currently investigating a solid freeform fabrication approach that will be able to produce veneers and cores with optimized properties independently. This approach increases the complexity of the restoration system since it introduces new layers (the joins) with different elastic modulus and bond strength. Our laboratory has developed a high modulus composite to join the two layers while providing the needed mechanical support.

This thesis is organized in the following manner. A background and pertinent literature review is done in Chapter 2. Current techniques in dental crown fabrication are discussed and a background for the thesis motivation is presented. It is followed by Chapter 3, which contains information on the processing of a high modulus composite and the experimental procedures in sample preparation. Composite properties, microstructure and the rheology of uncured paste are also covered. When considering the proposed use of the composite as an interlayer, the join developed by our laboratory has properties that are an improvement over current dental materials.

Chapter 4 covers single cycle and multiple cycle Hertzian contact testing on brittle laminate structures. The use of Hertzian indentation on flat layered structures is a model system for the occlusal point contacts that dental crowns are exposed to in the mouth. The effect of the joining interlayer elastic modulus on the critical loads for radial crack formation, P_{cr} , during single cycle loading is investigated. Multiple Hertzian cycles on brittle laminates are done in order to characterize possible long term behavior of model crowns in clinical environments. Join performance during both testing methods and their post mortem condition (adhesion) of the interfaces are also presented.

In Chapter 5, the behavior of cracks toward and through interfaces with compliant layers is studied. Four experimental techniques are used to drive crack propagation between brittle layers joined with two different materials. In two of the studies, a two-dimensional crack is produced with sufficient driving forces to propagate them into adjacent brittle layers using novel testing systems. The impact of

both joint elastic modulus and surface condition of the brittle layers on crack behavior is discussed.

Chapter 6 is a discussion of the results of the dissertation and Chapter 7 presents future paths of investigation.

Chapter 2: Background

2.1 Introduction

One of the hallmarks of biomedical engineering is the design and fabrication of prosthetics to replace diseased or lost biological organs and tissue. The greatest challenge in doing this is the fact that biological systems are honed to extremely efficient tolerances. Man-made implants that are designed to either replace or supplement existing biologics have many hurdles to overcome. One of the most successful prosthetics is the dental crown, which accounts for \$2 billion dollars a year in revenue and is anticipated to continually grow with an aging population [1]. The natural tooth seen in Figure 2.1 shows a schematic of its basic design [5, 6]. The outer enamel layer is primarily the mineral hydroxyapatite, a crystalline calcium phosphate, giving it strength and good wear characteristics [7, 8]. The enamel is a brittle layer supported by a compliant substrate, known as dentin, which attaches the enamel to the rest of the tooth substructure [7, 8]. Disease can cause the tooth decay and lead to the eventual need for tooth repair and restoration [5, 6, 8]. The tooth therefore must be restored with a prosthetic in order to maintain proper oral health and offer comfort to the patient. The reconstruction is generally a dental crown that is mounted onto the retained tooth structure (which is usually just dentin). Dental crowns are fabricated with different materials and can be categorized into two families; crowns that contain metal and all-ceramic crowns. The work presented in this dissertation focuses on the considerations surrounding all-ceramic crowns and seeks to elucidate variables that control crown performance.

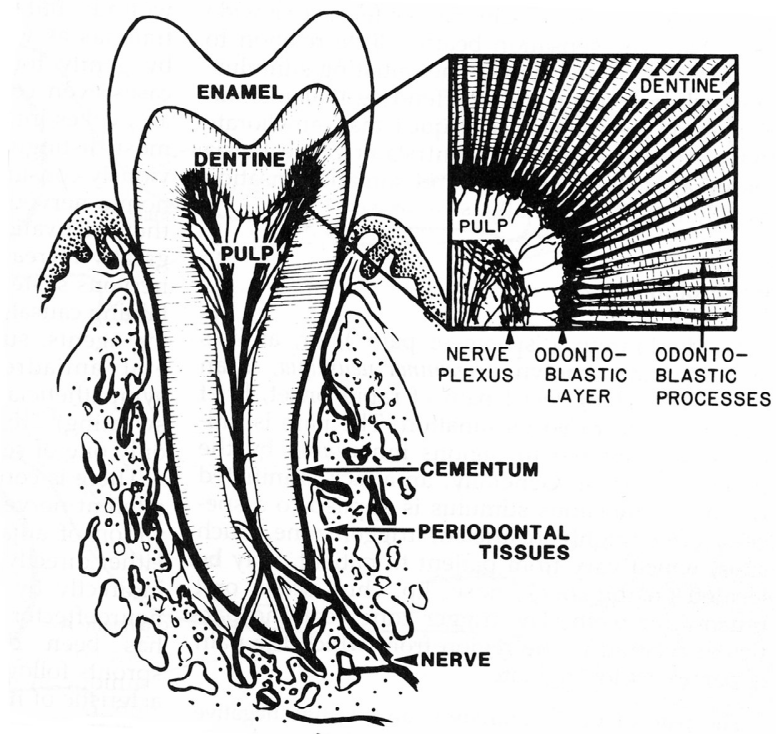


Figure 2.1: A schematic of the basic natural tooth design. The enamel is the contact bearing surface supported by bone-like dentine. The contact of opposing teeth during chewing causes point contact loading on the occlusal surface of the enamel [5].

2.2 Dental Crowns

All-ceramic crowns offer good biocompatibility due to their intrinsic inertness and excellent aesthetics from translucency that mimics natural teeth. However their failure rates exceed the more common porcelain-fused-on metal (PFM) crowns [1]. All-ceramic crowns account for about 20% of the dental crown market and should grow with the continued advancement of ceramic science [1]. The challenges to improve all-ceramic crown design, including fabrication approaches and performance are the core issues around dental restoration research. The work presented in this dissertation focuses on failure mechanisms and possible future crown design.

2.2.1 Current All-ceramic Crown Fabrication

Current techniques of making all-ceramic crowns are labor intensive and require trained artisans to hand-form the crown. This is done with the technician applying individual thin layers of porcelain slurry onto a ceramic core and firing it in an oven. The slurry application and firing is repeated until the porcelain layer has reached the appropriate thickness determined by spatial imprints made by the dentist. Figure 2.2 shows the application of the porcelain slurry and the unfired all-ceramic crown.

An issue which can influence structural integrity that arises from the repeated firing of the crown during fabrication is CTE (Coefficient of Thermal Expansion) mismatch [9-12]. While manufacturers work to minimize CTE mismatch and to make the stresses in the veneer layer at the interface with the core mildly

compressive, CTE mismatch can cause the bottom surface of the veneer layer to come under tension, thereby reducing performance [9, 10, 12]. When the CTEs are not closely matched, large tensile stresses can result. Work performed by Hermann et al shows that in a flat model systems of glass fused to strong cores made from alumina the magnitude of stress close to the interface is as high as + 66 MPa, a considerable amount compared to the strength of the veneer [12]. Such stresses can induce premature failure of a dental crown, as it leaves the structure exposed to the effects of creep and viscoplastic deformation in the crown substructure during the cool down cycle, with resultant enhanced crack initiation in service [1]. Figure 2.3 has micrographs of Vickers indentations (10 N) placed on the top surface of a glass monolith (control), and a 2-layered laminate structure, where soda lime glass is fused to a alumina core, mimicking a dental crown [12]. Both the monolith and the 2-layer specimens have cracks emanating from the corners of the indent, as expected in brittle materials. However the cracks in the monolith are much longer than the 2-layer specimen, signifying a compressive field on the top of the glass in the layered structure. Therefore it can be assumed that the bottom surface of the glass near the interface with the alumina is under tension, as described before.

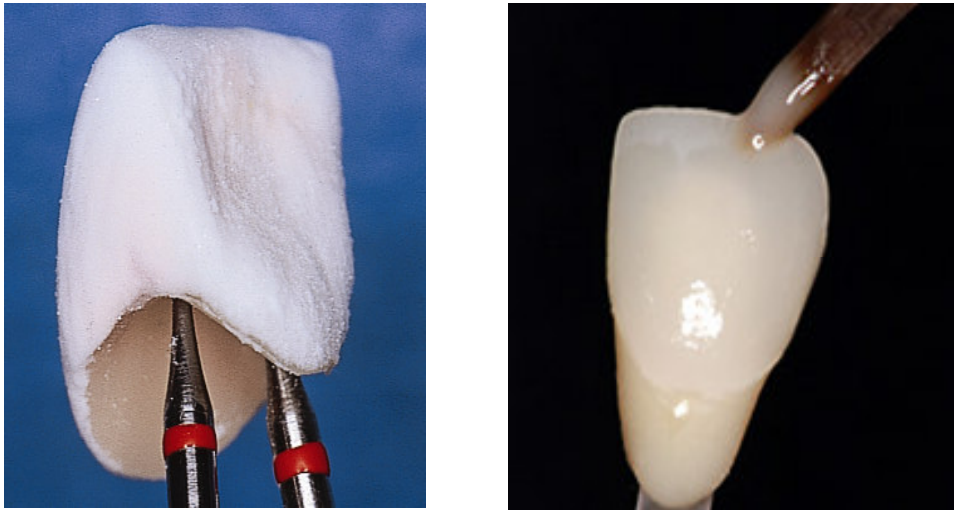


Figure 2.2: Crown fabrication technique of current all-ceramic dental crowns. Unfired surface (left) and the application of porcelain slurry performed by technician. Multiple coatings and firings are performed to achieve the proper veneer thickness. Figures obtained from personal communication from Mariano A. Polack, DDS, MS

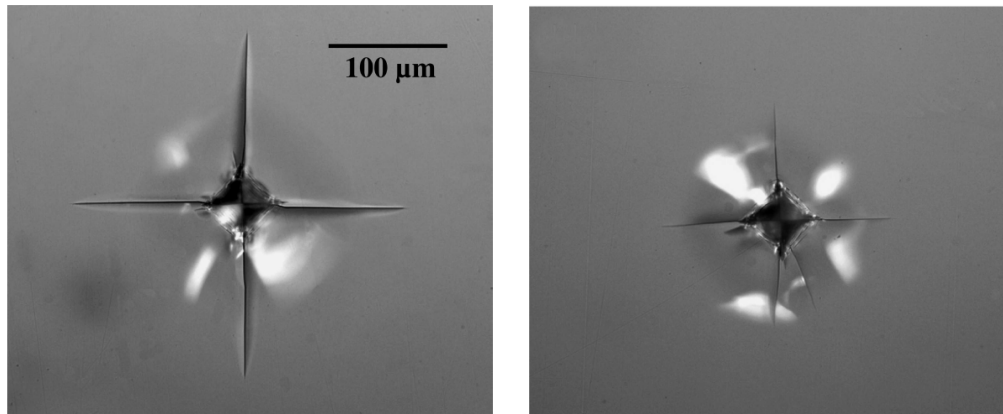


Figure 2.3: Micrographs of Vickers indentations (10 N) placed on the top surface of a glass monolith (left) and a 2 layered laminate structure (right). Note the difference in the length of crack emanating from the corners of the indenter [12].

The basic geometry of dental crowns is limited by the need to fit into the physical space dictated by a patient's teeth. It is generally thought that dental crowns should have a 1.5 mm minimum thickness in total, with veneers taking up 1 mm and the stronger core 0.5 mm, as seen in Figure 2.4. The crown is then mounted onto a prepared surface done by the clinician with a dental adhesive that has a relatively low elastic modulus [1]. Dental crowns used in posterior positions sometimes have smaller thicknesses than the 1.5 mm minimum prescribed by most clinicians due to complex geometries [1]. Indeed this can be problematic because of the higher loads seen in posterior positions during chewing and other physiologic conditions. All-ceramic dental crown fail at a rate up to 3% [1, 13]. It has been reported that so-called bottom surface radial cracks are present in tests done by pressing hard spheres into curved laminates [14]. Such failures are seen in clinically failed all-ceramic dental crowns as shown in Figure 2.5 [1, 14].

2.2.2 Freeform Fabrication

All-ceramic crowns have benefited with recent advancements in the material sciences. Novel fabrication techniques have been employed by clinicians and engineers alike to make recent generations of crowns more quickly and more precise than in previous years. Computer-aided design and computer-aided manufacturing (CAD/CAM) are now being implemented by dentists to manufacture crowns at the office while patients wait. There are also new fabrication methods that may revolutionize the way ceramics are used in dentistry. Robocasting and direct writing use similar technology to that seen in ink jet printers to make 3-dimensional ceramic

structures [15-17]. Robocasting can allow for the precise production of ceramic materials into dental crown components as seen in Figure 2.6, where the shape capability is illustrated. Part of the work in our laboratory is to employ these technologies to make independently free-form-fabricated veneers and cores. By independently manufacturing a porcelain veneer and a tough ceramic core, we may optimize each individual layer and overcome threat of residual stresses associated with their CTE mismatch. However the two layers must be joined after they have been engineered. In order to accomplish this, our lab has attempted to make a high modulus joining material to mate veneers to cores.

Figure 2.7 shows a schematic of our laboratory's proposed design. Using a high modulus adhesive our intention is join the strong core and aesthetic veneer without the high temperature firing required in current fabrication techniques. The proposed joining material should 1) have a strong bond to both the veneer and core; 2) contain no voids or gaps in the adhesive layer; 3) not cause degradation of the individual layers; 4) maintain stiffness and strength even in thin areas $< 20 \mu\text{m}$. The ongoing work in our laboratory is the development of a new class of dental crowns that exploit recent advancements in fabrication technology and a study of the efficacy of implementing a different crown structure.

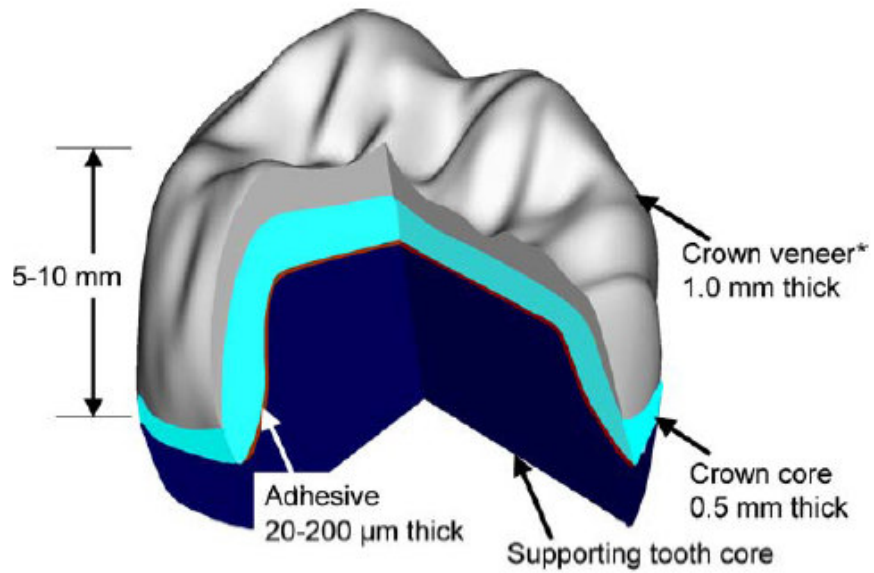


Figure 2.4: A cross section view of the layers of a all ceramic dental crown. Generally total crown thickness is approximately 1.5 mm with a variable cement thickness of 20 – 200 μm [1].

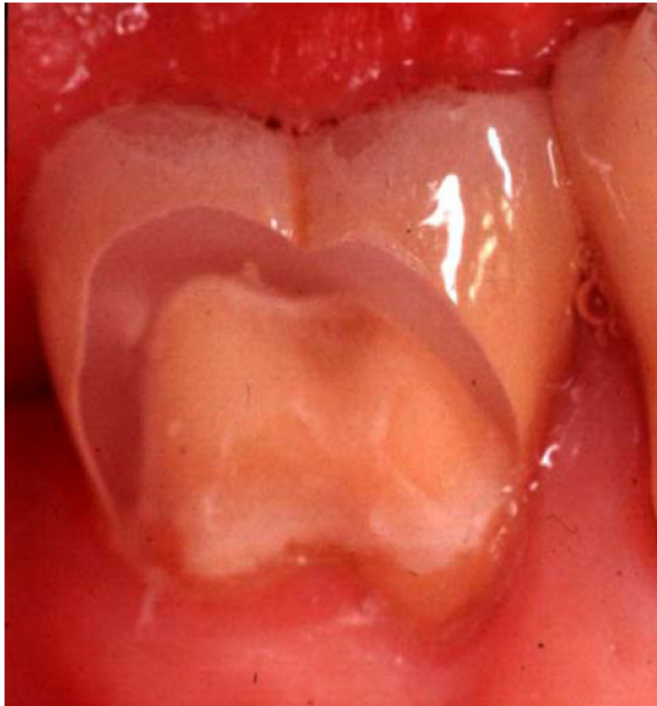


Figure 2.5: A failure of an all ceramic crown presented in a patient from of Ken Malament DDS [1, 14]



Figure 2.6: An assortment of different ceramic products fabricated by direct writing techniques from Dr. Jim Smay (Oklahoma State University).

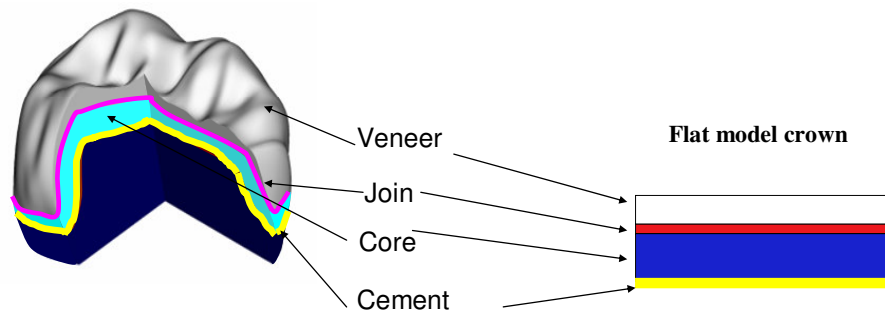


Figure 2.7: The proposed CAD/CAM dental crown design with independently fabricated veneers and cores that would have to be joined and placed in the mouth. On the right, is the relevant flat layered structure for mechanical testing. (Left figure from Dr. Guangming Zhang)

2.3 Flat Model Testing

The use of pressing hard spheres onto flat laminates to model the behavior of dental crowns is well established in dental research [18, 19]. Physiologic occlusal loading causes point contacts between either the opposing teeth or a tooth on foreign particle interaction. The indentation of a sphere onto a flat surface is extensively used to investigate the deformation and fracture of brittle ceramics since the first tests performed by Heinrich Rudolf Hertz over a century ago. Following are two studies performed that are pertinent to our group's proposed crown design. The elucidation of fracture of brittle laminates is central to the efficacy of a new crown.

2.3.1 Testing of Brittle Laminates

Elastic mismatch between stiff plates and compliant joins is a design property of many engineered structures. Brittle layers are used to provide good wear resistance and stiffness, while the compliant layers give stress shielding and confine damage within the laminate structure [20-29]. Compliant layers are sometimes required to overcome fabrication difficulties of bonding multiple brittle layers [30, 31]. A study performed by Drs. Herzl Chai and Brian Lawn showed a dependency of the critical loads, P , for the formation of both radial and ring cracks on brittle and compliant layer geometries [32]. In the experiments "overlayer" soda lime glass plates of different thicknesses (80 to 2000 μm) are joined to thicker (5.6 mm) "underlayer" soda lime glass slabs. Hertzian indentation, where a hard sphere is pressed into the top surface of the overlayer, is used to investigate the fracture behavior of the laminate structure. The strength and flaw population of the glass surfaces are controlled with abrasion. The issues relevant to this dissertation are that

the work showed the thickness of both the adhesive (epoxy) and overlayer controlled the initiation of bottom surface radial cracks in the overlayer. Figure 2.8 shows the data collected and the relationship between different overlayer thicknesses and adhesive thickness on the critical loads for radial crack formation, P_{radial} . Inset in the top right of the figure is the experimental schematic. The radial crack forms at the bottom surface of the top layer of glass. As the thickness of the overlayer falls, the critical load for radial crack formation drops accordingly to $P_{radial} \propto d^{1.49}$, approximately. The data in Figure 2.8 also show a strong dependence of radial crack formation on adhesive thickness. The thicker the adhesive layer the lower the critical load for radial cracks P_{radial} . Chai and Lawn concluded that subsurface radial cracks formed with greater ease than other transverse cracks investigated. Radial cracks are therefore one of the primary modes of failure due to point contacts when brittle overlayers are supported via compliant adhesives.

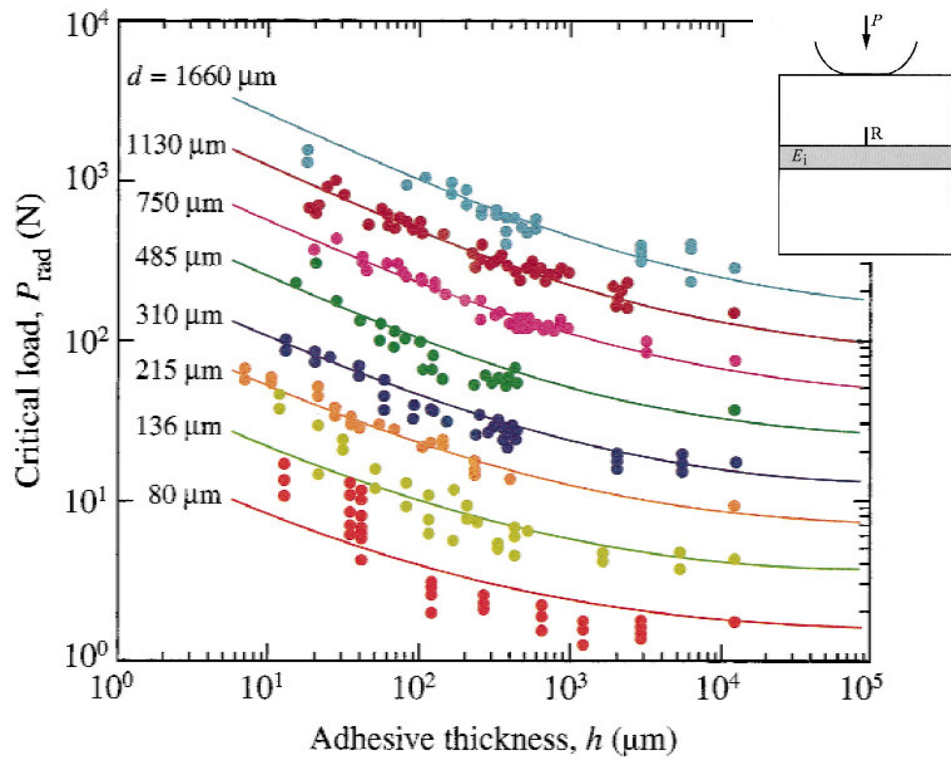


Figure 2.8: Critical Load, P_{rad} vs adhesive thickness for different overlayer thicknesses d (inset in the top right is the experimental schematic) [32].

2.3.2 Current Dental Adhesives as an Interlayer

A prior investigation into the critical loads for under surface radial crack formation of brittle laminates shows a dependence on adhesive modulus and thickness. Dr. Jong Ho Kim and co-workers studied 9 different adhesives and luting agents commonly used in restorative dentistry, Figure 2.9 [33]. The different materials are used to bond a flat brittle veneer layer to a supportive core, mimicking the structure of a dental crown. Hertzian contact tests are used to load the top surface of the veneer, thereby subjecting the bottom surface to tension and leaving it vulnerable to radial crack initiation. Kim *et al* experimented with different adhesives. The elastic mismatch between the top stiff layer and the interlayer causes biaxial flexure of the veneer under point loading. In their experiments, 1 mm thick monocrystalline silicon plates, used as the veneer layer, are bonded to a soda lime substrate, representing a support core, with the different dental adhesives. The bottom surface of the silicon veneer is abraded with 600 grit SiC, silicon carbide, to control its strength. This multilayer structure has the top surface veneer layer subjected to Hertzian contact loading and simultaneously monitored for the onset of radial cracks [32, 34-39]. The thicknesses of the assorted interlayers are varied to characterize the impact on critical loads for radial crack initiation.

The studied revealed that current dental adhesives allow for radial crack initiation at loads comparable to the occlusal loading seen in everyday biological function such as chewing. Of the 9 adhesives investigated, 5 of them showed delamination between the adhesive interlayers and the brittle layers either prior or during loading of the model system [33]. Figure 2.9 shows a plot of the critical loads

seen in the various adhesives/cements investigated for a fixed veneer thickness $d = 1$ mm and join thickness of $h = 150 \mu\text{m}$. The dental adhesives/cements are sorted by the 3 colors of the bars in the graph. The interlayers with black bars showed good adhesion with the brittle layers before and after testing. Gray bars represent joins that delaminated during testing and joins with white bars delaminated even prior to testing. Delamination in the dental crown is a highly unacceptable outcome which could result in the total loss of the prosthetic and would require the prosthodontist to replace the crown [1]. The Kim *et al* study shows that the use of current dental adhesives/cements veneer/core joining adhesives cannot protect the veneer from radial crack formation at loads seen even in normal loading environments that dental crowns are exposed to. Poor performance seen in the adhesive/cements is due to the fact that they are designed to provide mechanical or frictional locking when used in conventional dental crowns. Therefore there is a need to develop a high elastic modulus resin based adhesive that can provide chemical bonding as well as support against radial fracture in the veneer.

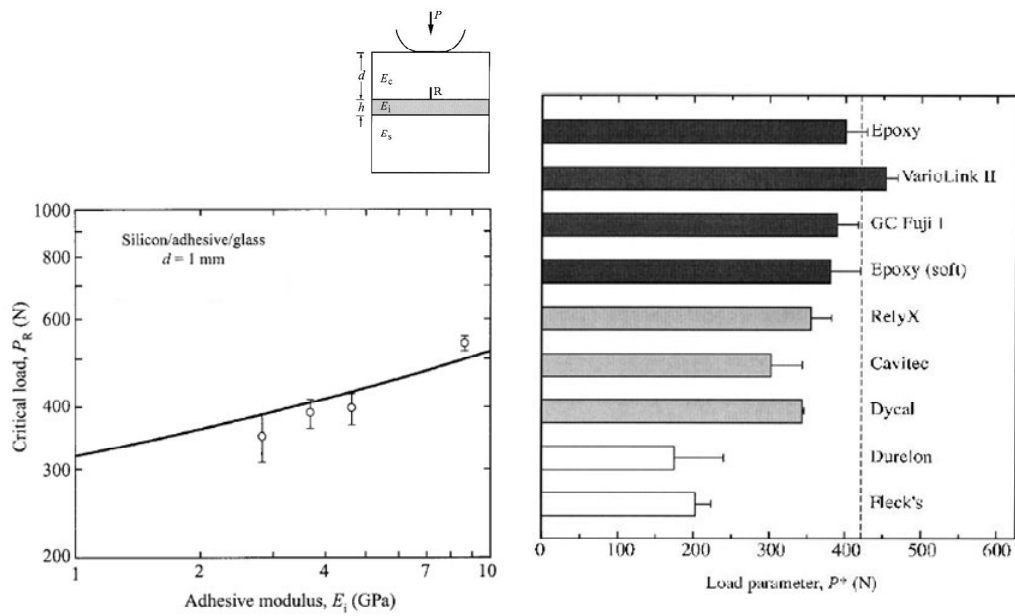


Figure 2.9: Point loads can cause radial fracture in the top layer of glass. Critical load dependence (Radial Crack) on modulus of support material, E_i . A total of 9 adhesives are studied. Black bars: good bond after testing; Gray bars: delamination after testing; White bars: delamination prior to testing [33].

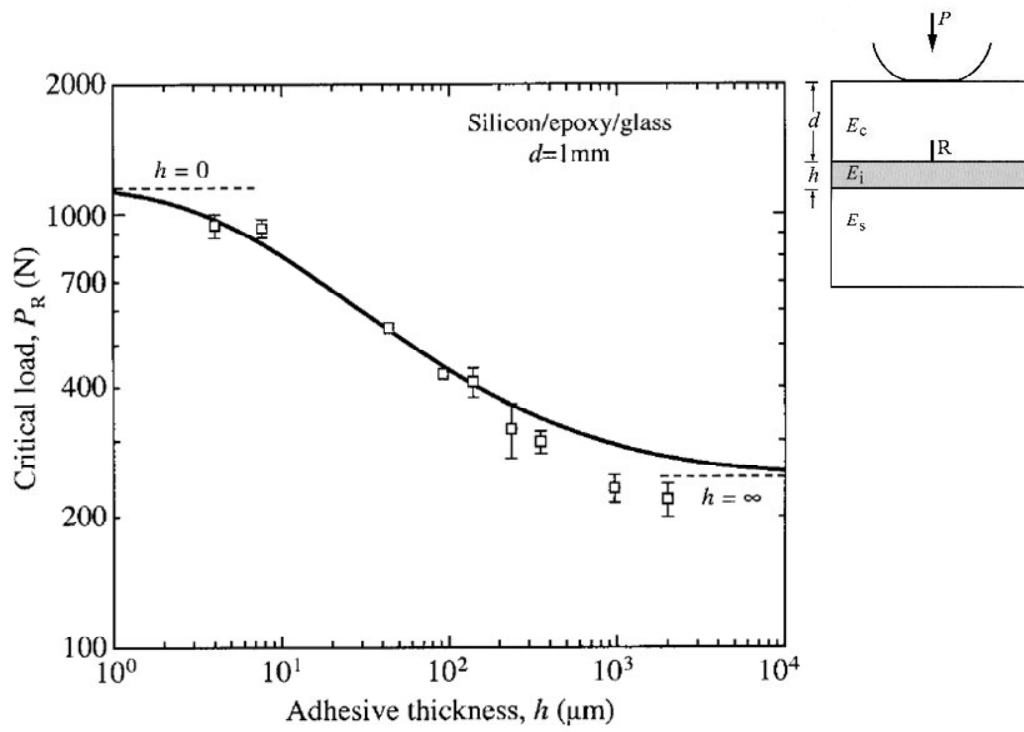


Figure 2.10: Critical Load Dependence (Radial Crack) on thickness of adhesive interlayer [33].

2.4 High Modulus Composite Joins

Composite interlayers used to adhere veneers to cores may offer benefits over current dental crown fabrication techniques. Joining independently fabricated brittle ceramic layers with an adhesive allows for the separate processing of layers and can overcome the need to match CTE of veneers and core materials [40, 41]. However, elastic mismatch between the veneer and adhesive can introduce new failure modes like bottom surface radial cracking of the veneer. The recent development of high elastic modulus composites may mitigate the lack of substrate support found in current dental adhesives [40, 41].

Cements are widely used in biomechanical applications such as adhering crowns to the remaining tooth structure or providing fixation for hip implants [42-45]. The focus of this chapter is to use an adhesive composite to join independently fabricated layers together in an optimized laminar structure and to evaluate this material as a potential new type of cement. Laminar structures of interest include multilayer crowns where the layers are produced by independent computer aided design and manufacturing (CAD/CAM) processes, and ceramic crowns on remaining tooth structures. Laminar structures are important since they allow different layers to serve different purposes, such as the addition of an esthetic veneer layer to a strong supporting core in a dental crown. They also mimic the multilayer structure of natural teeth.

2.5 Summary

Current adhesive cements used in dentistry are inadequate to join independently freeform fabricated layers [30, 33, 34, 44, 46]. There is a need to fabricate a joining adhesive with high elastic modulus and good bonding that can join brittle laminates without reducing the overall structural integrity of the dental crown. Any newly fabricated join must be tested for performance in order to confirm the underlying principles for crown design.

Chapter 3: Composite Processing and Specimen Preparation

3.1 Introduction

This chapter describes the development of a high modulus, non-porous composite with Bis-GMA-TEDGMA matrix. A high modulus is desirable for situations where the layers have low strengths [18, 34]. A veneer layer can experience tensile loading via flexure if it is attached to the core layer with a compliant join. Under tensile loading radial cracks may form, leading to failure. This is expected to be a problem when the join layer is relatively thick (> 10 microns) and compliant [32]. Given current practice in both CAD/CAM manufacturing and the preparation of crowns and teeth, we expect that join layers in laminar crowns and the cement layer under a crown would be between 20 and 200 μm . Crowns are thus vulnerable to radial fractures of veneer layers or of the crown itself.

While highly loaded (> 50 wt% filler) polymers are used to provide temporary plasticity for the shaping of ceramic products (injection molding, tape casting, or extrusion), analogous loaded adhesive systems are uncommon, especially nanoparticle filled systems. Such systems present fabrication challenges since they are extremely viscous. This is a particular problem when the filler is a nanopowder since nanopowders tend to have strong surface interactions due to their high surface-to-volume ratio. We use a nanopowder filler to provide greater flexibility in join thickness due to the small filler size. While some applications can be designed with uniform join thickness, other applications, such as multilayer dental crowns, may require variable thickness joins to accommodate both manufacturing uncertainty and

complex crown geometry [19]. With a nanopowder filler, even thin areas of the joint will have many particles through the cross-section to provide stiffness and strength. Viscosity, microstructure and density are used to characterize the bulk composites. Indentation modulus, calculated elastic modulus and hardness are discussed in detail in the dissertation of collaborator Yijun Wang [40, 41].

3.2 Materials and Methods: Bulk Composite Fabrication

Uniform loading of nanosized alumina into a bisGMA (Bisphenol A glycidyl methacrylate - Esstech, Essington, PA) and TEGDMA (triethylene glycol dimethacrylate - Sigma-Aldrich Inc., St. Louis, MO), matrix requires careful preparation of materials used and attention to the order in which steps proceed. Table 3.1 shows the materials used, their sources and characteristics. Figure 3.1 is a flow chart of the overall process. It is imperative that the alumina filler is well dispersed through the organic matrix to prevent agglomeration of particles and provide uniform material properties.

The polymeric matrix consists of an equal combination by weight of bis-GMA and TEGDMA (50/50 wt%). The ratio of filler to monomer matrix depends on the desired stiffness of the final composite mixture. To make the composite paste, equal parts of the two monomers are mixed. Then benzyl peroxide (BPO - Acros Organics - Geel, Belgium), the initiator, is added in powder form. BPO is dissolved into the monomers via sonication over a few hours in an ice bath to inhibit cross linking. Then the nanosized alumina powder is added. For low filler loading, mixing the alumina into the matrix is not difficult. At high filler loading the composite paste

is extremely viscous, so the special mixing apparatus shown in Figure 3.2 was developed. The composite paste is mixed in one polypropylene cup nested inside a second polyethylene cup that is secured to the top of a vibration table with zip ties. The nesting provides additional rigidity and stability. A spacer between the cups is used to minimize heat transmission from the vibration platform. The entire portion of polymer is added to the mixing vessel before the nested cups are tied down to the vibration platform. The inorganic powder is then added piecewise (increments of 0.05-0.1 g at a time for a composite with a total final mass of 20 g) to the monomer blend with the vibration platform turned on. It is critical that the powder is mixed into the monomer blend with not only the vibration platform, but also by the shear provided by mechanical stirring. The stirring is done with a PTFE (polytetrafluorethylene) coated spatula (Fisher Scientific – Pittsburgh, PA) as shown in Figure 3.2. The mechanical agitation with the coated spatula is continuous as the powder is added to the monomer blend. Since the viscosity of the organic matrix increases rapidly as the powder is added, a variable speed drill is used to drive the mixing, allowing more efficient incorporation of the powder at a wide variety of viscosities.

Material	Commercial Name	Source	Characteristics
Nano-alumina powders	NanoTek	Nanophase Technologies Corporation 1319 Marquette Drive Romeoville, IL 60446	Al ₂ O ₃ , Purity 99.95 +%, APS 47 nm SSA = 35 m ² /g (BET) Bulk Density = 0.26 g/cc, True Density = 3.6 g/cc Morphology = Spherical Crystal Phase = 70:30 Delta: Gamma
Bisphenol A Glycidylmethacrylate Molecular Formula: C ₂₉ H ₃₆ O ₈	bis-GMA	Esstech 48 Powhattan Ave Essington, Pennsylvania	Formula Weight 512 grams/mole
Triethyleneglycol Dimethacrylate Molecular Formula: C ₁₄ H ₂₂ O ₆	TEGDMA	Esstech 48 Powhattan Ave Essington, Pennsylvania	Formula Weight 286.36 grams/mole
Surfactant	Triton H66	Dow Chemical Midland, MI 48674 USA	Phosphate based
Initiator	Benzyol Peroxide	Sigma-Aldrich Corp. St. Louis, MO, USA	Molecular Formula C ₁₄ H ₁₀ O ₄

Table 3.1: Materials list.

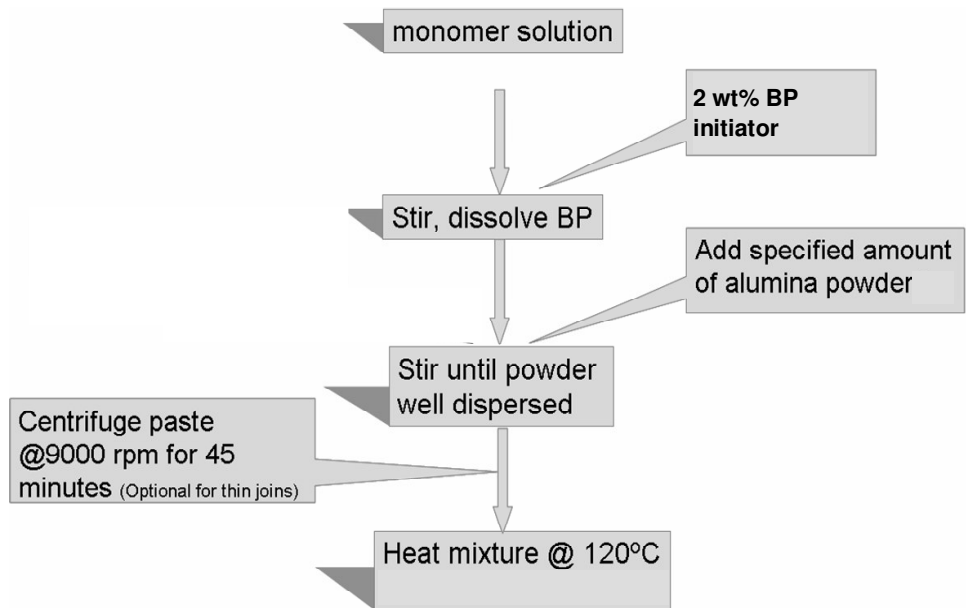


Figure 3.1: Flow chart of composite processing.

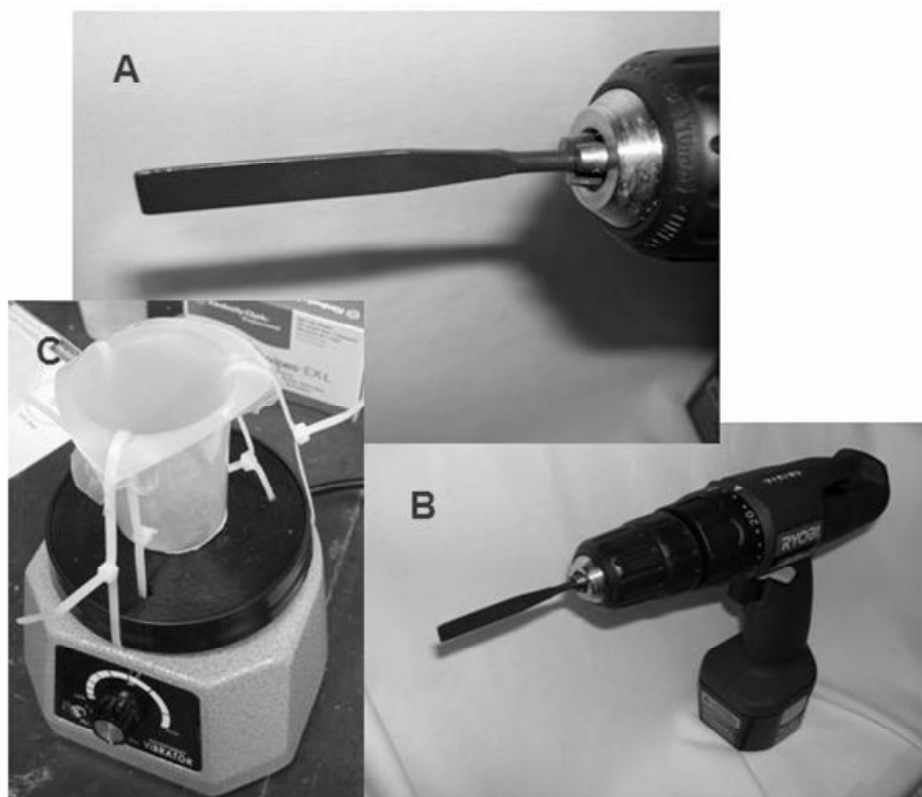


Figure 3.2: Mixing apparatus. A) PTFE coated spatula. B) Spatula with drill mount. C) Mixing cup mounted onto vibration platform.

The amount of powder added to the organic matrix to meet our target elastic modulus is approximately 80 weight percent. At these loading levels, the viscosity is so high that it is necessary to add a surfactant to help ‘compatibilize’ the nanopowders and slightly decrease viscosity. The surfactant, Triton™ H66 (Dow Chemical), has phosphate groups that interact with the alumina and improve particle dispersion. Table 3.2 shows representative particle loading levels and surfactant additions. Viscosity measurements are done on uncrosslinked pastes using a Rheometric Scientific (Rheometrics RDA III - Piscataway, NJ) parallel plate rheometer. Measurements are collected at room temperature (21°C) and ambient pressure. Figure 3.3 shows representative viscosity measurements.

<u>Composition</u> <u>Percent of</u> <u>Alumina Particles</u>	<u>Polymer</u> <u>Matrix Wt. %</u>	<u>Surfactant</u> <u>Wt.%</u>
50 wt.%	Bis- GMA/TEGDM A: 50 wt%	0 wt.%
60 wt.%	Bis- GMA/TEGDM A: 40 wt%	0 wt.%
70 wt.%	Bis- GMA/TEGDM A: 30 wt.%	0 wt.%
72wt.%	Bis- GMA/TEGDM A: 28 wt.%	0 wt.%
76.64 wt.%	Bis- GMA/TEGDM A: 22.09	1.27 wt.%
80 wt.%	Bis- GMA/TEGDM A: 16.49	3.5 wt.%

Table 3.2: Weight Percents of matrix, alumina filler and any surfactant additions.

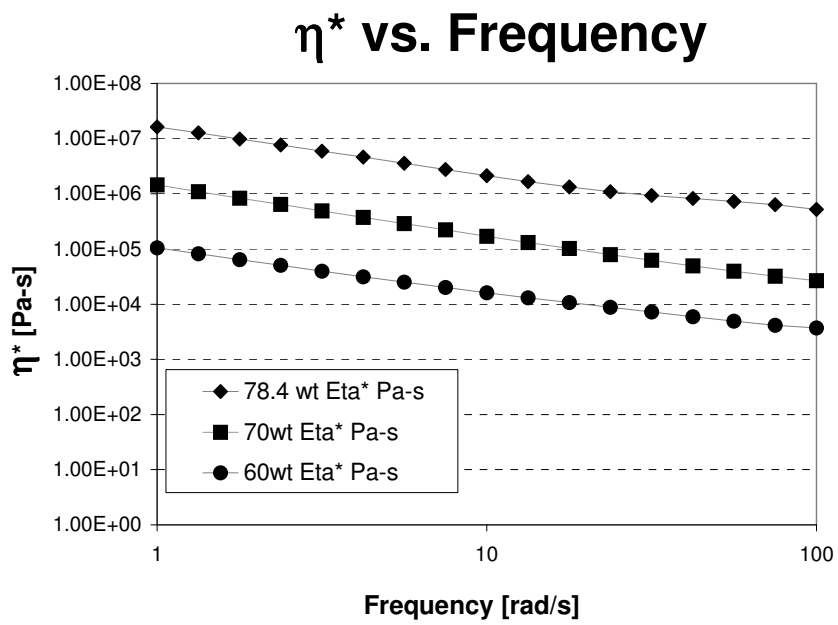


Figure 3.3: Relative Viscosity vs. Frequency.

After the pastes are prepared, bulk samples for characterization are shaped by either low or high speed centrifuging (Beckman Avanti® J-25 Series – Fullerton, CA) in a cylindrical glass vial. The centrifuge is used to help compact the paste and make uniform samples. Lower speeds (≤ 2500 rpm/1,500 g's) are sufficient for low loading levels. For loading levels above 70 wt.% high speed (9000 rpm/15,000 g's) is used. After the samples are prepared, they are heat cured at 120 C for 90 min.

Densities and relative porosities are measured using an adaptation of ASTM D 792 and ASTM C 373 standards for density and open porosity measurements [47]. The density measurements are done on centrifuged and crosslinked samples that are cut into cylindrical disks.

Samples are prepared for microstructural observation two ways. Some samples are polished using diamond paste for indentation measurements as detailed elsewhere [40]. These polished surfaces are examined using optical microscopy. Scanning electron microscopy (SEM) is done on a Hitachi S-2500 SEM. Samples are prepared by first fracturing the surfaces and then lightly coating them with gold using a Bio-Rad SEM Coating Apparatus (argon atmosphere, 1.5 kv, 12 mA for 15 seconds).

3.3 Composite Properties

3.3.1 Mixing and Viscosity

The process for the incorporation of nanosized alumina powder into a bis-GMA/TEDGMA or TEDGMA organic matrix yields a well dispersed composite with high elastic modulus and hardness for a composite of its type. Preparing a composite with loading levels less than 50 wt% required little effort to mix the alumina nanopowder into the matrix. Around 60 wt% loading, mixing became noticeably more difficult, as shown by the relative viscosity in Table 3.3. When loading levels reach 72 wt% it is necessary add surfactant. At this level unless surfactant is added alumina agglomerates are clearly visible and the unincorporated nanopowder remains on the external surface of the paste. The maximum loading attempted is 80 wt.% alumina powder with 3.5 wt.% of surfactant, Triton H66[®]. This composite has an elastic modulus of 32 GPa and a nanohardness of 950 MPa [40].

Table 3.3 shows both the qualitative perceived viscosity and the measured relative viscosity for the composite pastes in the as-mixed state. The loading refers to the level after incorporation. Note that measured relative viscosity increases one and a half decades between 60 and 70 wt.% alumina. This supports the qualitative perceptions. The composite paste was viscoelastic at all loading levels. However, above 70 wt.% alumina, our perception is that there is little viscous contribution to the behavior and the composite paste is dominantly elastic.

The loaded, uncrosslinked composite paste is not generally stable for long periods of time. The paste starts to cross link if it is exposed to sunlight. Therefore storage of the pastes requires a cool and dark place.

Weight Percent of Alumina Filler	Qualitative Viscosity	Relative Viscosity
50	Very smooth consistency and extremely flowable	at shear rate of 0.007 s^{-1} $2.8\text{E}4 \text{ Pa s}$
60	Very tacky and viscoelastic	at shear rate of 0.007 s^{-1} , $1.68\text{E}5 \text{ Pa s}$
70	Very viscous and extremely tacky; elastic contributions to deformation seem much greater than viscous contributions	at shear rate of 0.007 s^{-1} , $6.53\text{E}6 \text{ Pa s}$
80	Extremely viscous, nearly fully elastic	at shear rate of 0.007 s^{-1} , great than $1.52\text{E}7 \text{ Pa s}$

Table 3.3: Perceived and Measured Viscosity.

3.3.1 Microstructure and Bulk Density

The composite at all loading levels is a relatively dense solid with low levels of porosity. Figure 3.4 is a SEM image of a representative 80 wt.% composite. It shows a uniform microstructure with well dispersed alumina particles and little apparent porosity. Observation under the optical microscope (100X) indicated that there are occasional large pores (20-100 μm) in the samples with higher loading levels (above 70 wt.%), indicating that our processing approach is not yet optimized. Note that there is no evidence of alumina agglomeration in Figure 3.4 (the features in the micrograph are of the order of the size of the nanoparticles). We did not observe obvious agglomeration in any of the highly loaded samples of bis-GMA/TEDGMA composites containing surfactant.

Figures 3.5 and 3.6 show both the bulk density and open porosity as a function of the alumina loading level. The bulk density increases monotonically with the wt.% of alumina. The bulk density of the unloaded bis-GMA-TEDGMA is 1.22 g/cc. With higher loading levels the bulk density continues to increase and should approach an upper limit of 3.6 g/cc, the specific gravity of the pure alumina nanopowder [MDS Nanophase Inc. Romeoville, IL]. The open porosity of the solid composite also rises monotonically with increasing alumina loading levels rising to 1.4 vol.% at 80 wt% alumina.

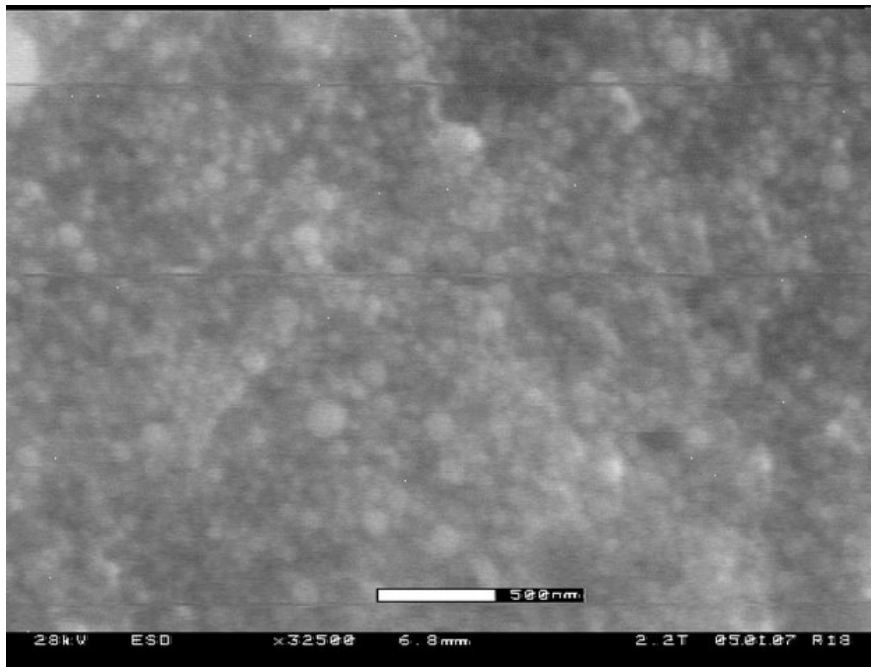


Figure 3.4: ESEM of 80 wt.% loaded composite.

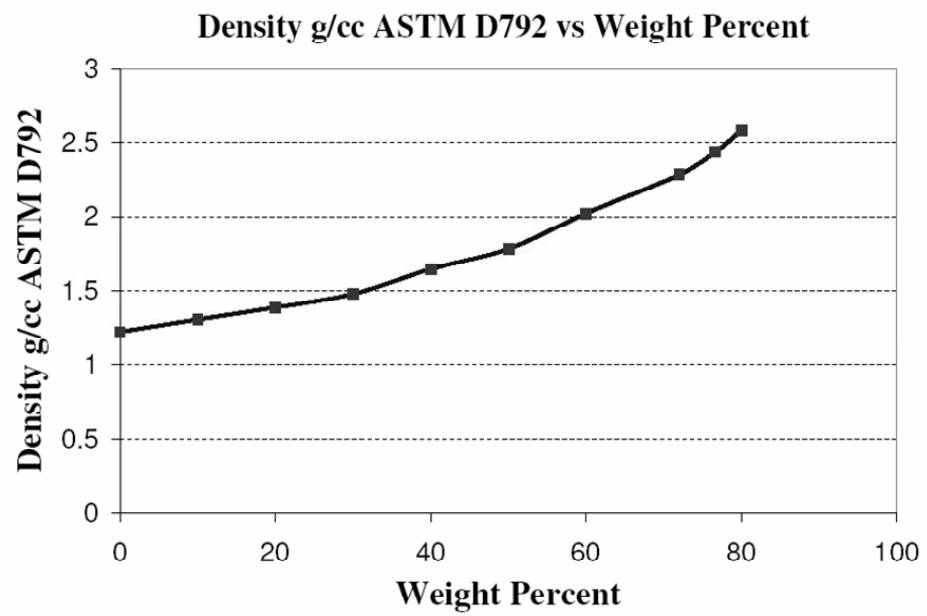


Figure 3.5: Density of Crosslinked samples versus Filler Weight percent.

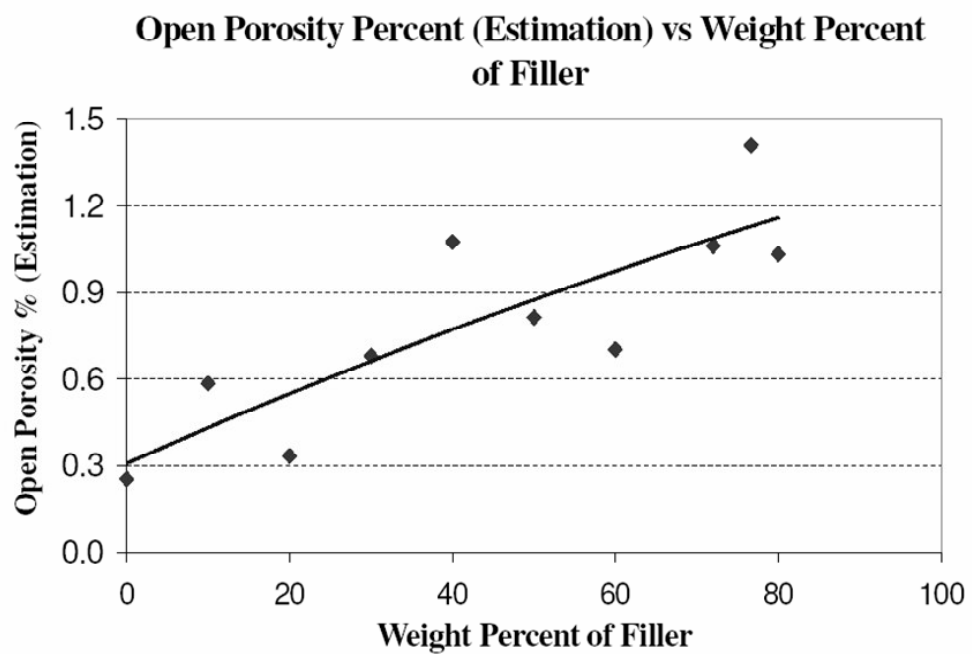


Figure 3.6: Porosity of Crosslinked samples versus Filler Weight percent.

3.4 Join Fabrication For Hertzian Contact Testing

Flat laminates used for Hertzian indentation tests are made from the joining of glass layers with either an alumina filled polymer composite (72 wt% Al₂O₃ – 28 wt% Bis-GMA/TEGDMA made in-house) or an epoxy resin (E = 2.3 GPa Harcos Chemicals – Bellesville, NJ).

Simple joins are formed between two flat soda lime glass slides. Glass lends itself well to *in situ* testing and crack observation due its transparency, and is isotropic. Glass slides are etched with 10% hydrofluoric acid for 30 seconds to remove surface flaws from handling. Glass strength is controlled by introducing flaws on appropriate surfaces using a 600 grit silicon carbide (SiC) slurry. The glass slabs are carefully placed over a small pool of slurry and light pressure is placed on top of the glass as it is moved over the slurry in a figure eight motion. Visual inspection insures that the flaw population is even over the surface of the glass. The resultant strength of the glass is $S = 120$ MPa. Even the highest loading levels of alumina in the organic matrix resulted in translucent joins. Glass surfaces in contact with the composite are treated with 3M™ ESPE™ RelyX™ Ceramic Primer (3M™ - St. Paul, MN), prior to joining to improve bonding. Utilizing the highly filled composite in “sandwiches” of glass/composite/glass, joins can be made as thin as 50 μm. All joins are cured at 120° C with a static load of approximately 100 N in an oven for 6 hours. The range of join thicknesses that would result from independently fabricating veneers and cores is 50 – 200 μm. The filled composites fabricated by our lab are able to produce joins in this range.

3.5 Aesthetic Properties of Bulk and Joins

Prosthetic dental crowns should have both good mechanical and aesthetic properties. Natural teeth have multiple layers that are translucent to light. Better crowns incorporate this translucent property of natural teeth without compromising performance [48]. Many dental crowns use metal cores as supporting substrates with porcelain veneers covering the unnatural looking post [38]. Crowns that are made with metal post as substrates discolor the surrounding tissue and generally do not have the coloration and translucency of natural teeth. All-ceramic crowns are designed to have superior aesthetic properties and mimic the appearance of natural teeth [1, 18, 49].

Optimal joining materials for all-ceramic crowns would bond different layers, provide support to the veneer and have translucency to help mimic natural teeth aesthetically. The composite joins in this chapter which provide improved performance over regular epoxy have a resin matrix and ceramic filler. The ceramic filler is nano-sized alumina with particles that are spherical with an average diameter of 45 nm [40]. At this size the alumina particles are smaller than the wavelength of visible light, and partially scatter light when mixed into the composite. Figure 3.7 shows 4 laminate structures formed with two glass slides joined the same composite (72wt% alumina and polymer – BisGMA/TEGDMA) that have been placed over printed type. At this filler loading level the volume of filler and resin are almost equal [40]. As the thicknesses of the joins increases the translucency predictably decreases. Pictured are a) join contains no composite, b) join thickness $h = 50 \mu\text{m}$, c) join thickness $100 \mu\text{m}$ and d) join thickness $250 \mu\text{m}$. It is noted that even at $250 \mu\text{m}$

the joins are somewhat translucent. In bulk form the composite is gray and opaque. Figure 3.8 shows 4 samples of bulk 72 wt.% alumina composite formed into 6 mm x 4 mm x 25 mm bars. However, when the composite layer is thin, there are fewer particles to scatter the light and the join is translucent as shown in shown in Figure 3.7. The composite joins is can easily range in thickness from approximately 50 - 200 μm , within the typical thickness range expected when joining CAD/CAM veneers and cores [1]. Therefore, using this composite to join independently fabricated veneers and cores would allow light to penetrate the veneer, mimicking natural tooth aesthetics.

3.6 Composite Novelty

To maximize the elastic modulus of an adhesive based composite it is necessary to use a very high loading level of a high modulus filler [50]. Frequently, loading level is maximized by using a bi- or tri-modal particle distribution. Dental composites typically utilize this approach. But they have not generally used nanosized alumina as the filler. In addition, while high modulus is generally considered to be a desirable attribute, it is unusual to see hardness or modulus values approaching our target magnitude of 30-40 GPa [50, 51]. Our target modulus is intended to minimize the elastic modulus mismatch between the join material and adjacent brittle ceramic materials (porcelain, elastic modulus 70-80 GPa) used as veneering layers. Elastic modulus mismatch is a critical factor in some of the failure modes in multilayer dental composites [34, 52]. Compliant joins may allow for radial cracking at the veneer join interface and lead to accelerated crown failure.

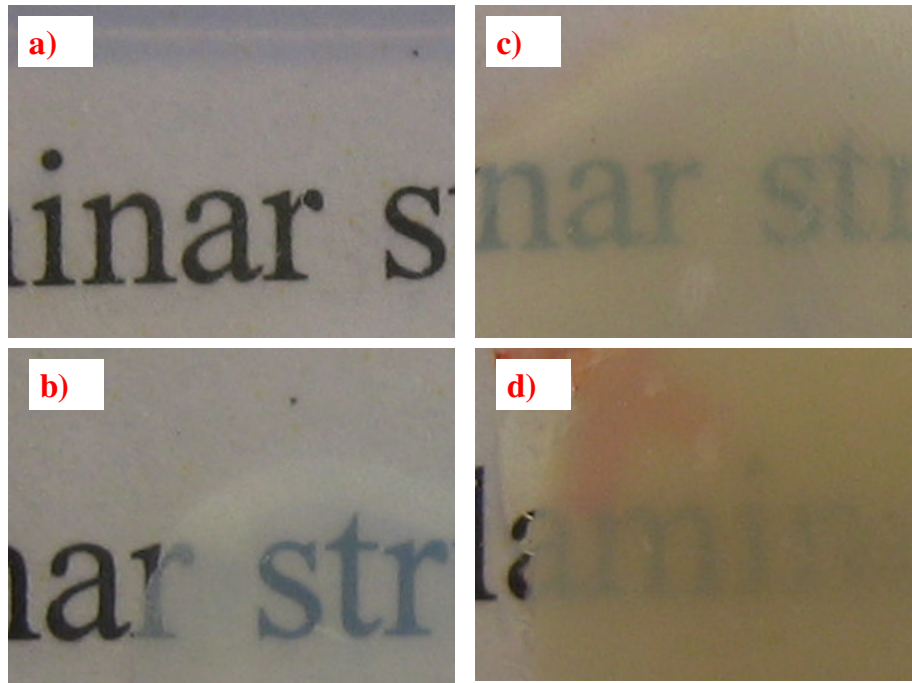


Figure 3.7: Flat laminates placed over type. Note the change in translucency as the thickness of the composite (72wt% alumina, 28wt% BisGMA/TEDGMA) interlayer is increased. a) no composite b) 50 μm join thickness c) 100 μm join thickness d) 250 μm join thickness.



Figure 3.8: Bulk composite specimens (72wt% alumina, 28wt% BisGMA/TEDGMA)

Highly loaded adhesive composite pastes are viscous, and viscosity generally increases with increasing filler content. However, the high surface area of nanosized powders increases the interactions between the particles, and between the particles and the matrix, enhancing the viscosity with increasing filler content. This can make it very difficult to incorporate increasing amounts of inorganic powder into the organic matrix while keeping the mixture well dispersed. This problem was addressed two ways. One was the design and construction of the mixing apparatus shown in Figure 3.2. The other was the use of a surfactant that was expected to bond well with the alumina due to its phosphate groups and still be compatible with the methylacrylate matrix. In the future, we will replace the surfactant with a ‘bonding agent’ that will minimize interaction of the particles and also bond them to the polymer matrix since that will provide a more robust composite.

The vigorous mixing approach using both vibration and shear works well until a loading level of 72 wt.% nanoalumina filler. At this point, the stirring and mechanical manipulation of the sample becomes extremely difficult. As noted in Table 3.2, the composite is extremely viscous and its behavior is more like an elastic material than a viscous material. Adding a small amount of surfactant directly to the composite paste is beneficial. It helps the alumina to mix into the paste and decreases the viscosity slightly. It is expected that the surfactant would act as a mediator between the alumina powder and the Bis-GMA/TEGDMA, since the surfactant molecules would attach to the alumina surface with their phosphate ends. The surfactant’s hydrophobic tails should then help to “compatibilize” the particles with the methylacrylate matrix. However, given the decrease in viscosity observed with

surfactant addition, the relatively small surfactant molecules may also be acting as a plasticizer within the methacrylate matrix.

While our composites are generally dense as shown in Figure 3.4, some pores are evident. The vigorous mixing approach, the extremely high viscosity of the paste and the relatively large sample size make it easy to introduce air into the composite during the mixing process. The extremely high viscosity makes it difficult for this air to escape. The centrifuging step is included to help remove voids and is relatively successful as evidenced by the small number of large voids. Experiments indicate that voids will be much less of a problem when the composite paste is used to make thin joints ($< 100 \mu\text{m}$) under slight pressure.

The work shown here indicates that up to 80 wt.% nanoalumina filler can be loaded into an organic polymeric resin matrix without perceivable agglomeration. At these loading levels the mixing is extremely laborious and great care must be taken not to load the system too quickly. Composites with similar loading levels have not been made with nanosized alumina particles. As shown in Figure 3.4, the nanoparticles of our system seem well dispersed under SEM. The mechanism by which the surfactant aids mixing with higher alumina additions is not yet clear.

The elastic modulus of our system dramatically increases with high loading levels of alumina, as shown in Figure 3.9. Further loading should be possible with the optimization of surfactant and matrix compositions. The relationship between the weight percent of alumina and the corresponding elastic modulus is detailed elsewhere [40]. As the weight percent of alumina increases the modulus rises roughly exponentially at high loading levels. The elastic modulus of pure alumina is about

360 GPa, which is two orders of magnitudes greater than the pure 50:50 weight percent of Bis-GMA/TEGDMA [40, 41]. Thus even higher alumina loading levels above the already achieved 80 wt.% would be expected to raise the elastic modulus even further. However, additives are required to drive the loading level above 72 wt% alumina. Therefore in order to simplify the testing of the laminates made within this dissertation and to preclude any reactions that involve the additives, only the 72 wt% alumina/28 wt% (Bis-GMA/TEGDMA), with elastic modulus 22 GPa are used to form the composite joins.

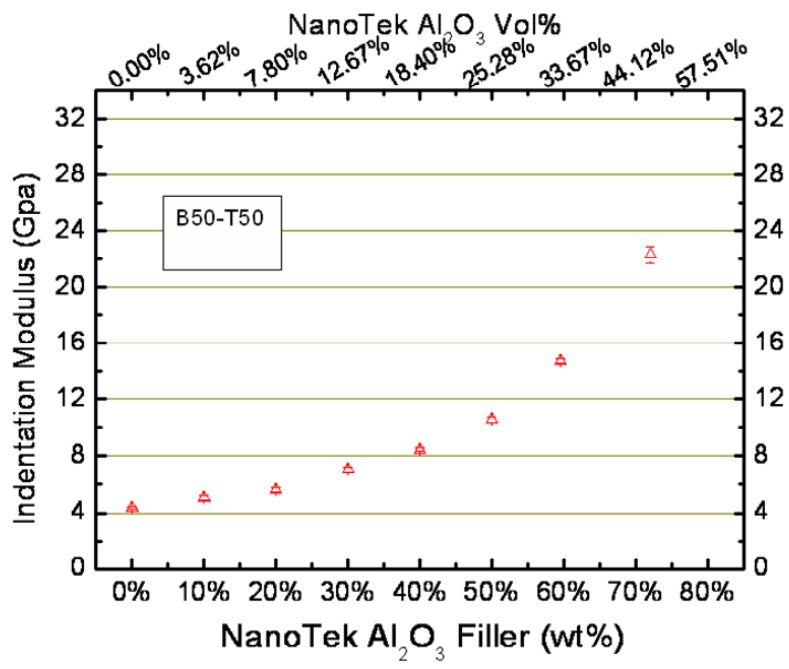


Figure 3.9: Indentation obtained elastic moduli versus the amount of nano alumina filler additions to polymeric matrix.

3.7 Summary

1) Nanoparticle-filled composites are generally dense and appear to have uniform properties that are a function of loading level. At loading levels greater than 72 wt.% it is necessary to add chemical agents, such as surfactants, to improve mixing and homogeneity.

2) It is possible to obtain very uniformly loaded composites with up to 80 wt.% nanoalumina with little porosity and no obvious agglomeration of particles. At very high loading levels the elastic modulus is greatly enhanced compared to current composites using similar organic matrices.

3) Laminate structures fabricated using the high modulus composites are uniform, well bonded to glass layers and have acceptable translucency. Although uncured composite viscosity is higher than current adhesives, it does not limit its use even in very thin joints.

4) Using our high modulus composites materials as an adhesive does not preclude translucent dental crowns. Such crowns are more aesthetic and mimic the translucency of natural teeth and therefore are preferred over opaque dental crowns.

Chapter 4.0: Hertzian Loading of Layered Structures and the Effect of Join Elastic Modulus

4.1 Introduction

Laminar structures are particularly important in dental restorations since they can help to mimic the structure and function of natural teeth. A particularly important issue in laminar composites is elastic mismatch between layers. Compliant inter-layers allow flexure and can lead to failure of brittle veneering layers. Ceramic dental restorations typically include at least an aesthetic veneer layer and a stronger core layer [18, 30, 36, 53]. The veneer may fail under point contact if it is not well supported. This chapter focuses on understanding the failure modes and mechanisms of laminar structures under single cycle loading.

4.2 Experimental Setup: In Situ Hertzian Contact Testing

The purpose of this experiment is to use Hertzian contact to find the critical loads at which radial cracks form in the veneer. Initial formation of the radial cracks is experimentally observed using a combination of high speed video capture and a screw driven mechanical test rig, Figure 4.1. During the experiment the multilayered samples are placed on a test platform consisting of a 10 mm soda lime glass block supported on a stainless steel test station. The veneer of the multilayer sample is subjected to Hertzian contact using a tungsten carbide ball. As the load of the indenter is increased a critical load will be reached at which a radial crack will form in the veneer. The load of the indenter and a visual observation of the veneer must be

simultaneously recorded to enable one to experimentally determine the critical load of radial crack formation.

Indentation is controlled by a system of screw driven test rigs and computer controlled actuators. An Instron 5500R and Instron 4501 (Instron Corporation, Canton, MA) is mounted with a steel rod equipped with a holder at one end where a tungsten carbide spherical indenter is placed. The loading of the Instron 5500R/4501 is controlled by computer software supplied by Instron, Merlin version 4.2. Once the multilayered sample is placed on the test station the indenter is lowered onto the top layer until a minimum load of 1 N is reached. A video camera, Canon XL1 3CCD (Canon, New Hyde Park NY) is pointed toward the side of the polished edge of the glass veneer. Since the glass is polished it is optically transparent and therefore the formation of radial cracks can be videoed. Radial cracks are observed by magnifying the side view of the glass veneer using an Optem Zoom 200D magnifying lens (Optem International, Fairport NY) connected to the video camera. In addition, the glass veneer is back lit with a halogen light with two separate beams in order to increase the amount and angle of light entering the glass, increasing light visible to the camera. During the execution of the experiment the video feed from the camcorder is recorded onto a video cassette, and another external camera that is focused on the load readout from the computer monitor is also placed onto the video feed (picture in picture). Therefore it is possible to record the instantaneous condition of the glass veneer and the load simultaneously. This technique allows for the observation of initiation of a radial crack in the veneer and the exact critical load at which they occur.

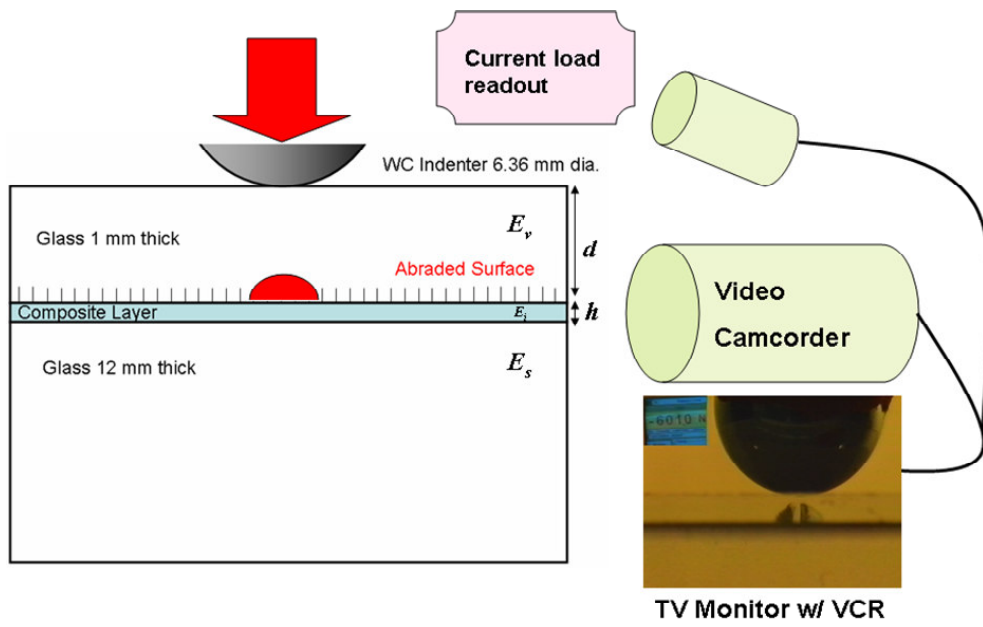


Figure 4.1: Specimen schematic for flat model testing with Hertzian contact.

4.3 Radial Crack Testing in Single Cycle Loading

Hertzian indentation with ever increasing monotonic loading on the test samples produces radial cracking in the veneer layer as seen in the video sequence shown in Figure 4.2. The image sequence is a series of still pictures taken from video during testing. The images are a side view of the layered model structure as the spherical indenter is loaded onto the veneer layer. As the load increases, eventually a critical load is reached that initiates a radial crack in the veneer. When the critical load for radial crack initiation, P_{cr} , is reached, a radial crack “pops in”, reflecting the light, and is recorded. The load at which the crack initiates is determined by the value projected from the computer monitor image. As the load continues to increase a cone crack may also appear, emanating from the contact with the spherical indenter, if the loads are sufficiently high. These cone cracks do not appear before the radial cracks in the veneer thicknesses investigated here. This is due to the fact that the top surface of the glass has been etched and there are relatively small flaws on the top of the veneer in comparison to the flaws introduced at the interface between the veneer and adhesive layer. Delamination is another potential mode of failure. It is important to note that no instances of delamination of the joining material from the veneer or core are observed in our experiments. The bond strength between the composite or epoxy performed well even after thousands of loading cycles are conducted. Radial crack initiation is the primary failure mode in these tests.

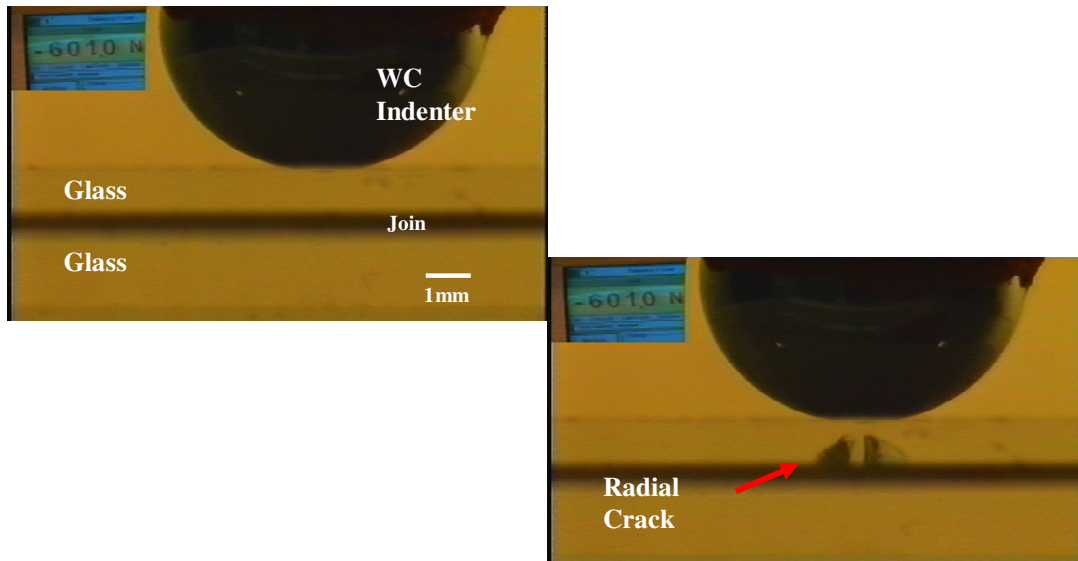


Figure 4.2: Image sequence of single cycle Hertzian contact taken from video. Radial crack initiation is apparent in veneer layers. No delamination is present between the composite join and the glass layers.

Figure 4.3 shows the critical load, P_{cr} , for radial crack formation in 1 mm thick veneers as a function of joint thickness. The data demonstrate an average increase in P_{cr} with decreasing joint thickness in the composites and epoxy joins. Most notably, there is a significant difference in P_{cr} between the 22 GPa composite and epoxy joins. Using a standard t-test for joint thicknesses near 150 μm , the P_{cr} values for epoxy and composite are significantly different, with a $p < 0.000002$. On average, P_{cr} for the 22 GPa composite joins is 3 times higher than that for epoxy joins for all the thicknesses investigated.

The plotted lines in Figure 4.3 represent calculated values for the P_{cr} in the veneer versus joint thickness. Each plot line represents P_{cr} versus joint thickness for given joint elastic moduli. All of the joins are made using 1 mm thick veneer. The governing equations, from Kim *et al*, for the formation of radial cracks in the veneer are as follows [33].

$$P_{cr} = BSd^2 / [\log(E_v/E^*)] \quad 4.1$$

where S is glass strength, d the thickness of the veneer, E_v the veneer modulus and $B = 2$ is a dimensionless constant. The quantity E^* is an effective support modulus given by

$$E^* = E_i (E_v/E_i)^L \quad 4.2$$

The effective modulus, E^* , of the veneer supporting structure (join and substrate) is related to both the elastic modulus of the join layer, E_i and the substrate, E_s . The exponent, L , is a function of the thickness of the adhesive.

$$L = \exp [- [\alpha + \beta \log (h/d)]^\gamma] \quad 4.3$$

where $\alpha = 1.18$, $\beta = 0.33$ and $\gamma = 3.13$ are constants obtained from plotting L versus h/d to a Weibull function as describe by Kim *et al* [33, 54]. The 2 plots of P_{CR} from the governing equations for radial crack formation (solid lines) fall on the data for E_i values of 2.3 GPa (epoxy joins) and 22 GPa (composite joins). The rest of the variables in the model are the strength of the glass, $S = 130$ MPa, the veneer modulus $E_v = 70$ GPa, the substrate modulus $E_s = 70$ GPa and the veneer thickness, $d = 1$ mm.

The other two plotted lines in Figure 4.3 (dashed lines) represent hypothetical adhesive or interlayer elastic modulus of 10 GPa and 40 GPa. As mention, current commercial dental cements have elastic moduli near 10 GPa. However these higher elastic modulus cements are inadequate for adhering laminate structures, and in prior studies have failed by delamination after Hertzian contact loading [33]. Note that for the plot representative of a 40 GPa layer, P_{CR} is always greater than 1000N. There are no existing dental adhesives in this elastic modulus range. However our laboratory has made composites with elastic modulus ~ 40 GPa. Preliminary data for 40 GPa and 10 GPa composites do not fit the predictive curves as well since sample preparation procedures were still under development. However they fit the trend for varying thickness and a shift in P_{cr} due to elastic modulus of the interlayer.

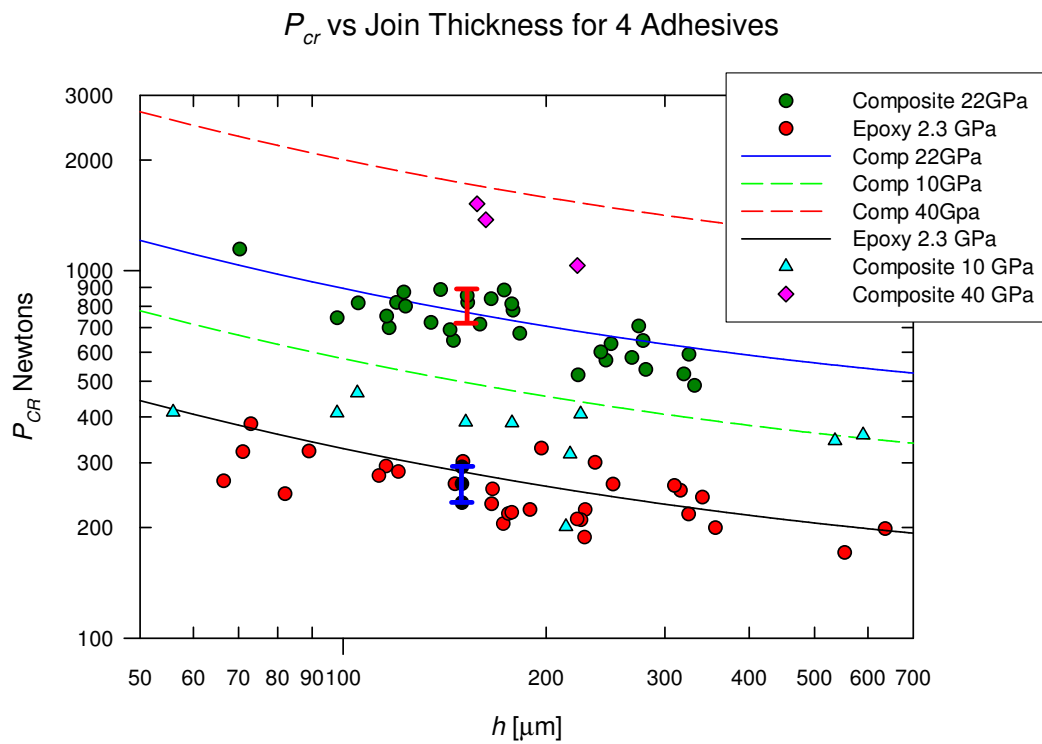


Figure 4.3: Plotted P_{cr} for epoxy and 3 composites joined specimens (veneer thickness = 1mm).

The advantage of the relations in equations 4.1-4.3 is their capacity to make predictions for hypothetical adhesive layers. The effect of modulus on the predicted critical load for radial crack formation, P_{cr} , is shown in Figure 4.4 for different joint thicknesses using these equations. Regardless of the thickness of the adhesive, the model predicts that the P_{cr} will rise to infinity as the elastic modulus of the adhesive approaches the elastic modulus of the veneer. Clinically, the biting forces that teeth are exposed to during chewing are on the order of 100 N [55]. Therefore in the design of crowns and in our consideration for joints supporting veneers critical loads should be much greater than 100 N. From Figure 4.4 only the plot for the 10 μm joint has P_{cr} values at or above 1000 N for all elastic moduli of the adhesive layer. As a margin of safety and for acceptable lifetimes of dental crowns, the P_{cr} should be near or above 1000 N which is ten times the typical biting forces. P_{cr} for 10 μm joints are 2.75 times larger than P_{cr} for 50 μm joints for all investigated joint moduli. As joint thicknesses increase further, P_{cr} continues to fall from the levels seen in the 10 μm joints. Indeed, if very thin joints between the veneer and core were the norm for these CAD/CAM dental crowns, the concern of failure due to radial cracks in the veneer would be mitigated. However current techniques for fabricating these materials do not have tolerances for fitting separately fabricated veneers and core such that the gap between them will 10 μm or less over the entire crown. Therefore it is necessary that joints are able to limit veneer flexure during occlusal loading regardless of their thickness.

P_{cr} vs Elastic Modulus of Adhesive for Varying Join Thickness

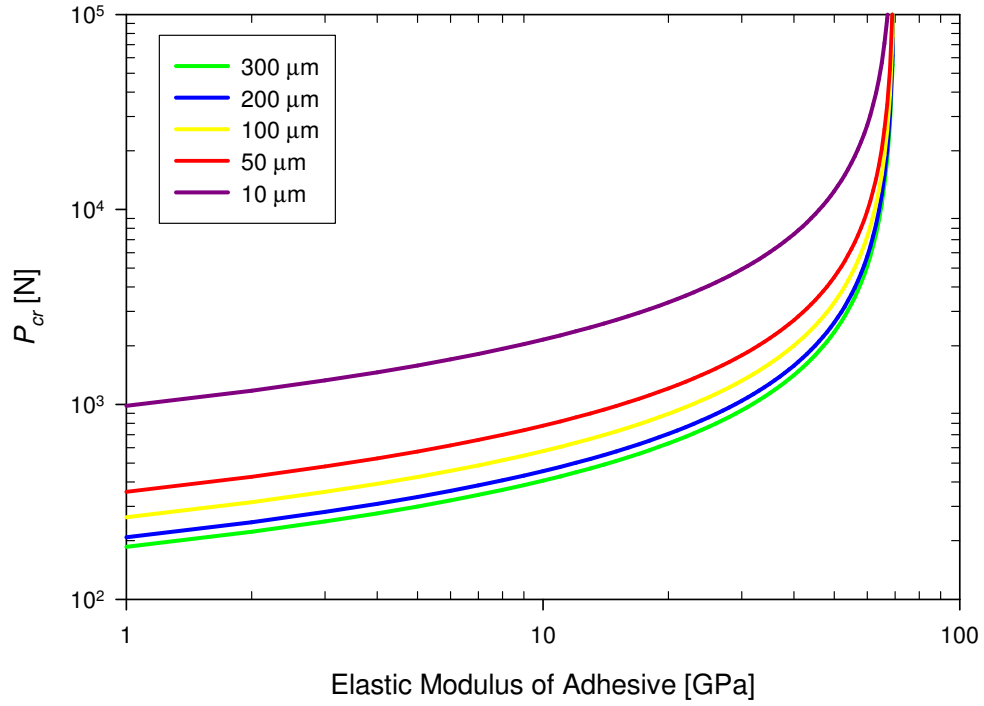


Figure 4.4: P_{cr} versus join elastic modulus for different adhesive thicknesses (veneer thickness = 1mm).

Radial cracks will form in the veneer at even lower loads when the veneer thickness decreases as seen in equation 4.1 ($P_{cr} \propto d^2$). Figure 4.5 plots the critical loads for radial crack formation in 100 μm joints against joint elastic modulus as a function of veneer thicknesses. For 2 mm veneers the critical loads are in excess of 1000 N for all joint moduli. However a veneer thickness of 2 mm is beyond the typical range of current veneers. In fact, the entire crown (veneer/core) has an average thickness in the range of 2 mm. Typical veneers have approximate thicknesses of 0.5-1 mm. Some veneers can be even thinner, depending on the processing techniques and geometric constraints. Thinner veneers are even more vulnerable to radial crack formation than thicker veneers. Figure 4.5 shows a P_{cr} of 70 N when the joint's elastic modulus is that of current dental adhesives, ~ 3 GPa. At this level of occlusal loading radial cracks would form during normal chewing, where loads are close to 100 N. A high elastic modulus composite joint would raise the P_{cr} to roughly 180 N. This is not much higher than the loads seen in chewing and so is insufficient for the desired margin of safety in crown design. A joint elastic modulus around 56 GPa would be needed to raise P_{cr} to 1000 N and thereby provide the veneer with sufficient support to suppress radial crack formation. Therefore equations 4.1-4.3 and figures 4.4 and 4.5 indicate that by choosing veneer thickness and joint modulus the detrimental effects of introducing a relatively compliant layer between the core and veneer can be limited.

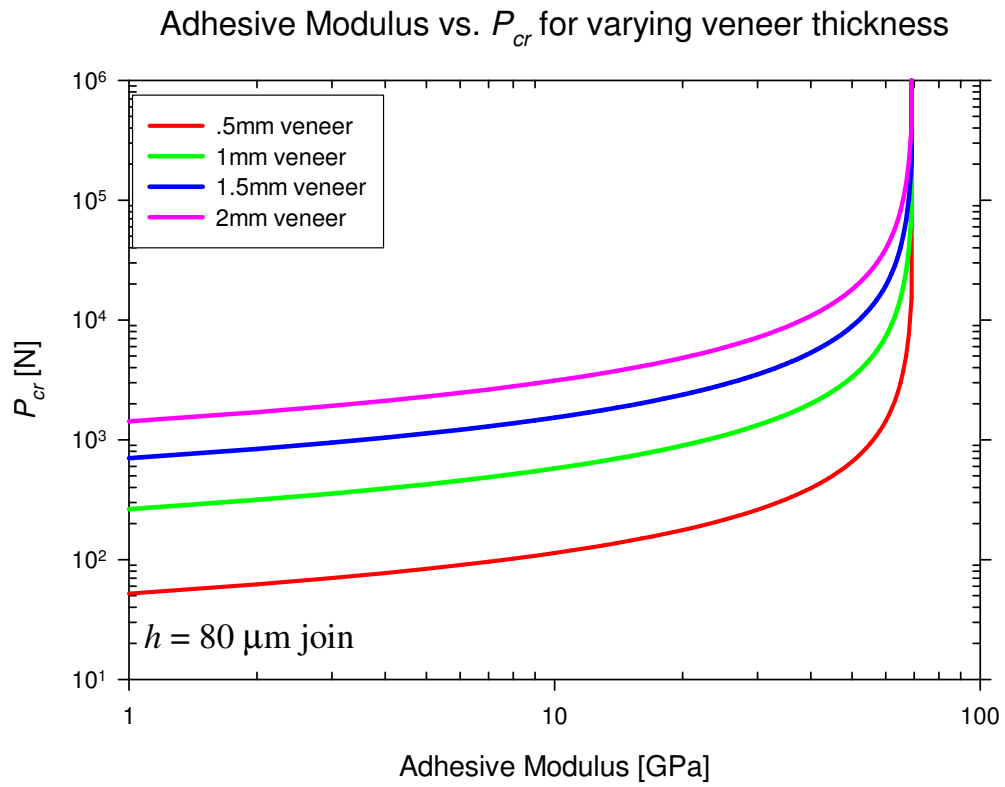


Figure 4.5: Effect of veneer thickness on P_{cr} for all joint moduli.

4.4 Radial Crack Testing in Multi Cycle Loading

The ultimate purpose of the “crown like” structures tested here is to represent real crowns and the variables that contribute to their performance. However, single cycle indentation of laminate structures is limited in estimating long term performance with repeated loading. The Hertzian indentation methods covered in the previous section deal exclusively with single cycle loading. These experiments illustrate the role of geometry and material properties on radial crack initiation as well as the critical loading for crack initiation. Cyclic Hertzian loading is more useful in estimating lifetime since dental crown are subjected to 1500 chewing cycles a day or approximately 550,000 cycles a year [55, 56]. When model laminate structures are subjected to sinusoidal loading, it is possible to track the number of cycles to failure and the loads at which failure occurs to predict long term performance[12, 57].

The laminate model structures for cyclic Hertzian testing are fabricated using similar methods to that of those used for single cycle testing [40, 58]. The number of cycles to radial crack initiation in a veneer $d = 1$ mm and join thickness $h = 80$ μm is plotted in Figure 4.6. The join thickness of $h = 80$ μm is chosen due to the fact that it well within the like range of likely thickness for our proposed laminate structure [1]. Figure 4.6 shows that at a Hertzian contact load of 200 N, 2.7×10^6 cycles are required to form a radial crack in the veneer that is joined using a composite interlayer. For epoxy a 200 N indentation load need only 1.55×10^5 cycles to form a radial crack in the veneer. If we are to consider that there are 1500 chewing cycles a day, laminates made with composite joins would function nearly 5 years without radial cracks and 100 days for epoxy. This test provides a simple means to examine

possible long term behavior. In addition, the joints fabricated with composite adhesives did not show any signs of delamination with either the veneer or core even after the 2.7 million cycles. Recall that in the study by Kim *et al*, the highest modulus joints did not even survive after a single Hertzian loading cycle [33]. This suggests that the adhesion between composite and veneer or core is robust not only in single cycle, but also in prolonged cyclic loading. Therefore delamination of the model laminate structure may be excluded as a possible damage mode in our tests [59].

The reduction of strength in the veneer over repeated loading is due to slow crack growth of the flaws in the glass layer, according to a crack velocity equation of the form $v \sim K^N$, where K is the stress intensity factor N is an exponent. As the corresponding strength of the glass falls over time the critical loads, P_{cr} , also falls, according to a relation of the kind $n \sim P^{-1/N}$ (where n is the number of cycles) [60]. The dashed lines in Figure 4.6 represent this dependence, with $N = 17$ for glass [60].

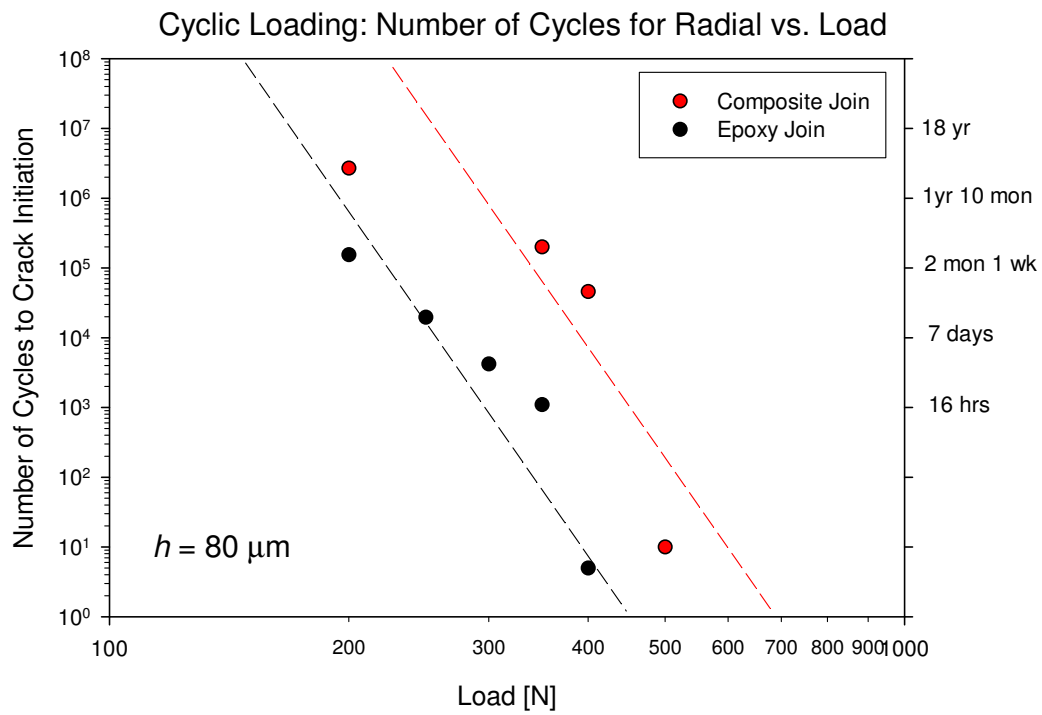


Figure 4.6: Indentation load vs the number of cycles required to generate a radial crack in a 1 mm glass veneer layer. Both epoxy ($E = 2.3 \text{ GPa}$) and composite joints ($E = 22 \text{ GPa}$) have joint thickness $h = 80 \mu\text{m}$.

4.5 Summary

1) Higher modulus join layers limit failure by radial fracture from contact loads in single cycle. Joins made with composite materials are well bonded and do not delaminate even after radial cracks appear and veneers fail. Radial cracks are suppressed from forming in the veneer up to loads where top surface cone cracks may form when they are joined to the core with the high elastic modulus composite.

2) Composite joins do not delaminate even after being subjected to loading cycles numbering near 2.7 million. Lower loads with cyclic testing yields longer lifetimes of veneer in respect to radical crack initiation.

Chapter 5: Crack Containment Between Layers Joined with Composite/Epoxy Interlayer

5.1 Introduction

The use of adhesives in crown construction offers potential benefits over current methods. Joining with a compliant adhesive in lieu of the traditional labor intensive firing and hand layering of the veneer to cores overcomes the need to reduce residual stresses associated with CTE mismatch [12, 36, 57, 61, 62]. Using a composite join is appealing since it allows the optimization of the individual layers in the laminar structure. This is particularly important for the veneer layer since hand layering porcelain veneers can result in residual porosity. In addition brittle layers that are glued to cores have relatively low susceptibility to radial crack formation when the adhesive layers are relatively thin and have a high elastic modulus [30, 32, 34, 58]. These improvements are not without potential drawback. Very stiff adhesives may potentially allow cracks that originate in one layer to cross into adjacent layers through the adhesive. This chapter explores the behavior of crack propagation between layers and factors that dictate this damage mode.

5.2 Experimental Set-up

This chapter covers three unique experiments that propagate cracks from one layer of glass through adhesives into an adjacent brittle layer. Each experiment is conducted with video capture of the crack growth *in situ*, in a similar manner to that described in Chapter 3. Experiments follow cracks as they approach the adhesive and

eventually go through the join into the next layer. The loads at which cracks enter adjacent layers are noted.

5.3 Hertzian Contact Radial Crack Growth: Core/Join/Veneer

In order to facilitate mechanical characterization of the composite joining layer and to provide a foundation for the proposed work, a model system based on an extension of the configuration in the preceding chapter is used. In these preliminary experiments soda lime glass is used as both a veneering layer and core layer with a composite join between the two. Glass is a good transparent substitute for the veneer layer because it has similar modulus and toughness values to aesthetic porcelain [18]. Since glass is transparent, crack behavior can be observed in real time. Glass is used as a preliminary core layer to simplify the system by having the veneer and core layer modulus matched.

Figure 5.1 shows a schematic of a Hertzian test setup. The white areas are the glass layers, the composite is the light blue layer between the glass and the entire “sandwich” is supported by a polycarbonate block. The sandwich structure is not bonded to the polycarbonate support in this case. Above the sandwich a spherical indenter places loads on the veneer layer in Hertzian contact testing. The purpose of this experiment is to investigate crack behavior at the interface between the upper glass layer mimicking the veneer and the composite join layer. To facilitate this, a Vickers indent was used to place a flaw or crack nucleation site on the bottom surface of the lower glass plate directly below the contact area of the spherical indenter. This produces more reproducible experiments, since the flaw population is controlled and

allows control over crack propagation through the lower glass plate. The sandwich structure test setup exposes the bottom of the top plate to tension under loading with the spherical indenter. Under tension, the crack generated by the Vickers indentation on the lower plate grows towards the interface with the high modulus composite. The propagation of the crack is monitored through the highly polished surfaces of the glass and recorded using high speed video. The test setup allows for the characterization of crack behavior at the join interfaces and performance of composite as an adhesive layer.

The variables that may impact the performance of composite joining layers under Hertzian contact loading include, but are not limited to: 1) the thickness of the individual layers, 2) the modulus of the individual layers, 3) the interfacial join toughness, 4) surface treatment of the joining layers and 5) toughness of the composite join. In order to limit the number of variables and to focus on the crack propagation and composite join performance, an initial standard geometry and composite formulation was chosen. The layers of glass were 1 mm thick and the join thickness averaged about 80 μm . A composition 72 wt% alumina nano powder (50 nm diameter spherical particle size) and 26 wt% blend of two polymers, bis-GMA, Bisphenol-A-glycidylmethacrylate and TEGDMA, triethylene glycol dimethacrylate (1:1 weight ratio) was utilized in the composite joining layer. This composition was chosen because it has the highest modulus, 22 GPa, of our 'simple' composites, those without surfactants and plasticizers to aid in mixing. These additions add another variable may impact in crack behavior. The Hertzian indenter was limited to a radius of 3.18 mm, which simulates contact area during

mastication. The polycarbonate support not only allows for the biaxial flexure of the sandwich structure during Hertzian loading but also has a similar modulus to the dentin layers that support dental crowns [12, 33, 39, 63].

Hertzian contact experiments were conducted at a relatively slow loading rate, 3 μm per minute, to allow observation of crack evolution. The initial testing setups used 1 mm glass layers whose surfaces were etched using 10% hydrogen fluoride and then polished to provide optically transparent surfaces. Optimal lighting conditions were chosen during videoing of the crack propagation. However due to the differences in crack planes in the glass layers some variability in appearance of the cracks was noted.

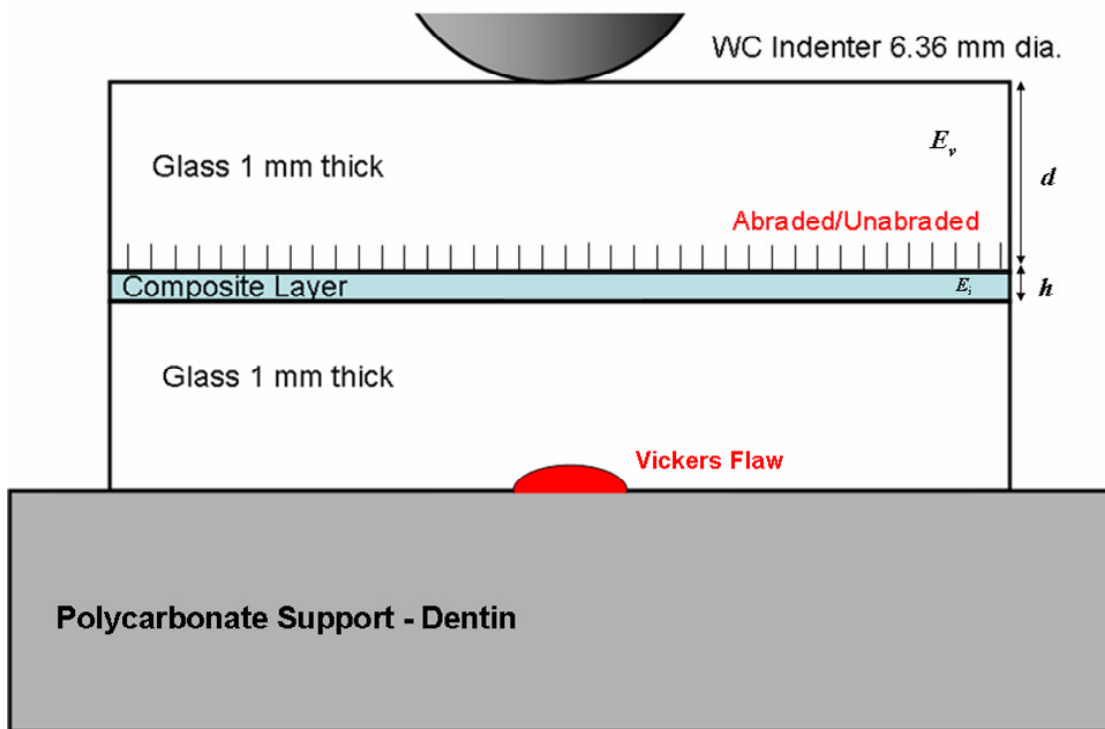


Figure 5.1: Etched, unabraded or abraded glass layer mounted onto polycarbonate substrate. Vickers indent bottom of lower layer. No delamination observed.

Figure 5.2 shows the result of a single cycle Hertzian contact experiment. The individual figures are taken from the video captured during the loading via Hertzian contact. In the top left figure dimensions have been indicated and the induced flaw by Vickers indentation is clearly seen at the bottom of the lower glass. As the load increases, the lower glass is under tension. This induces a crack at the Vickers indentation that grows towards the composite/glass interface. When the crack reaches the join interface there appears to be no delamination of the join. In this sample, no other flaws were induced, except for the Vickers indentation the surfaces were in the etched and polished state. The crack in the lower glass extended laterally over the entire span of the sample. Since there were no significant stress concentrators, the top glass fails spontaneously after the material reaches its failure stress since the bottom layer no longer supports it. In addition, the lack of flaws in the bottom surface of the upper glass layer does not allow for a single crack to nucleate and cause failure. However once the stresses reach a threshold the glass fails catastrophically and the origin or damage mode cannot be captured using video.

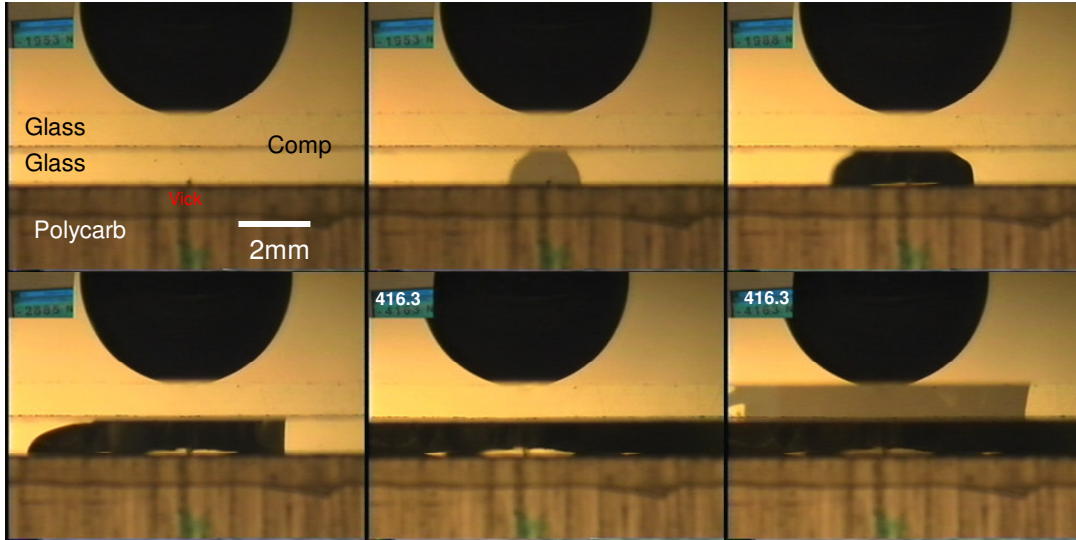


Figure 5.2: - Video sequence of Hertzian Contact experiment. Bottom surface of top glass is left unabraded. Catastrophic failure at high loads. No delamination is apparent.

In order to control the crack propagation in the upper glass layer, the glass interfaces with the composite layer were abraded prior to joining. Again Figure 5.1 is a schematic of the experiment with the addition of an abraded/unabraded interface. The abrasion was performed with a mixture of water and 600 grit silicon carbide (SiC) powder. Abrading the bottom surface of the upper glass layer produces stress concentration sites that can nucleate cracks in a controlled manner and allow for videoing in situ. Figure 5.3 is a series of pictures from a video taken during the loading of a sandwich structure with the abraded surface. The onset of cracks in the upper glass is visible in the first slide on second row. As the cracks in the lower glass reach the interface under increasing applied load, a threshold is reached that allows cracks to appear in the upper glass. The critical loads for cracks appearing in the upper layer are different between the abraded and unabraded glasses by more than 2:1.

The stresses required to initiate a crack for an unabraded glass versus an abraded glass are much higher since the etching and polishing removed scratches etc. that would serve as stress concentrators. From the experiment in Figures 5.2 and 5.3 it may be concluded that the mechanism of crack propagation through the composite join from the lower to upper glass is that of reinitiation. This means the cracks seen in the lower glass of the abraded experiment do not propagate continuously into the upper glass through the interface. The cracks seen in the upper glass are new cracks created by tension during loading. Propagation of the crack from the lower to upper glass was the other possible outcome of the Hertzian contact loading. If the cracks in the upper glass had directly propagated from the lower glass the surface treatment of

the interface would not affect the cracking behavior. Thus, the need for an abraded surface before cracks appear in the upper glass implies that reinitiation rather than continuous propagation occurs. It is also significant that no delamination between the composite and glass was observed after the failure of the samples in either case as seen in Figure 5. This join integrity after failure implies that the interfacial join is relatively strong [33]. Upon post mortem inspection of samples, Figure 5.4, it is noted that the crack planes in the upper and lower glass had nearly identical crack planes. While, this might be construed as evidence of direct crack propagation in the absence of real time observation, it is not. In fact, the crack planes in adjacent layers are not exactly the same. Similar behavior was observed in a study by Shaw and Marshall, where the renucleated cracks between alumina and metal plates had similar cracking planes [64].

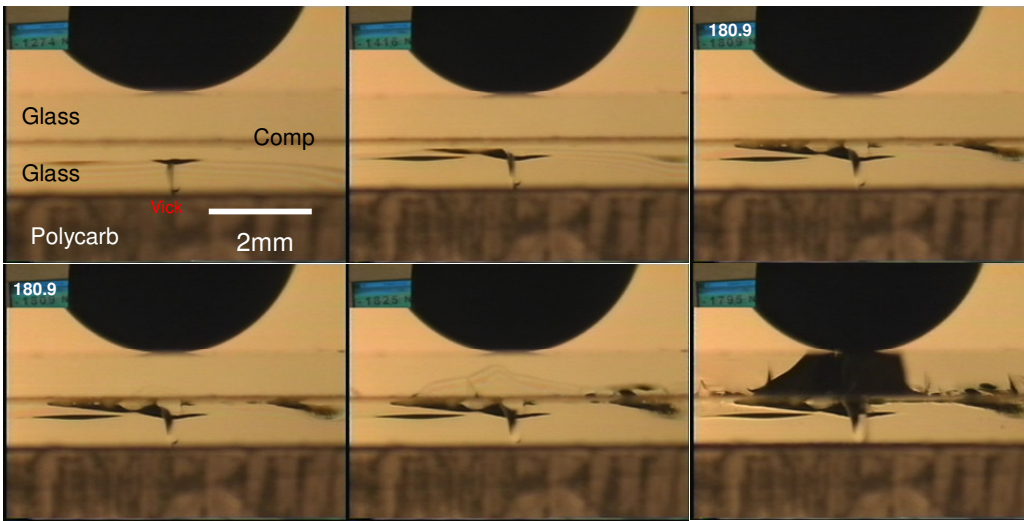


Figure 5.3: - Video sequence of Hertzian Contact experiment. Bottom surface of top glass abraded. Catastrophic failure at high loads. No delamination observed.

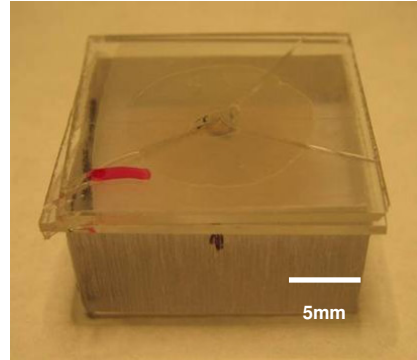
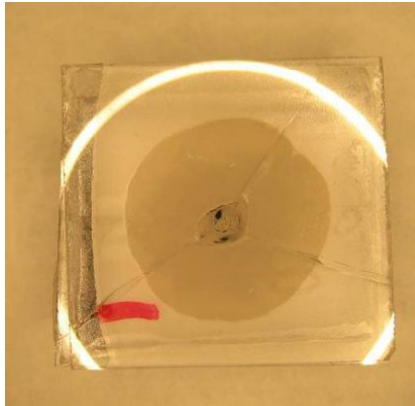


Figure 5.4: Fractured Specimen, renucleation is concluded. No apparent delamination. Cracks planes in lower & upper layers similar. Joins are translucent.

In order to further elucidate the fracture mechanisms in the layers, Vickers indents were placed near the composite/glass interfaces of cross sections of the joins, Figure 5.5. This technique was employed by J.W. Kim *et al* [65] to elucidate crack behavior at the interfaces [65, 66]. Dr. Kim studied flat porcelain layers fused to either yttria-tetragonal-zirconia-polycrystal (Y-TZP) or alumina cores. He showed that when Vickers indentations are placed in the porcelain layer the cracks either arrest at or deflect along the porcelain/core boundary. However when Vickers indents are placed in the core, the resultant cracks pass unimpeded into the weaker porcelain. In this case there is no containment of crack in the tougher and stronger core. In our experiments, by placing Vickers indents close to the join/glass interface, transverse cracks can also be directed into adjacent layers in a similar fashion to the Hertzian radial crack experiments in the previous section, while visually observing cracks in cross section [31]. This method allows for a passive investigation into possible crack arresting characteristics of our joins. We found that cracks originating from the Vickers indentation always arrested in the tougher composite layer and joins did not delaminate, Figure 5.6. The composite layer of 200 μm thickness here is the same as in the radial crack experiment, i.e., a 72 wt% alumina that yields a composite with an elastic modulus of 22 GPa. The dark area close to the glass interface is due to the wear characteristics of the composite surface in relation to the glass. (During sample preparation the faces of the cross sections are polished, which causes the edge of the composite to wear away from the glass edge due to the difference wear characteristics.) The Vickers indent is placed with a load of 30 N close to the interface with the corners of the indenter either perpendicular or parallel to the join,

thereby producing cracks in the glass that either run transverse towards the join or parallel to the interface. Figure 5.6 shows a crack entering the composite join and arresting in the composite layer. There is no delamination between the glass and the composite layer. As described in a similar study by He and Hutchinson, the crack has entered the composite layer, and therefore the join toughness is a factor greater than that of the bulk composite itself [66]. In addition, the cracks that are parallel to the interface follow away from the indent and curve toward the indentation due to the elastic modulus mismatch between the composite layer and glass, which is 1:4 [32, 66]. This 30 N Vickers indentation cannot drive a crack across the join and into the adjacent glass layer.

The experiment is repeated with an indentation load of 90 N at a distance 80 μm from the interface, with a thinner join layer, Figure 5.7. Even with the tripling of the load and the thinner join relative to the prior experiment the crack cannot traverse the composite join layer. Once again the crack has entirely arrested within the join layer, and there is no sign of delamination, confirming the strong join between the composite and glass [59].

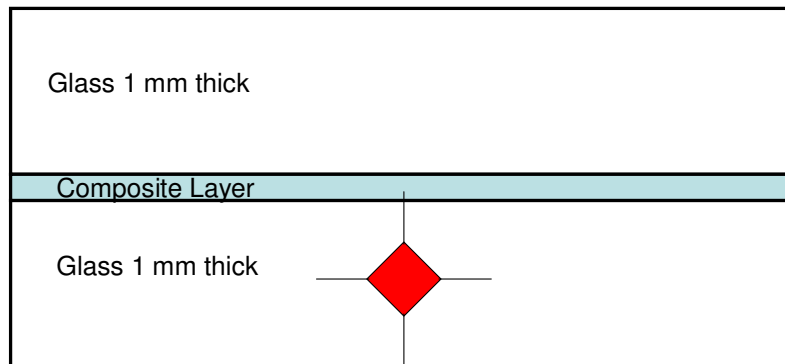


Figure 5.5: Vickers Microhardness. Cross sections of laminate joined structure. Crack propagation is observed between layers. Glass surfaces etched. Composite Layer, 72wt% nano alumina, $E = 22$ GPa.

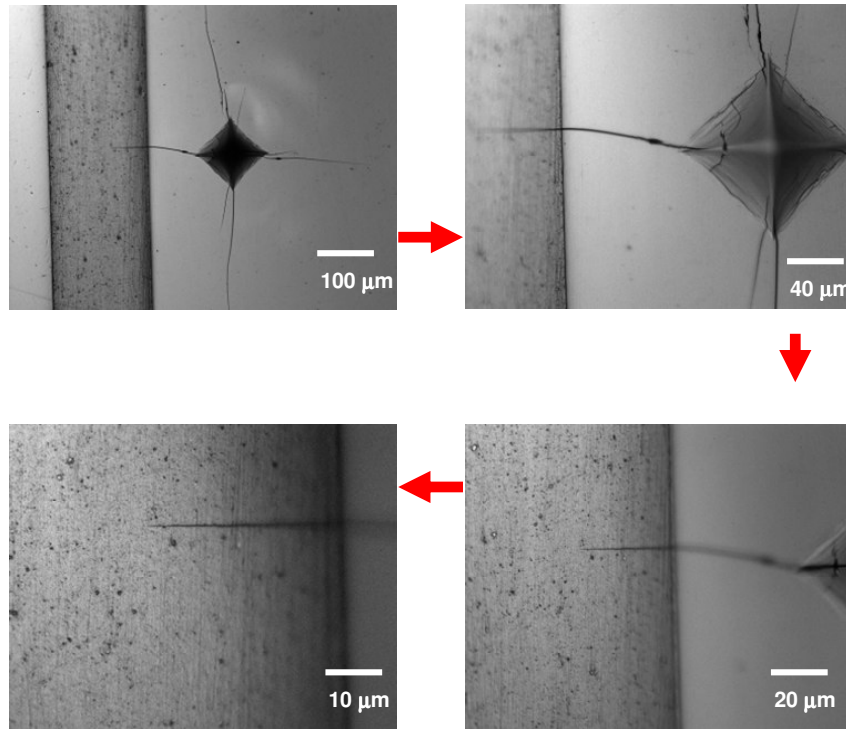


Figure 5.6: 30 N Vickers indent close to interface. Crack arrests in composite, no delamination.

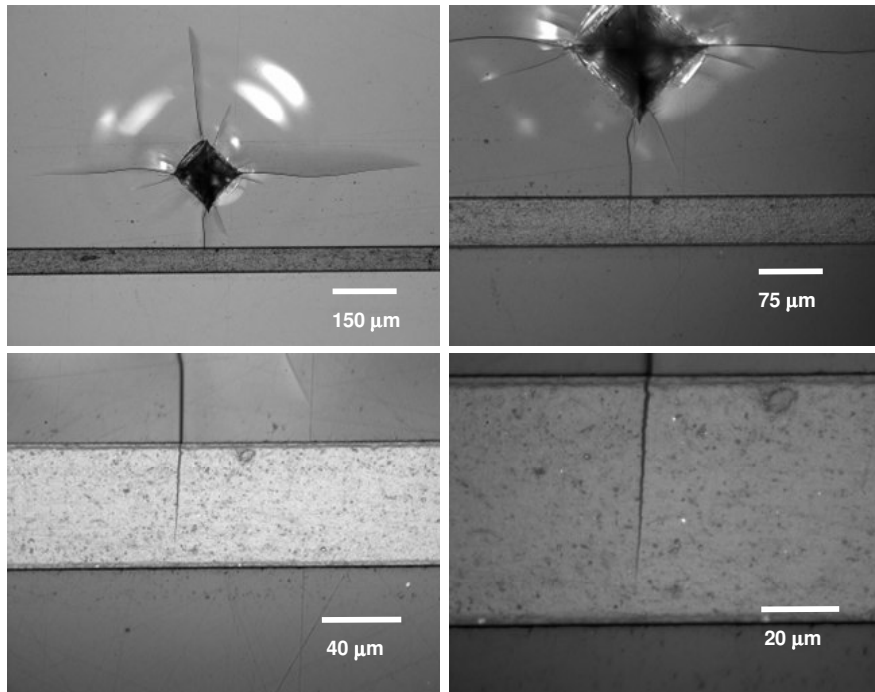


Figure 5.7: 90 N close to interface. Crack arrests in composite, no delamination.

Placement of such Vickers indentations cannot be too close to the interface due to local failure of the glass. Figure 5.8 shows such a Vickers indentation, which results in chipping of the glass layer. The spurious chipping causes the local stress field to fall off significantly and causes the driving force for the crack to drop, resulting in a short crack length in the composite layer. The crack length depends on glass integrity during the indentation. When the glass chips the stress field is reduced and thereby reduces the driving force pushing the crack across the join layer. Even a Vickers indent with a load of 200 N cannot produce cracks that traverse the composite joining layer, as seen in Figure 5.9. The crack here has traversed the composite layer but fails to enter into the adjacent glass layer. Close examination reveals that the crack appears to be following the interface [59]. However any possible crack deflection by the adjacent glass layer cannot be confirmed with cracks produced by Vickers indentations.

We find that cracks propagate from the glass into the composites by way of a penetration mechanism and arrest within the composite. Cracks do not traverse the interlayer due to stress shielding due to the lower elastic modulus of the joining layer. Reinitiation seems to be the method for cracks to enter from one glass layer to the next. Identification of the conditions that would control a switch from a renucleation to direct penetration through the composite to the glass would be very helpful in the design of dental restorations as well as other laminar systems.

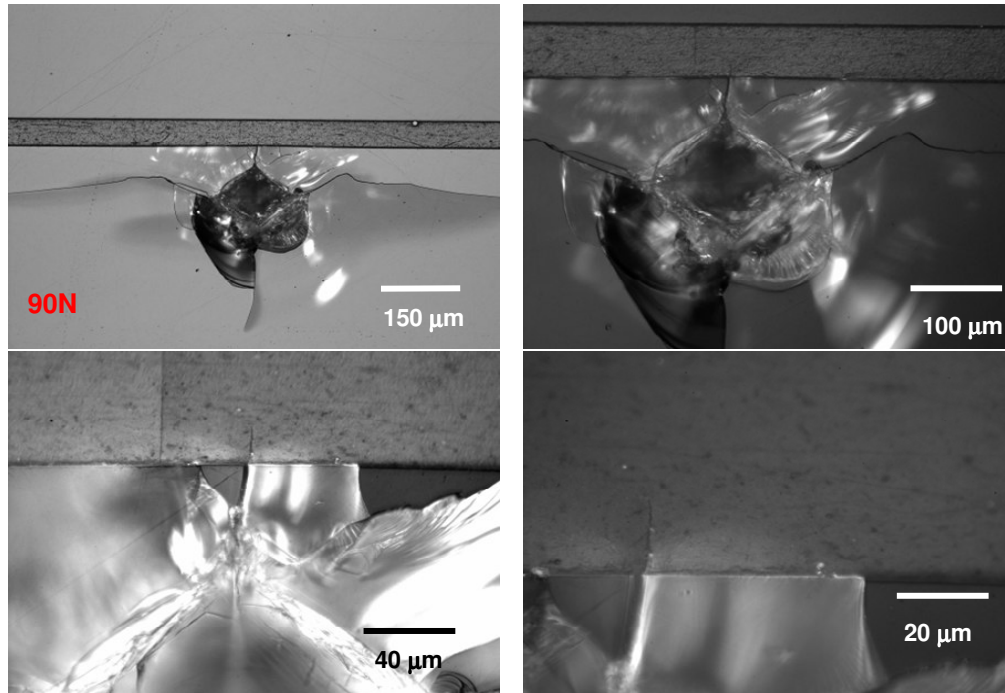


Figure 5.8: 90 N close to interface. Spurious chipping causes the crack tip to arrest inside the composite layer.

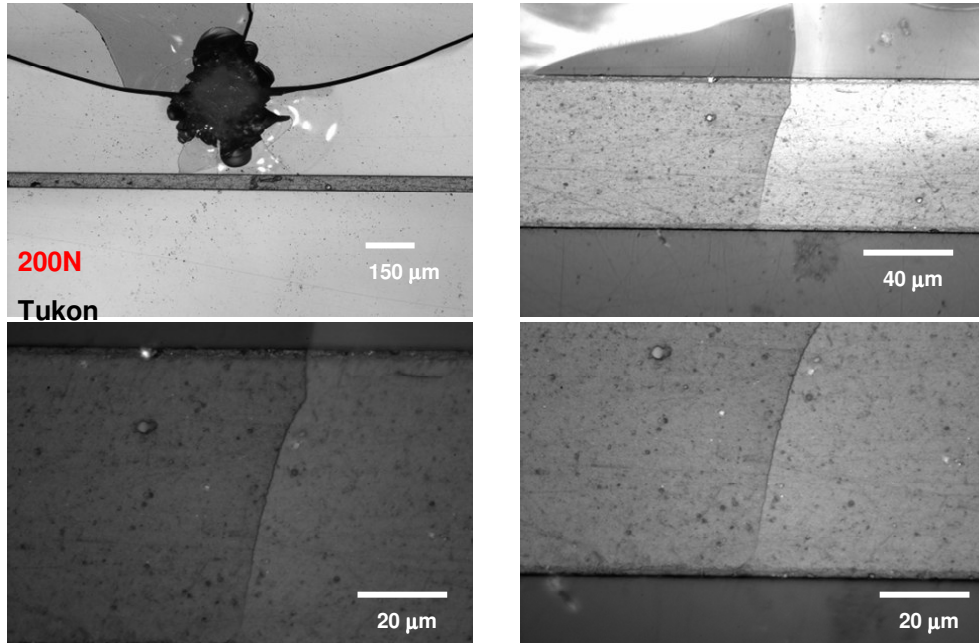


Figure 5.9: Maximum load of 200 N. Crack arrests in composite, no delamination. Crack cannot be driven into opposite glass layer using Vickers indentations.

5.4 Plane Strain Driven Cracks: 4 Point Bend Bar

In situ observation of crack propagation in radial crack experiments is difficult due to the fact that cracks traverse the center of the sample beneath the glass free surface. To properly characterize crack behavior through interfaces into a second brittle layer, observation of the tip during crack evolution is necessary. An experiment has therefore been designed to drive cracks into adjacent layers without the limitation of far-field loading of crack tips inherent in Vickers indentations. A Mode I crack model is implemented, whereby plane strain cracks are driven perpendicular to the crack direction [67]. The continual application of strain across the crack forces it to continue growing once it reaches the interface. At each interface (glass/join or join/glass) the crack may either arrest and deflect, delaminating the bond, or penetrate into the next glass layer, or reinitiate ahead of the crack [66, 68].

5.4.1 Bend bar: Experimental Setup

Four-point bending allows for the application of uniform tensile strain on the bottom surface of the test sample, as shown in Figure 5.10. The four-point bend test is based on a modification of ASTM C 273 where the lower rollers are 2 cm apart and the upper rollers are 1 cm apart [47]. The rollers have a diameter of 3 mm and are 3 cm long. Samples are made with 5 alternating layers of brittle and polymeric materials (3 glass layers joined by 2 layers of epoxy). Glass layers are made from the same soda lime glass plates as used in prior experiments. Epoxy layers are also made from the same resin (Harcos Chemicals, Bellesville NJ). The center glass layer is 1 mm thick while the outer glass layers are 2.2 mm thick. The outer glass thickness is

greater in order to promote the observation of cracks entering the outer layer. The thicknesses of the 2 epoxy layers are always equal; however those thicknesses vary as a part of the experimental design from 1 μm to 1 mm. The joined laminates of glass and epoxy are then made into rectangular bars 5.5 mm tall, 30 mm long and 5.4 - 6.4 mm wide, depending on joint thickness. Again the glass is etched in the same manner as prior experiments. Some bars have the inner surface of the outer glass (the one facing the epoxy) abraded, and others are left un-abraded. Abrasion of the surface introduces flaws and reduces strength of the glass in a controlled manner, to $S = 130$ MPa [32]. The top and bottom of the bars, where the cross sections of all layers are visible, is polished for a flat surface. The edges of the sample bars are etched to remove surface flaws created during polishing and to reduce the chance of cracks starting at the edge.

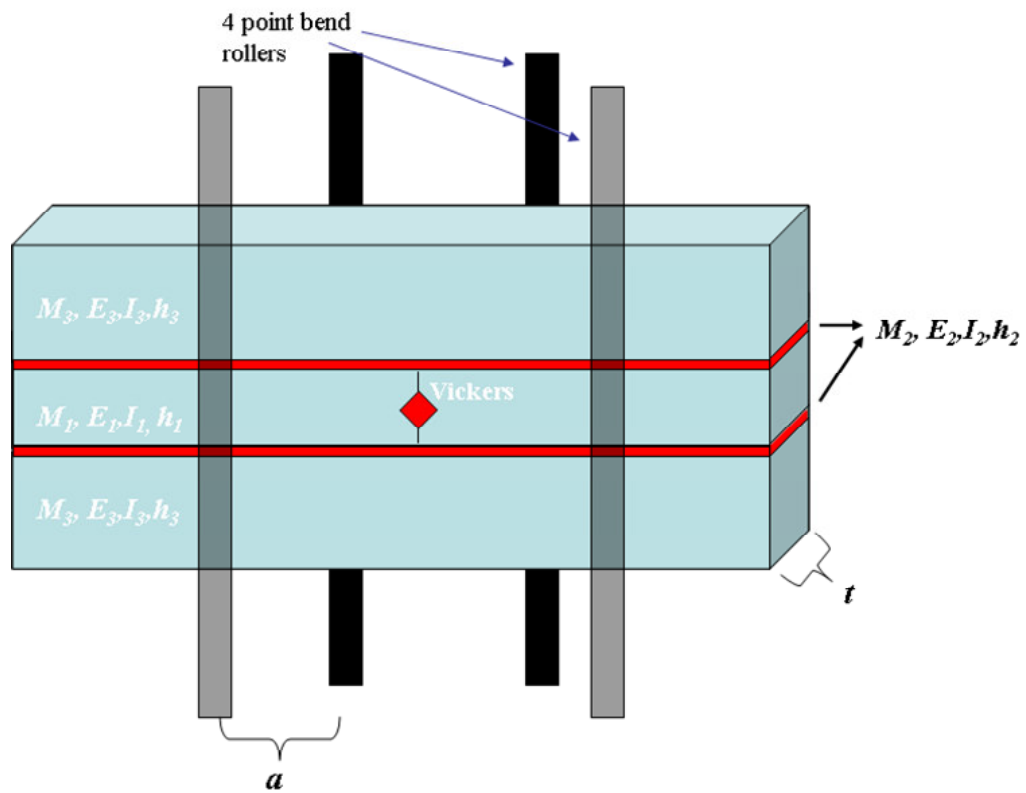


Figure 5.10: Beam Test, place lower surface under tension and drive cracks from Vickers indent into opposite interfaces.

5.4.2 Bend Bar Experimental Results

Mode I cracks are driven into adjacent layers via the application of planar tensile strain at the bottom surface of the bend bar samples. A starter flaw is placed in the middle of the center glass layer. The flaw is a Vickers indentation with a load of 10 N. The center axes of the Vickers indent are either perpendicular or parallel to the join/glass interfaces. The bend bar sample is then placed with the Vickers indentation, “induced flaw”, surface face down on and centered between the bottom rollers. As load is applied the bottom surface of the bend bar is subject to strain along the long axis of the specimen. Strain forces the cracks perpendicular to the join/glass interfaces to grow away from the Vickers indent and approach the interfaces. The cracks continue to the adhesive layer in a similar fashion to that of the prior experiment where Vickers indentations are placed close to the interface. However in this case strain is continually applied in a monotonically increasing manner. Therefore there is sufficient force to drive the crack into the adjacent glass layer. The crack may then deflect, penetrate or reinitiate, as before.

Figure 5.11 shows a sequence of frames taken from video captured as the cracks from the Vickers indentation approach adjacent joined layers. The side of the adjacent glass layers that face the interface are abraded here with an epoxy joint thickness of 2 μm (in other experiments the surfaces are left polished). At low loads the cracks emanating from the corners of the Vickers indent have similar lengths. As the load increases, the cracks perpendicular to the tensile forces from the bending begin to grow outward. The cracks continue to grow until they meet the interface, and appear to arrest. The load continues to increase until cracks have initiated in one

of the outer layers. Once cracks are present in the outer layer they are unstable and the sample fails quickly. Images of cracks entering the outer glass layer cannot be recorded due to the speed at which failure of occurs; the sampling rate of 32 frames per second for the video is too slow to image cracks propagating in the outer layer. Once the sample has failed the bend bar goes out of focus on the video, and there is a large load drop. All bending experiments result in similar crack growth toward the interface. This is seen when relative crack length is plotted against applied strain, Figure 5.12. At low level strain, $\epsilon < 0.0004$, the relative crack length c/c_t (c = the current crack length and c_t = the distance from the center of the Vickers indent to the interface) remains somewhat stable at around 0.2. The relative crack length is the length of the crack from the center of the Vickers indent to the tip of the crack divided by the distance from the center of the Vickers indent to the interface. Therefore the relative crack length is normalized for the initial position of starter flaws.

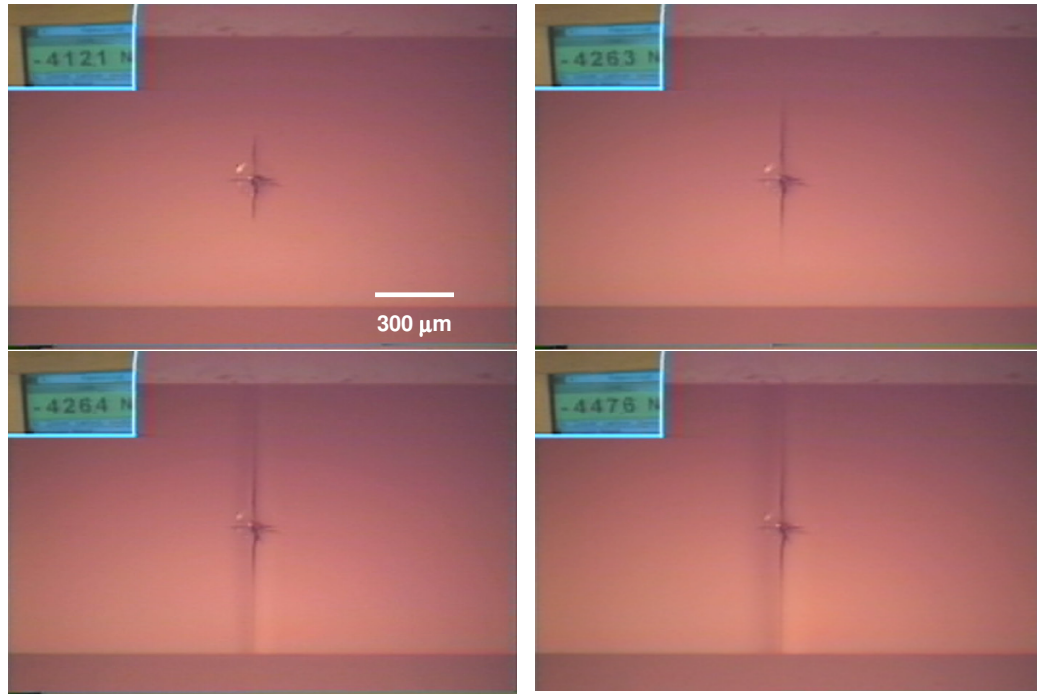


Figure 5.11: Video sequence of cracks reaching joint interfaces for a sample made with 2 μm thick epoxy joins.

An analysis of this problem has been provided by Dr. Herzl Chai. The strain is calculated from the solution of a bend problem of essentially a five layered structure subjected to a moment M . M_1 is the moment of the center 1mm glass and M_2 and M_3 are moments of the joining layer and outer glass layer respectively. Then

$$M_{total} = M_1 + 2(M_2 + M_3) \quad (5.1)$$

Therefore the total moment is the sum of five individual moments. The strain and moment of inertia can be described below where h is the layer thickness and t is the layer width.

$$\varepsilon = M(t/2)/EI, I = ht^3/12 \quad (5.2)$$

It is assumed that there is no slippage between layers and therefore the strain in each layer is equal and can be expressed in terms of the moment, elastic modulus and moment of inertia of each layer:

$$2\varepsilon/t = M_1/E_1I_1 = M_2/E_2I_2 = M_3/E_3I_3 \quad (5.3)$$

Substituting for each M into equation 5.1 the strain can be separated out,

$$M_{total} = 2\varepsilon t [E_1I_1 + 2(E_2I_2 + E_3I_3)] \quad (5.4)$$

The total moment is equal to $Pa/2$, where P is the load and a is the horizontal distance between the upper and lower rollers. The load is divided by 2 because there are 2 rollers on each side of the 4 point bend fixture. Therefore substituting $Pa/2$ into equation 5.2, the equation can be written as follows:

$$M_{\text{total}} = Pa/2 = \epsilon^2/6 [1 + 2(E_2h_2/E_1h_1 + E_3h_3/E_1h_1) E_1h_1] \quad (5.5)$$

The strain can then be expressed as

$$\epsilon = (3Pa/E_1t^2h_1) (1 + 2E_2h_2/E_1h_1 + 2E_3h_3/E_1h_1)^{-1} \quad (5.6)$$

In Figure 5.12, when the strain approaches 0.00055, the cracks grow precipitously towards the interface. Independent of geometry, cracks grow in a similar manner in all our bend bar experiments. The growth of the crack is universally halted at the interface, regardless of join thickness and independent of the surface condition of the outer glass layer (abraded or unabraded). At higher load, the cracks suddenly reappear in the adjacent layer, and jump spontaneously to failure. The load at which this happens is much higher for unabraded adjacent glass surfaces, suggesting that cracks that eventually enter the outer glass are new cracks rather than a continuous crack emanating from the Vickers indent during bending of the sample. If the cracks that originated in the inner glass propagated continuously into the outer glass then the surface condition of the outer glass would not matter. In these experiments the presence of surface flaws directly influences the load at which cracks

enter the outer glass as seen in Figure 5.12. For samples with abraded outer glass surfaces, cracks reinitiate at a strain level around $\varepsilon = 0.0006$. Unabraded samples have cracks reinitiating in the outer layer when the strain approaches $\varepsilon = 0.0014$, i.e. more than twice as high.

Even with extremely thin joins, $h \sim 1 \mu\text{m}$, cracks arrest at the interface prior to appearing in the outer glass layer. Additional force is required to reinitiate the crack on the other side of the interface. Absence of any join interlayer would result in the crack traversing the bar unimpeded. Figure 5.13 plots the strain level at which cracks appear in the outer glass layer versus the join thickness. Despite the scatter in data typical of glass fracture, there is a moderate benefit of thicker joins, requiring higher level of strain to reinitiate cracks in the outer glass. Again, even at the thinnest joins, higher strain is required to reinitiate cracks across the interface. Figure 5.13 also contains as the solid curve a FEM prediction using ANSYS software (Version 6.0, ANSYS Inc., Cannonsburg, PA) (courtesy of Dr. Herzl Chai). From both acquired data and FEM prediction, the strain required to reinitiate cracks in the outer glass increases by a factor of 3 when the thickness of the adhesive layer is increased from $1 \mu\text{m}$ to 1mm . Therefore increasing join layers better shield adjacent glass layers from the existing crack tip present in the inner glass.

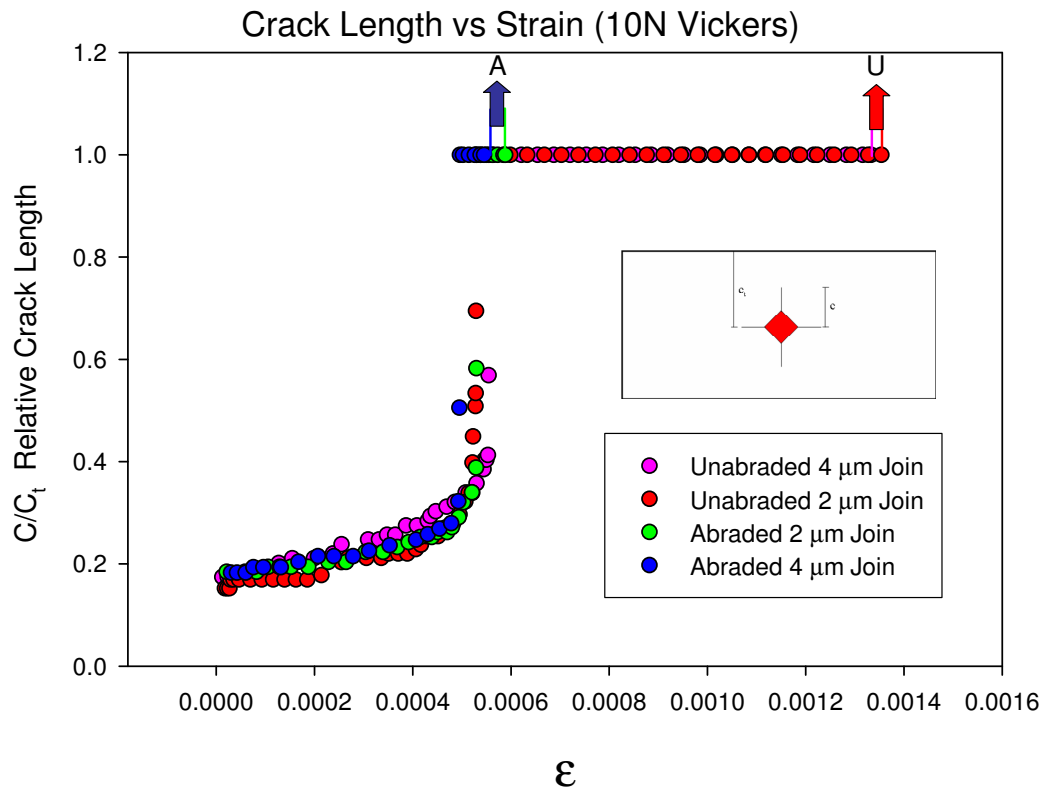


Figure 5.12: Crack length plotted against applied strain. Abrasion of glass surfaces reduces the loads at which reinitiation take place. A = abraded reinitiation and U = unabraded reinitiation of cracks in outer layer.

The presence of surface flaws deeply impacts the crack morphology as the cracks traverse the adhesive interlayer into adjacent glass layers. Figure 5.14 shows micrographs of a bend bar experiment done with a join thickness of 2 μm and with an abraded outer glass layer. The bend bar is halved with a remarkably clean fracture across the inner glass layer that continues into the outer glass layer. The presence of an abraded surface provides an abundance of surface flaws, so that the crack reinitiates seamlessly on the opposite glass layer. At first glance this may appear to be a continuation of the same crack that simply has penetrated the outer glass layer. However if that were the case the presence of surface flaws would not influence the manner or loading level at which cracks enter the outer layer. Figure 5.15 shows micrographs of a bend bar experiment with 2 μm join thickness similar to that of Figure 5.14, but with unabraded glass surfaces. The absence of starter flaws hinders the formation of cracks in the outer glass layer and interrupts the propagation of cracks from the inner glass, similar to that of the previous experiment. The bend bar does eventually fail when the forces are sufficient to grow a minute flaw that is inherent in the outer glass layer. The point of crack reinitiation is typically remote from the crack tip in the inner glass layer. Therefore the fractured surfaces are not closely aligned to the crack in the originating layer Figure 5.15. Unlike the abraded case, the crack tip has had to "search" for an appropriately large flaw in the adjacent glass layer. It is not likely that the crack tip has deflected and followed the interface and then entered the outer glass. More likely is that a new crack has formed in the outer glass and the adhesive join is pulled away from the glass layers, giving the impression of crack deflection or delamination prior to bend bar failure.

Again reinitiation of cracks between joined layers appears to be the mechanism of crack bridging across interfaces. As the crack moves into the more compliant adhesive layer from the stiffer glass, there is stress shielding at the crack tip due to lower elastic modulus of the joining interlayer. The importance of the presence of surface flaws for crack propagation via reinitiation is once again highlighted.

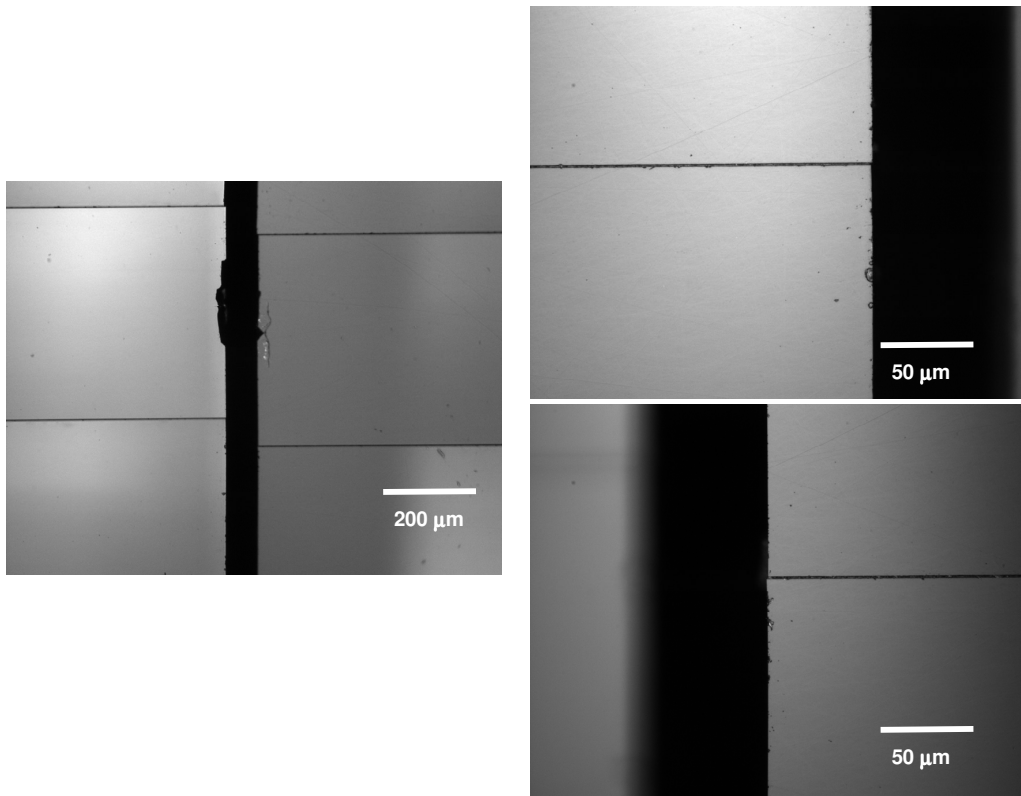


Figure 5.14: Micrographs of sample made with epoxy and abraded glass surfaces 2 μm joints.

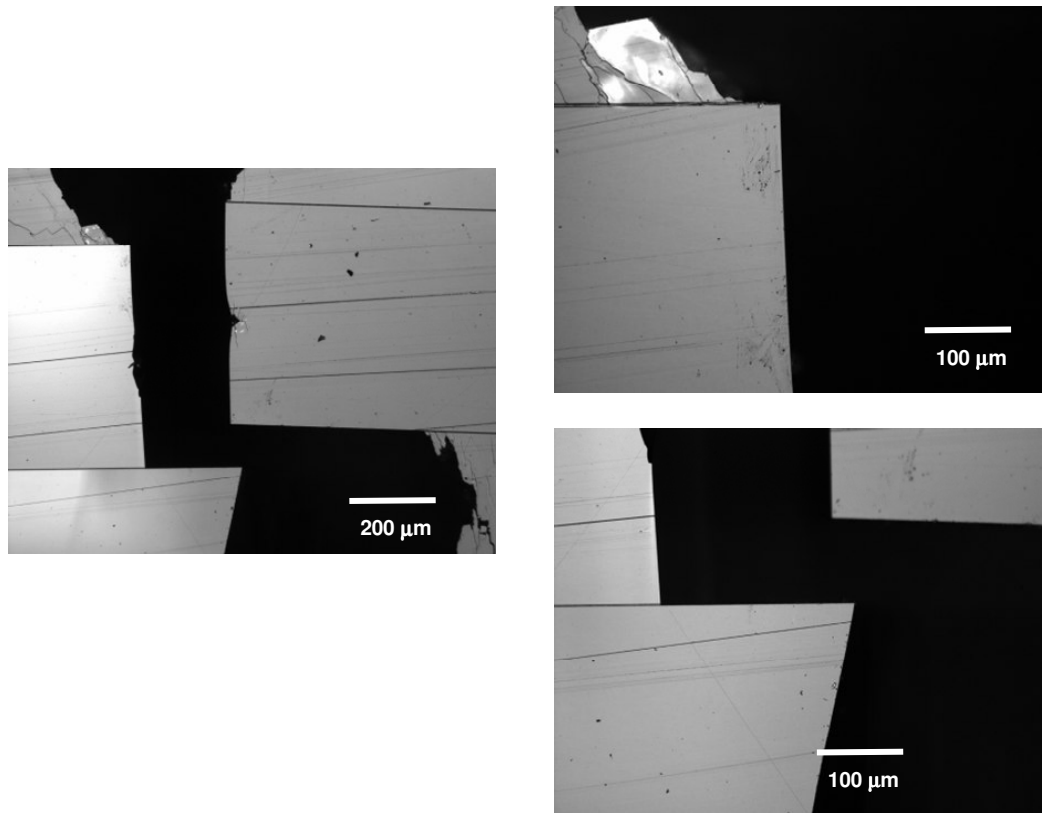


Figure 5.15: Micrographs of sample made with epoxy and unabraded glass surfaces 2 μm joins.

5.5 Two-Dimensional Transverse Cracks: Line Load via Knife Indenter

The visualization of cracks traveling from one layer into another and across interlayers is the culmination of the previous experiments described in this chapter. Direct *in situ* observation of transverse cracks driven by far field loading would elucidate crack behavior similar to the loading conditions seen in dental crown occlusal contacts. To that end an experiment is applied here where a two dimensional crack is driven into joined layers with either epoxy or composite adhesives using a knife indenter. Crack propagation is directly observed entering adjacent glass layers.

5.5.1 Knife Indenter: Experimental Setup

The use of a knife indenter creates a two-dimensional crack emanating from the indenter and propagation toward the interface as seen Figure 5.16. Samples are formed by bonding glass plates with either epoxy or composite joining material in a similar fashion to prior experiments. The top surface of the bottom glass is abraded using the SiC slurry and sides of the samples are polished until transparent. Specimen have a length of 25 mm with a top glass layer 1 mm thick and bottom glass plate 12 mm thick and 3 mm wide. The specimen bars rest on a glass stage and the indenter is lowered down onto the top surface of the bar [68]. The indenter is a rectangular tungsten carbide (WC) glass cutter (Wale Apparatus Co., Hellertown, PA) with corner radius $< 10 \mu\text{m}$ and length 40 mm. The sides of the knife are polished down using a $1 \mu\text{m}$ diamond slurry to enhance the corner sharpness. The knife is then mounted onto a aluminum wedge with sides at a 45° angle to the specimen so that the line edge of the indenter rests on the surface of the test sample.

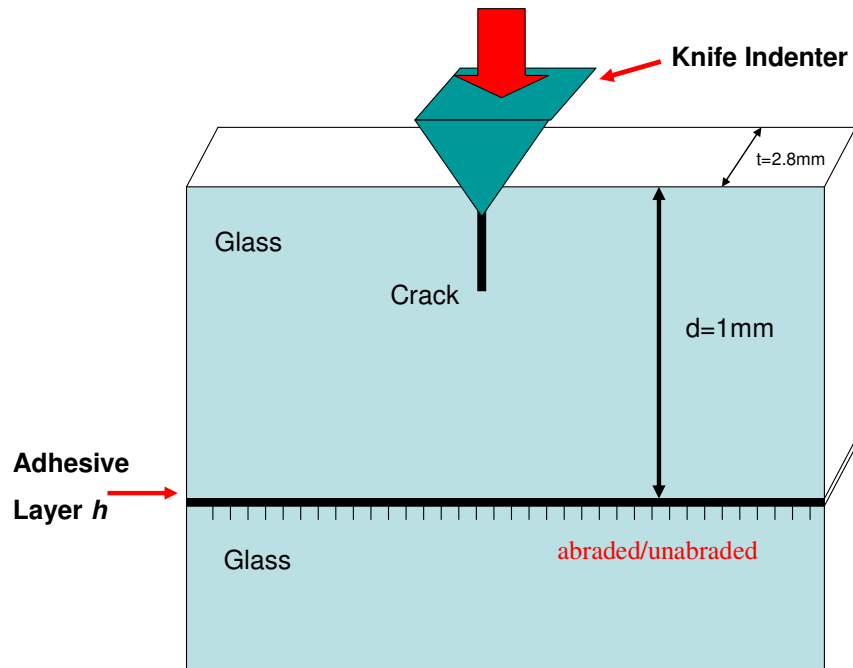


Figure 5.16: Experimental schematic of Knife indenter experiment. A line load is placed on the top glass layer and a crack is driven toward the interface. Top surface of the lower glass layer is either abraded or unabraded.

5.5.2 Knife-Indenter Experimental Results

The use of the knife indenter produces a stable crack that grows downward from the contact with the specimen. Figure 5.17 shows a series of frames taken from video where the crack originates at the contact zone and stably propagates towards the interface. The sample is made with a thin epoxy layer, 2 μm thick and the top surface of the lower glass is abraded. When the crack has reached the interface the crack arrests momentarily until the load is doubled, at which stage the crack reinitiates on the other side of the interface. Without the abrasion of the lower glass the load for reinitiation is extremely high, on the order of 1000 N. This suggests that reinitiation of cracks again controls the failure process.

In order to compare the behavior of crack with joins made from epoxy and particle-filled resin composite the experiment is repeated with join thicknesses of 50 μm . Figure 5.18 plots the line load P_l against crack length c as the crack tip approaches the interface. In both specimens the cracks reach the interface at relatively the same line load level, $P_l^I \approx 80 \text{ N/mm}$. What separates the crack morphology is that the specimens made with epoxy interlayers require higher loads to reinitiate the crack into the bottom glass layer, $P_l^I \approx 250 \text{ N/mm}$, compared to $P_l^I \approx 150 \text{ N/mm}$ in composite joins. The higher modulus of the composite interlayer reduces the load needed to reinitiate the crack in the adjacent glass layer. A detailed fracture mechanics-of this phenomenon is given in the Appendix section (courtesy Dr Brian Lawn). The composite layer with its higher elastic modulus has a higher stress intensity at the crack tip, yielding a lower load threshold to push the crack through the adhesive.

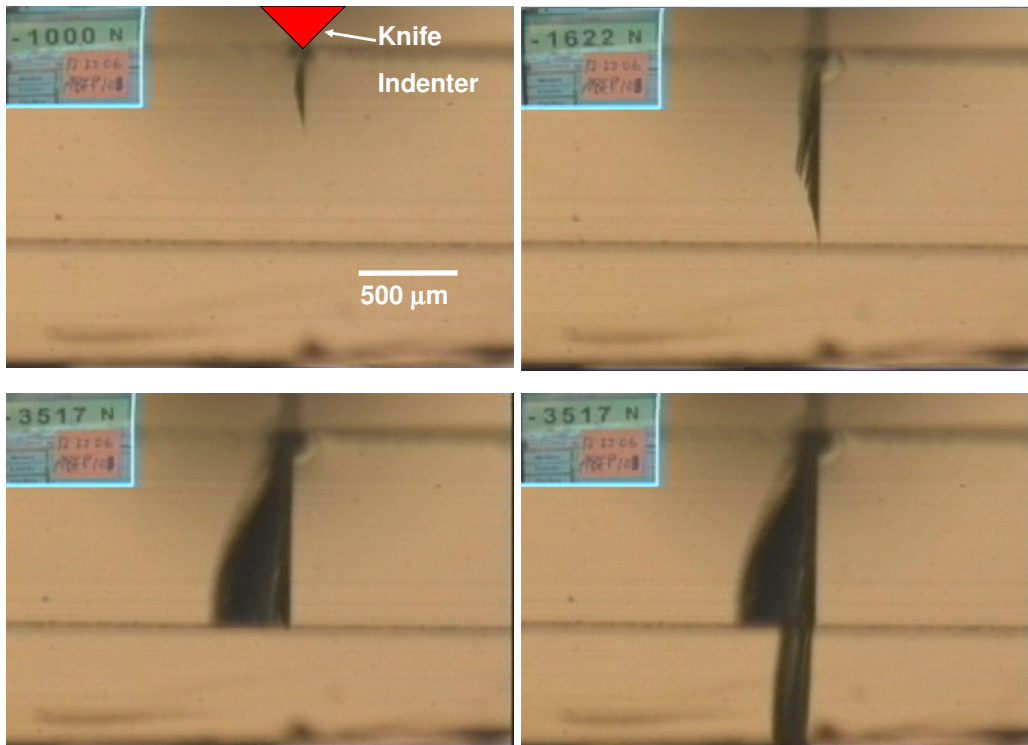


Figure 5.17: $h = 2 \mu\text{m}$, $d=1\text{mm}$, Reinitiation Mechanism is observed in the lower glass.

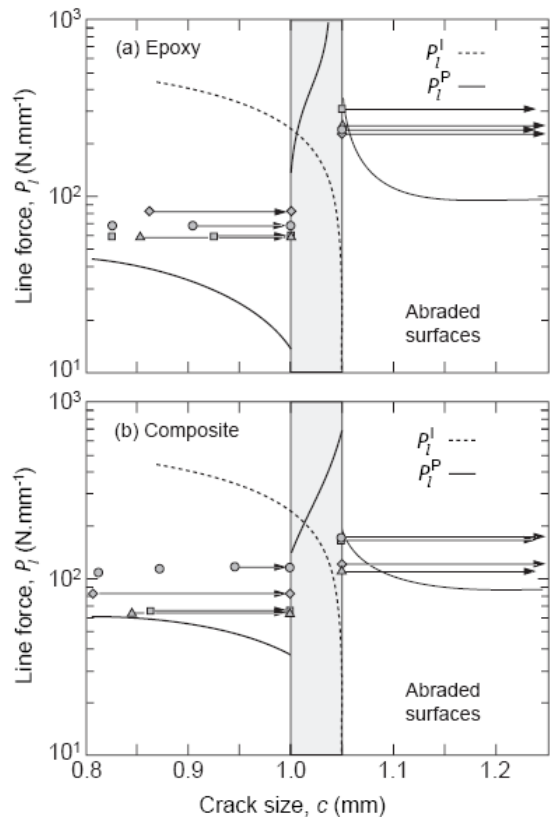


Figure 5.18: Plots of the line load P_l in N/mm as a function of crack length. The less stiff epoxy requires a higher line load to reinitiate cracks into the lower glass than the samples made composite joints [67].

The effect of adhesive thickness is shown in Figure 5.19 where the reinitiation load is plotted against joint thickness over a range 1 to 50 μm for epoxy interlayers. Even at the minimum thickness of 1 μm the cracks continue to arrest at the interface with the epoxy. The reinitiation load, expressed as $P_l^I(c^*) = (S_1 d / \chi_e) (2\pi h / d)^{1/2}$ (where S is the strength, d is top layer glass thickness, χ_e is a constant obtained from FEA and h is the joint thickness), is plotted (solid line) along with the FEM prediction (dashed line). The reinitiation loads obtained experimentally conform reasonably to the analytical and FEM solutions. Even at the lowest joint thicknesses there is some crack containment in the upper layer from the stress shielding of the crack tip by the compliant joint. The data highlight the increased difficulty in driving a crack to reinitiation at clinically thin joint thicknesses of 50 μm or more. It is unlikely that CAD/CAM veneers and mated cores would be fitted more accurately than this. However from 1 to 50 μm the reinitiation load increases by a factor of 3.

The role of a compliant interlayer in arresting crack propagation is to diminish the capacity to transmit stress from one brittle layer to another. This is known as stress shielding and is the primary mechanism of crack containment in our systems.

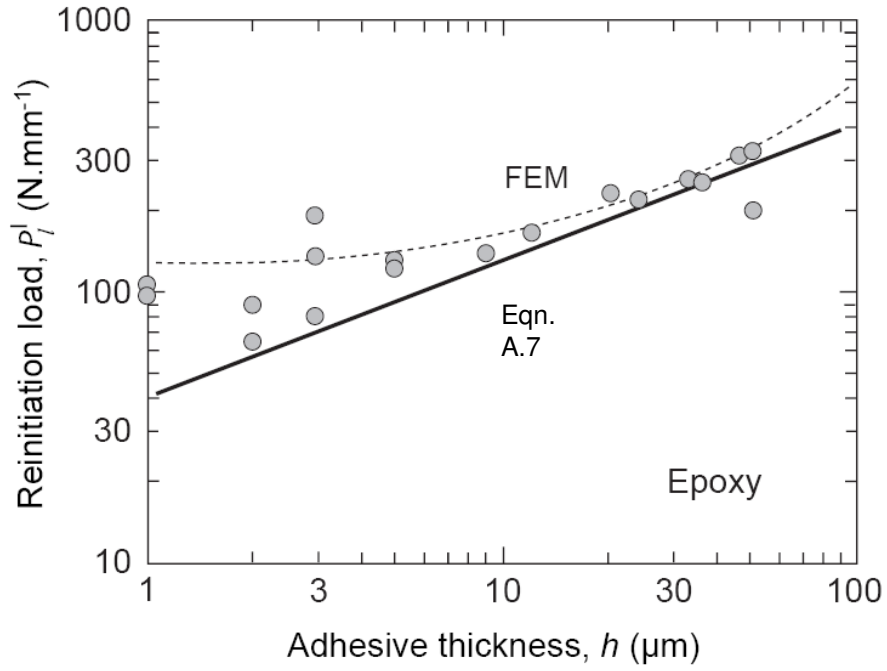


Figure 5.19: Plot of the effect of the epoxy joint thickness on the reinitiation of crack in the lower glass. It is experimentally observed that crack arrest at the interface even for thin joints prior to cracks entering the lower glass layer [67].

5.6 Summary

A higher modulus composite joins allow cracks to reinitiate into secondary glass layers at lower loads than epoxy joins. Although the benefit of using thick, high modulus composites in layered structure is clear in preventing the formation of radial crack from occlusal contact loads, care should be taken to preserve the crack containment characteristic of adhesive joins: the thinner the join, the lower the load required to reinitiate cracks into secondary glass layers.

Chapter 6: Conclusions

The suppression of new failure modes due to occlusal contact from the joining of laminar brittle structures using a polymeric interlayer has been presented. The joining of independently fabricated layers removes the need to match CTE to minimize the residual stresses and would automate current techniques for making all-ceramic dental crowns. The work presented here seeks to confirm the feasibility of using a high modulus joining material to mate brittle ceramic dental cores and veneers without compromising the performance of the overall structure during occlusal contact. The use of *in situ* testing techniques allows for the direct observation of crack initiation and propagation in brittle layers and the impact of material properties and structural geometry. From the collection of data concerning crack behavior several conclusions can be drawn.

I. For the first time it is shown that it is possible to suppress radial crack initiation in veneering layers with the use of a high modulus joining layer. The occlusal contact from opposing teeth and food particles causes flexure and can lead to the formation of radial cracks in the veneer layer when it is joined to the core via a compliant interlayer. The use of a high modulus composite allows for variable thickness of the joining layer including for thin joins, $< 50 \mu\text{m}$, without compromising particle distribution of the filler. Fundamental relationships for radial crack initiation are confirmed for the high modulus joining layer as describe by the following equations:

$$P_{cr} = BSd^2 / [\log(E_s/E^*)] \quad 4.1$$

$$E^* = E_i (E_s/E_i)^L \quad 4.2$$

$$L = \exp [- [\alpha + \beta \log (h/d)]^\gamma] \quad 4.3$$

II. The use of a high modulus composite improves the long term cyclic loading lifetime over interlayers that have similar moduli to current dental adhesives. Joining techniques developed through this work sufficiently preclude any delamination between the brittle layers. Delamination is often observed in weakly bonded systems and it can diminish the lifetime of the veneer.

III. Crack propagation between brittle layers joined with compliant materials is controlled by a reinitiation mechanism. The reinitiation loads are controlled by the elastic modulus and thickness of the interlayer and the surface condition of adjacent brittle layers. Current fabrication techniques of veneers and all-ceramics dental crowns leave the structure vulnerable to crack propagation across interlayers.

IV. Long term survival of all-ceramic crowns joined with compliant materials depends on the stiffness and thickness of the interlayer. The use of high modulus joins to prevent the formation of radial cracks in the veneer should be balanced against the prospect of crack propagation from one layer into another. Durable

ceramic dental crowns will require immunity from both radial crack formation and structural toughness.

V. A novel high elastic modulus composite has been fabricated via a particle-filled resin matrix. A regime of nano-sized fillers, using shear and vibration mixing techniques, has been developed. The procedure produces uniform low porosity joints that are strong yet translucent, a property that is desirable for aesthetics dental crowns.

Chapter 7: Future Work

- 1) The systems studied in this dissertation are flat layered structures. More complex and physiologically significant geometries may further elucidate clinical behavior. The use of high elastic modulus composites as joining layers in brittle curved structures may more closely mimic the behavior seen in the mouth. These studies should be done using composites where the filler is coupled to the matrix to minimize viscoelastic deformation and the potential for water absorption and swelling.
- 2) Recent work has revealed possible new failure modes in brittle laminate structures due to the presence of water at the point of contact during multiple cycle testing. The presence of water can cause accelerated crack propagation in brittle layers due to hydraulic pumping. The introduction of high elastic modulus joins as crack arresters of the veneer may be of clinical interest.
- 3) The studies presented here use laminate structures that have clear geometric boundaries. Structures that have graded mechanical properties may perform better in contact loading due to the distribution of stress. Work is ongoing to create functionally graded ceramic materials. Graded structures joined with high elastic modulus composites as a new type of dental crown would be of clinical interest.
- 4) Studying the competition between radial fracture in the veneer versus the core may reveal relevant geometric and material property variables in the production of laminate crowns.

Appendix: Fracture Mechanics of Line Load Indentation

This appendix provides a detailed fracture mechanics analysis for the line load problem discussed in Chapter 5.5 Two-Dimensional Transverse Cracks: Line Load via Knife Indenter and is provided courtesy of Dr. Brian Lawn [67].

A.1 General Mechanics

Consider the test configuration in Fig. 1. A brittle plate (material 1) of thickness d , modulus E_1 , toughness T_1 and strength S_1 is bonded with adhesive (material 2) of thickness h , modulus E_2 and toughness T_2 to a like brittle base plate (material 1) of thickness $\gg d$. A wedge indenter under line load $P_l = P/l$ along a specimen width l introduces a transverse plane crack of depth c within the upper plate, and drives this crack downward to the adhesive interface. The action of the indenter will generally induce a contact plastic zone, responsible for initiating the crack in the first place and subsequently augmenting the elastic driving force in the ensuing propagation stage [69]. However, by the time the crack nears the interface in the far field, any such plasticity-associated fields may be assumed to be negligible.

Suppose that the crack reaches the first adhesive interface, and that the bonding is strong enough that delamination does not occur. There are two possibilities for subsequent growth: (i) the crack penetrates into the adhesive, ultimately reaching and entering the second brittle layer; (ii) after arresting at the first interface or penetrating part way into the adhesive, the crack reinitiates in the second brittle layer ahead of the primary tip. These two modes may be expected to have different dependencies on material and geometrical (thickness) variables.

A.2 Crack penetration

Crack penetration might be expected to be the principal mode for adhesives that are relatively stiff, hard and brittle. Begin with a simple relation for a thick monolithic brittle specimen of material 1, and then modify to allow for presence of an intervening adhesive material 2. Assuming the principal driving force to come from the horizontal component of the applied line force, the stress intensity factor for such a crack may be written [69-71]

$$K_0 = \alpha P_l / [(\pi c)^{1/2} \tan \beta'] = \chi_e P_l / c^{1/2} \quad (\text{A.1})$$

where $\beta' = \beta + \arctan \mu$ is an effective indentation wedge half-angle, with β the true wedge half-angle and μ a friction coefficient, and α and $\chi_e = \alpha / \pi^{1/2} \tan \beta'$ are dimensionless constants. This relation ignores any influence from the vertical line force component on the crack growth, but any such contribution may be subsumed into α and χ_e in eqn. A.1. For a layer system with adhesive interlayer we may write

$$K = \Phi K_0 \quad (\text{A.2})$$

where $\Phi = \Phi(c/d, h/d, E_2/E_1, \nu_2/\nu_1)$ is a dimensionless function defining the influence of the interlayer, with E Young's modulus and ν Poisson's ratio. (Note the limiting case $\Phi = 1$ for a brittle monolith, $E_1 = E_2$ and $\nu_2 = \nu_1$.) The function Φ for any given ratio E_2/E_1 can be evaluated by 2D finite element analysis (FEA) by emplacing cracks of length c in structures with and without adhesive interlayers (Figure A.1) using the Irwin crack-opening displacement relation [72] to compute relative stress intensity factors at any given load P_l and crack size c [73]. A supplementary benefit of FEA

analysis is to confirm that all stresses in our system remain within the elastic limit, a necessary condition for validity of the fracture mechanics formalism.

Results of FEA calculations of the function Φ as a function of relative crack size c/d are shown in Fig. A.2 for a set of experimental conditions to be described in the next section, using ANSYS software (Version 6.0, ANSYS Inc., Cannonsburg, PA). The FEA system comprises upper and lower glass plates with an interlayer adhesive of relative modulus $E_2/E_1 = 0.22$ or 0.040 and relative thickness $h/d = 0.05$. Lateral dimensions for the system are $80d$, large enough to eliminate any boundary effects. Forces are applied at the crack mouth with an indenter of rectangular cross-section (i.e., $\beta = 45^\circ$). The mesh is refined until solutions converge. The plots in Figure A.2 indicate a modestly rising crack attraction on approaching the first interface ($\Phi > 1$), a pronounced crack inhibition within the compliant adhesive layer ($\Phi \ll 1$), and continued (but reduced) crack inhibition beyond the second interface ($\Phi < 1$). The positive deviations from unity in the first region are similar to those calculated for cracks approaching and crossing the interface between a stiff coating and compliant substrate in a simple bilayer [74]. The negative deviations in the second and third regions reflect the degree of stress shielding exerted by the adhesive on the crack propagation. Note the greater shielding effect in layers with greater mismatch, i.e. smaller E_2/E_1 .

The condition for equilibrium crack penetration at any given length c can be determined by equating the stress intensity factor K to the appropriate toughness T (K_{IC}). Using superscript P to denote penetration mode, eqn. A.1 and A.2 then yield

$$P_l^P = (Td^{1/2}/\chi_e)[(c/d)^{1/2}/\Phi(c/d)] \quad (3)$$

where $T = T_1$ within $c < d$, $T = T_2$ within $d < c < d + h$, and $T = T_1$ within $c > d + h$. Note P_l^P is independent of strength of the brittle materials—it is toughness that controls the crack growth in this mode.

To illustrate, P_l^P in eqn. A.3 is plotted in normalized form in Figure A.3 as a function of c/d , using $\Phi(c/d)$ from Figure A.2. For this case we take $T_2 = T_1$, to emphasize the modulus mismatch shielding effect. Note the monotonically increasing function for monoliths, ($E_2/E_1 = 1$, $\nu_2 = \nu_1$). For $E_2/E_1 < 1$, $P(c)$ actually passes through a maximum at $c \approx 0.5d$, corresponding to a small pop-in to the interface, the more pronounced for lower E_2/E_1 . Thereafter, within $d < c < d + h$, a substantial load increment is required to drive the crack through the adhesive, and the fracture becomes highly stable. The requirement in eqn. A.3 for the crack to reach the second interface at $c^* = d + h$ is given by

$$P_l^P(c^*) = (T_2 d^{1/2} / \chi_c) [(1 + h/d)^{1/2} / \Phi(c^*/d)] \quad (\text{A.4})$$

At this point the condition for propagating the crack into the second brittle layer is exceeded and fracture is spontaneous. Of course, such failure assumes that the load $P_l^P(c^*)$ is achieved before fracture occurs by any competing mode.

A.3 Crack Reinitiation

In this case a secondary crack initiates in the lower brittle layer within the K -field of the primary crack prior to penetration to the second interface. This is the expected mode for adhesives that are relatively compliant, soft and tough. Simplistically, the condition for reinitiation is that the maximum tensile stress in the near-surface of the second brittle layer just equals the strength $S_1 = T_1/(\pi c_f)^{1/2}$ of that layer, where c_f is a characteristic flaw size. This condition ignores any effects of crack tip stress gradients over the critical flaw, which could be substantial in the region $h < c_f$. Designating the distance ahead of the primary crack tip as $x = d + h - c$ (Fig. A.1), the normal stress at the surface of the second brittle layer can be approximated by [64]

$$\sigma_y = K_0/(2\pi x)^{1/2} \quad (\text{A.5})$$

within the region $x \ll c + h$. It is implicit in this relation that the intervening adhesive layer does not seriously perturb the K field in the second brittle layer (regardless of whether the crack resides in the first brittle layer or the adhesive layer). Inserting $\sigma_y = S_1$ along with $x = d + h - c$ in eqn. A.5 then yields a relation for reinitiation, designated by superscript I,

$$P_I^1 = (S_1 d / \chi_e) [(2\pi c/d)(1 + h/d - c/d)]^{1/2} \quad (6)$$

Note that it is now strength and not toughness of the second layer that determines the critical condition. Note also that P_I^1 is independent of E_2/E_1 in this approximation. Again, justification of the assumptions and approximations used in the derivation of eqn. A.6 requires numerical verification.

A plot of the normalized reinitiation load P_I^I as a function of relative crack size c/d , for relative thickness $h/d = 0.05$, is shown in Fig. A.4. The solid line is a direct representation of eqn. A.6, the dashed lines are FEA calculations for $E_2/E_1 = 0.22$ and 0.040 with a calibrated coefficient $\chi_e = 0.21$. The FEA curves deviate from eqn. 6 in the region $c < d$, which lies outside the range of validity of the Irwin crack-tip field. However, in the vicinity of the adhesive eqn. A.6 provides a fair representation of the critical conditions. The probability of reinitiation increases dramatically as the primary crack approaches the second interface. Once the condition for reinitiation is met, the crack pops in from a critical flaw in the surface of the lower brittle layer.

A special case of interest is that of reinitiation in the field of an arrested primary crack at the first interface. Inserting $c^* = d$ into eqn. A.6 yields

$$P_I^I(c^*) = (S_1 d / \chi_e) (2\pi h / d)^{1/2} \quad (\text{A.7})$$

This relation emphasizes the role of interlayer thickness h in the reinitiation process.

The issue of which mode wins, penetration or reinitiation, is then determined by the relative values of P_I^P in eqn. A.3 and P_I^I in eqn. A.6.

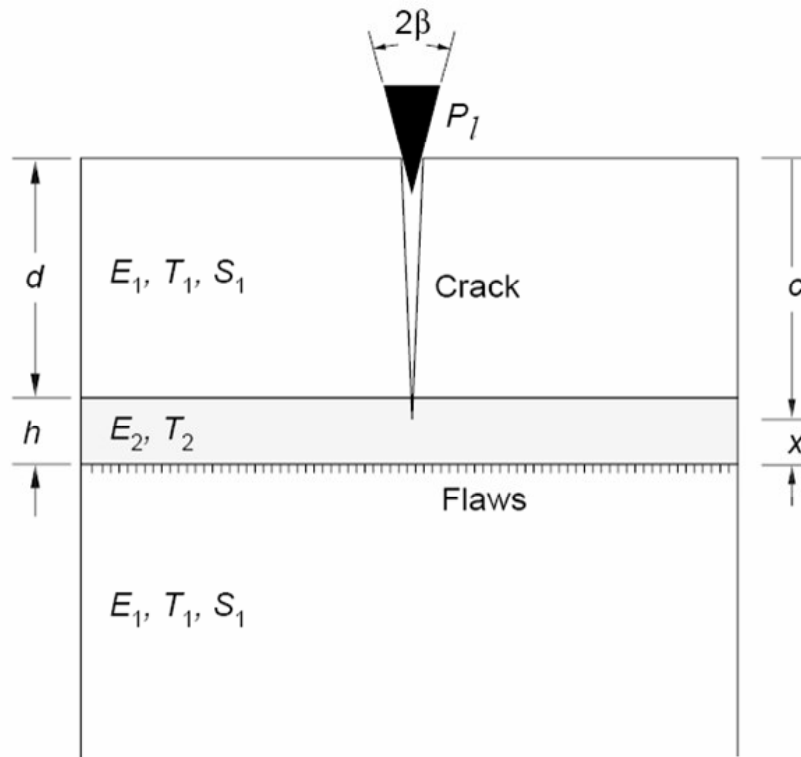


Figure A.1: Schematic of line force crack configuration in layer system consisting of two brittle plates bonded by a polymer-based adhesive. Crack can propagate into lower brittle layer either by continuous penetration or reinitiation from a surface flaw ahead of an arrested primary crack tip.

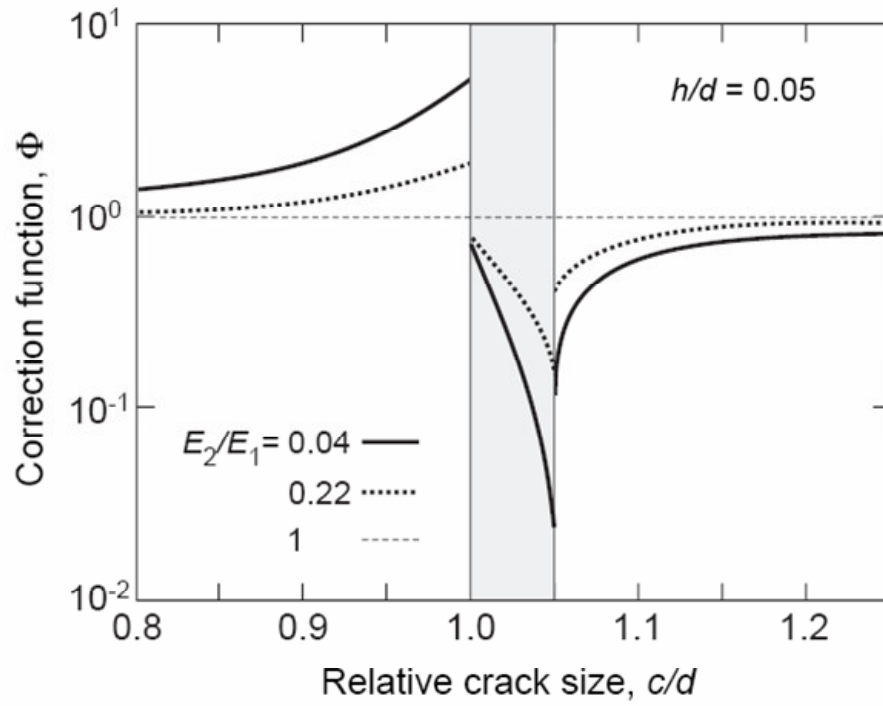


Figure A.2: Plot of function $\Phi(c/d)$ for brittle plates bonded with adhesives of relative thickness $h/d = 0.05$ and modulus $E_2/E_1 = 0.04$ and 0.22 .

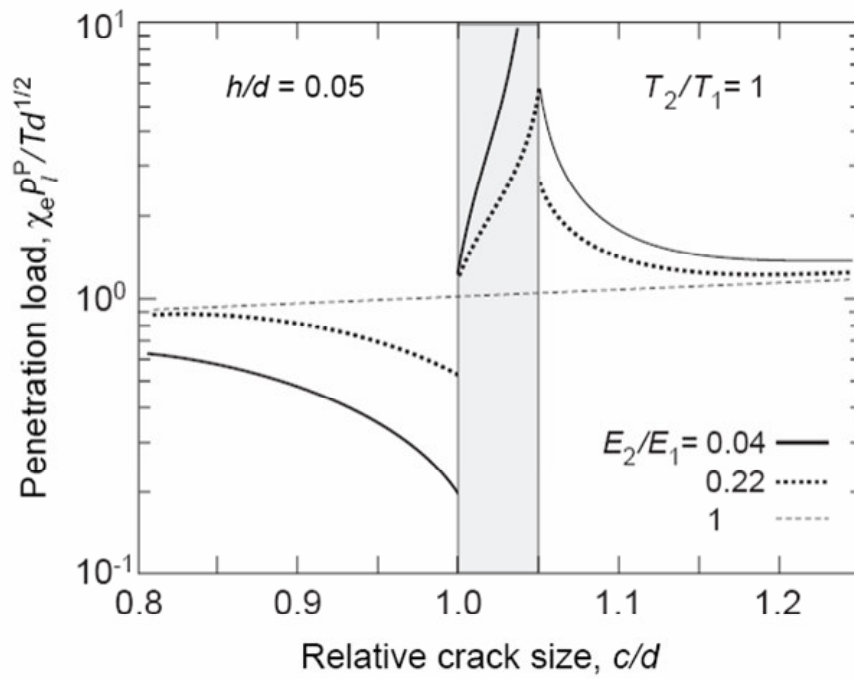


Figure A.3: Plot of $\chi_e P_1^P / Td^{1/2}$ versus c/d for given h/d and E_2/E_1 .

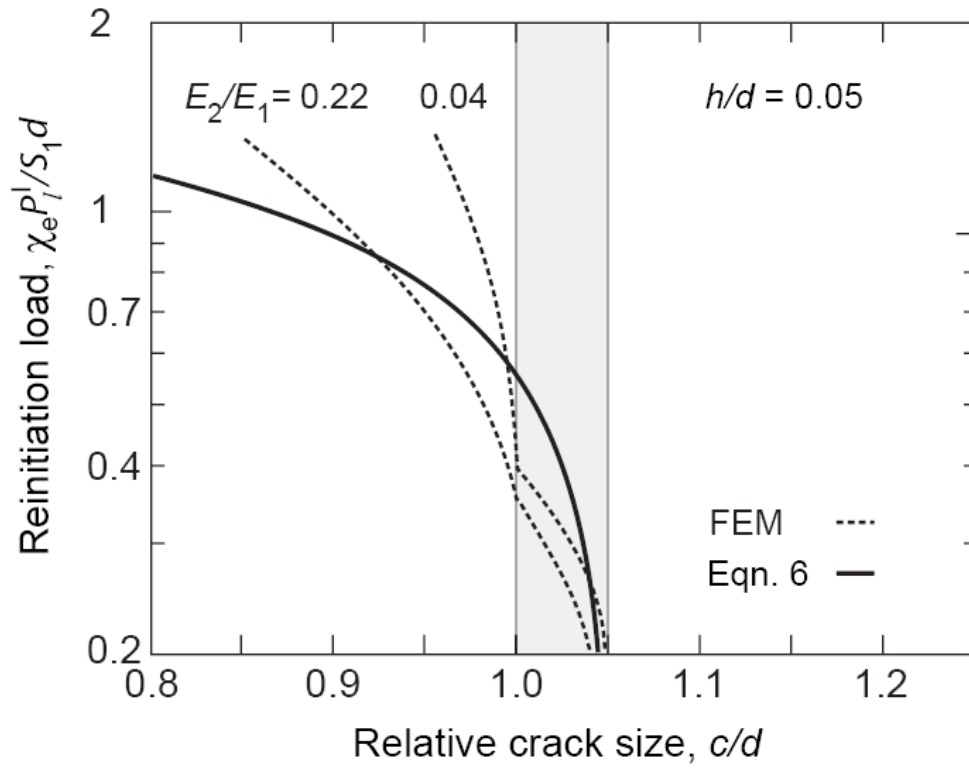


Figure A.4: Plot of $\chi_e P_1^I / S_1 d$ versus c/d for given h/d .

References:

1. Rekow, D. and V.P. Thompson, *Engineering long term clinical success of advanced ceramic prostheses*. Journal of Materials Science-Materials in Medicine, 2007. **18**(1): p. 47-56.
2. Zhang, Y., B.R. Lawn, K.A. Malament, V.P. Thompson, and E.D. Rekow, *Damage accumulation and fatigue life of particle-abraded ceramics*. International Journal of Prosthodontics, 2006. **19**(5): p. 442-448.
3. Xu, H.H.K., D.T. Smith, S. Jahanmir, E. Romberg, J.R. Kelly, V.P. Thompson, and E.D. Rekow, *Indentation damage and mechanical properties of human enamel and dentin*. Journal of Dental Research, 1998. **77**(3): p. 472-480.
4. Peterson, I.M., S. Wuttiphan, B.R. Lawn, and K. Chyung, *Role of microstructure on contact damage and strength degradation of micaceous glass-ceramics*. Dental Materials, 1998. **14**(1): p. 80-89.
5. Sessle, B.J., *The Neurobiology of Facial and Dental Pain - Present Knowledge, Future-Directions*. Journal of Dental Research, 1987. **66**(5): p. 962-981.
6. Patton, H.D. and W.H. Howell, *Textbook of physiology*. 21st ed. 1989, Philadelphia: Saunders. 2 v. (xv, 1596, lxx p.).
7. Chadwick, D. and G. Cardew, *Dental enamel*. Ciba Foundation symposium ; 205. 1997, Chichester ; New York: Wiley. ix, 284 p.
8. Robinson, C., J. Kirkham, and R. Shore, *Dental enamel : formation to destruction*. 1995, Boca Raton: CRC Press. 272 p.

9. Isgro, G., H. Wang, C.J. Kleverlaan, and A.J. Feilzer, *The effects of thermal mismatch and fabrication procedures on the deflection of layered all-ceramic discs*. Dental Materials, 2005. **21**(7): p. 649-655.
10. Isgro, G., C.J. Kleverlaan, H. Wang, and A.J. Feilzer, *The influence of multiple firing on thermal contraction of ceramic materials used for the fabrication of layered all-ceramic dental restorations*. Dental Materials, 2005. **21**(6): p. 557-564.
11. Bhowmick, S., Y. Zhang, and B.R. Lawn, *Competing fracture modes in brittle materials subject to concentrated cyclic loading in liquid environments: Bilayer structures*. Journal of Materials Research, 2005. **20**(10): p. 2792-2800.
12. Hermann, I., S. Bhowmick, Y. Zhang, and B.R. Lawn, *Competing fracture modes in brittle materials subject to concentrated cyclic loading in liquid environments: Trilayer structures*. Journal of Materials Research, 2006. **21**(2): p. 512-521.
13. Burke, F.J., G. Fleming, D. Nathanson, and P. Marquis, *Are Adhesive Technologies Needed to Support Ceramics? An Assessment of the Current Evidence*. Journal of Adhesive Dentistry, 2002. **4**(1): p. 7-22.
14. Qasim, T., C. Ford, M.B. Bush, X.Z. Hu, K.A. Malament, and B.R. Lawn, *Margin failures in brittle dome structures: Relevance to failure of dental crowns*. Journal of Biomedical Materials Research Part B-Applied Biomaterials, 2007. **80B**(1): p. 78-85.
15. Lewis, J.A., *Direct-write assembly of ceramics from colloidal inks*. Current Opinion in Solid State & Materials Science, 2002. **6**(3): p. 245-250.

16. Lewis, J.A., J.E. Smay, J. Stuecker, and J. Cesarano, *Direct ink writing of three-dimensional ceramic structures*. Journal of the American Ceramic Society, 2006. **89**(12): p. 3599-3609.
17. Smay, J.E., G.M. Gratson, R.F. Shepherd, J. Cesarano, and J.A. Lewis, *Directed colloidal assembly of 3D periodic structures*. Advanced Materials, 2002. **14**(18): p. 1279-+.
18. Lawn, B.R., A. Pajares, Y. Zhang, Y. Deng, M.A. Polack, I.K. Lloyd, E.D. Rekow, and V.P. Thompson, *Materials design in the performance of all-ceramic crowns*. Biomaterials, 2004. **25**(14): p. 2885-2892.
19. Lawn, B.R., Y. Deng, P. Miranda, A. Pajares, H. Chai, and D.K. Kim, *Overview: Damage in brittle layer structures from concentrated loads*. Journal of Materials Research, 2002. **17**(12): p. 3019-3036.
20. Folsom, C.A., F.W. Zok, and F.F. Lange, *Flexural Properties of Brittle Multilayer Materials .2. Experiments*. Journal of the American Ceramic Society, 1994. **77**(8): p. 2081-2087.
21. Folsom, C.A., F.W. Zok, and F.F. Lange, *Flexural Properties of Brittle Multilayer Materials .1. Modeling*. Journal of the American Ceramic Society, 1994. **77**(3): p. 689-696.
22. Gordon, J.E., *The New Sciences of Strong Materials*. 1968: Peguin, Harmondsworth, UK.
23. Clegg, W.J., K. Kendall, N.M. Alford, T.W. Button, and J.D. Birchall, *A Simple Way to Make Tough Ceramics*. Nature, 1990. **347**(6292): p. 455-457.

24. Swain, M.V. and J. Mencik, *Mechanical Property Characterization of Thin-Films Using Spherical Tipped Indenters*. Thin Solid Films, 1994. **253**(1-2): p. 204-211.
25. Diao, D.F., K. Kato, and K. Hokkirigawa, *Fracture Mechanisms of Ceramic Coatings in Indentation*. Journal of Tribology-Transactions of the Asme, 1994. **116**(4): p. 860-869.
26. An, L., H.M. Chan, N.P. Padture, and B.R. Lawn, *Damage-resistant alumina-based layer composites*. Journal of Materials Research, 1996. **11**(1): p. 204-210.
27. Liu, H.Y., B.R. Lawn, and S.M. Hsu, *Hertzian contact response of tailored silicon nitride multilayers*. Journal of the American Ceramic Society, 1996. **79**(4): p. 1009-1014.
28. Pajares, A., L.H. Wei, B.R. Lawn, N.P. Padture, and C.C. Berndt, *Mechanical characterization of plasma sprayed ceramic coatings on metal substrates by contact testing*. Materials Science and Engineering a-Structural Materials Properties Microstructure and Processing, 1996. **208**(2): p. 158-165.
29. Lee, K.S., S. Wuttiphan, X.Z. Hu, S.K. Lee, and B.R. Lawn, *Contact-induced transverse fractures in brittle layers on soft substrates: A study on silicon nitride bilayers*. Journal of the American Ceramic Society, 1998. **81**(3): p. 571-580.
30. Chai, H. and B.R. Lawn, *Cracking in brittle laminates from concentrated loads*. Acta Materialia, 2002. **50**(10): p. 2613-2625.

31. Wuttiphan, S., B.R. Lawn, and N.P. Padture, *Crack suppression in strongly bonded homogeneous heterogeneous laminates: A study on glass glass-ceramic bilayers*. Journal of the American Ceramic Society, 1996. **79**(3): p. 634-640.
32. Chai, H. and B. Lawn, *Role of adhesive interlayer in transverse fracture of brittle layer structures*. Journal of Materials Research, 2000. **15**(4): p. 1017-1024.
33. Kim, J.H., P. Miranda, D.K. Kim, and B.R. Lawn, *Effect of an adhesive interlayer on the fracture of a brittle coating on a supporting substrate*. Journal of Materials Research, 2003. **18**(1): p. 222-227.
34. Chai, H. and B. Lawn, *Fracture modes in brittle coatings with large interlayer modulus mismatch*. Journal of Materials Research, 1999. **14**(9): p. 3805-3817.
35. Jung, Y.G., S. Wuttiphan, I.M. Peterson, and B.R. Lawn, *Damage modes in dental layer structures*. Journal of Dental Research, 1999. **78**(4): p. 887-897.
36. Lawn, B.R., Y. Deng, I.K. Lloyd, M.N. Janal, E.D. Rekow, and V.P. Thompson, *Materials design of ceramic-based layer structures for crowns*. Journal of Dental Research, 2002. **81**(6): p. 433-438.
37. Deng, Y., B.R. Lawn, and I.K. Lloyd, *Characterization of damage modes in dental ceramic bilayer structures*. Journal of Biomedical Materials Research, 2002. **63**(2): p. 137-145.
38. Deng, Y., I. Lloyd, and B.R. Lawn, *Damage modes in all-ceramic crownlike bilayer and trilayer structures using contact testing*. Journal of Dental Research, 2002. **81**: p. A470-A470.

39. Deng, Y., P. Miranda, A. Pajares, F. Guiberteau, and B.R. Lawn, *Fracture of ceramic/ceramic/polymer trilayers for biomechanical applications*. Journal of Biomedical Materials Research Part A, 2003. **67A**(3): p. 828-833.
40. Wang, Y., J.J.-W. Lee, I. Lloyd, O.C. Wilson, M. Rosenblum, and V. Thompson, *High modulus nanopowder reinforced dimethacrylate matrix composites for dental cement applications*. Journal of Biomedical Materials Research Part A, 2007. **In Press**.
41. Wang, Y., *High Elastic Modulus Nanopowder Reinforced Resin Composite for Dental Applications*, in *Dept. of Material Sciences and Engineering*. 2007, University of Maryland College Park: College Park MD.
42. Xu, H.H.K., D.T. Smith, G. Schumacher, F.C. Eichmiller, and J.M. Antonucci, *Indentation modulus and hardness of whisker-reinforced heat-cured dental resin composites*. Dental Materials, 2000. **16**(4): p. 248-254.
43. Bayne, S.C., H.O. Heymann, and E.J. Swift, *Update on Dental Composite Restorations*. Journal of the American Dental Association, 1994. **125**(6): p. 687-701.
44. Bowen, R.L., *Properties of a Silica-Reinforced Polymer for Dental Restorations*. Journal of the American Dental Association, 1963. **66**(1): p. 57- &.
45. Cross, M., W.H. Douglas, and R.P. Fields, *The Relationship between Filler Loading and Particle-Size Distribution in Composite Resin Technology*. Journal of Dental Research, 1983. **62**(7): p. 850-852.

46. Kim, H.W., Y. Deng, P. Miranda, A. Pajares, D.K. Kim, H.E. Kim, and B.R. Lawn, *Effect of flaw state on the strength of brittle coatings on soft substrates*. Journal of the American Ceramic Society, 2001. **84**(10): p. 2377-2384.
47. ASTM, *ASTM C 273-00 (2000) Standard Test Method for Shear Properties of Sandwich Core Materials*. Annual Book of the ASTM Standards, 2000.
48. Kelly, J.R., *Clinically relevant approach to failure testing of all-ceramic restorations*. Journal of Prosthetic Dentistry, 1999. **81**(6): p. 652-661.
49. Azer, S.S., G.M. Ayash, W.M. Johnston, M.F. Khalil, and S.F. Rosenstiel, *Effect of esthetic core shades on the final color of IPS Empress all-ceramic crowns*. Journal of Prosthetic Dentistry, 2006. **96**(6): p. 397-401.
50. Xu, H.H.K., J.B. Quinn, D.T. Smith, A.A. Giuseppetti, and F.C. Eichmiller, *Effects of different whiskers on the reinforcement of dental resin composites*. Dental Materials, 2003. **19**(5): p. 359-367.
51. Sabbagh, J., J. Vreven, and G. Leloup, *Dynamic and static moduli of elasticity of resin-based materials*. Dental Materials, 2002. **18**(1): p. 64-71.
52. Lawn, B.R., K.S. Lee, H. Chai, A. Pajares, D.K. Kim, S. Wuttiphan, I.M. Peterson, and X.Z. Hu, *Damage-resistant brittle coatings*. Advanced Engineering Materials, 2000. **2**(11): p. 745-748.
53. Chai, H. and B.R. Lawn, *Fracture mode transitions in brittle coatings on compliant substrates as a function of thickness*. Journal of Materials Research, 2004. **19**(6): p. 1752-1761.

54. Hu, X.Z. and B.R. Lawn, *A simple indentation stress-strain relation for contacts with spheres on bilayer structures*. Thin Solid Films, 1998. **322**(1-2): p. 225-232.
55. Delong, R. and W.H. Douglas, *Development of an Artificial Oral Environment for the Testing of Dental Restoratives - Bi-Axial Force and Movement Control*. Journal of Dental Research, 1983. **62**(1): p. 32-36.
56. Gibbs, C.H., K.J. Anusavice, H.M. Young, J.S. Jones, and J.F. Esquivel-Upshaw, *Maximum clenching force of patients with moderate loss of posterior tooth support: A pilot study*. Journal of Prosthetic Dentistry, 2002. **88**(5): p. 498-502.
57. Zhang, Y. and B. Lawn, *Competing damage modes in all-ceramic crowns: Fatigue and lifetime*. Bioceramics 17, 2005. **17**: p. 697-700.
58. Lee, J.J.-W., Y. Wang, I. Lloyd, and B. Lawn, *Joining Veneers to Ceramic Cores and Dentition with Adhesive Interlayers*. Journal of Dental Research, 2007. **In Press**.
59. He, M.Y. and J.W. Hutchinson, *Crack Deflection at an Interface between Dissimilar Elastic-Materials*. International Journal of Solids and Structures, 1989. **25**(9): p. 1053-1067.
60. Lee, C.S., D.K. Kim, J. Sanchez, P. Miranda, A. Pajares, and B.R. Lawn, *Rate effects in critical loads for radial cracking in ceramic coatings*. Journal of the American Ceramic Society, 2002. **85**(8): p. 2019-2024.

61. Zhang, Y. and B. Lawn, *Long-term strength of ceramics for biomedical applications*. Journal of Biomedical Materials Research Part B-Applied Biomaterials, 2004. **69B**(2): p. 166-172.
62. Lawn, B.R., Y. Deng, and V.P. Thompson, *Use of contact testing in the characterization and design of all-ceramic crownlike layer structures: A review*. Journal of Prosthetic Dentistry, 2001. **86**(5): p. 495-510.
63. Miranda, P., A. Pajares, F. Guiberteau, Y. Deng, H. Zhao, and B.R. Lawn, *Designing damage-resistant brittle-coating structures: II. Trilayers*. Acta Materialia, 2003. **51**(14): p. 4357-4365.
64. Shaw, M.C., D.B. Marshall, M.S. Dadkhah, and A.G. Evans, *Cracking and Damage Mechanisms in Ceramic-Metal Multilayers*. Acta Metallurgica Et Materialia, 1993. **41**(11): p. 3311-3322.
65. Kim, J.W., S. Bhowmick, I. Hermann, and B.R. Lawn, *Transverse fracture of brittle bilayers: Relevance to failure of all-ceramic dental crowns*. Journal of Biomedical Materials Research Part B-Applied Biomaterials, 2006. **79B**(1): p. 58-65.
66. He, M.Y., A.G. Evans, and J.W. Hutchinson, *Crack Deflection at an Interface between Dissimilar Elastic-Materials - Role of Residual-Stresses*. International Journal of Solids and Structures, 1994. **31**(24): p. 3443-3455.
67. Anderson, T.L., *Fracture mechanics : fundamentals and applications*. 1995.
68. Lee, J.J.-W., I. Lloyd, H. Chai, Y.G. Jung, and B. Lawn, *Arrest, Deflection, Penetration and Reinitiation of Cracks in Brittle Layers Across Adhesive Interlayers*. Acta Materialia, 2007. **In Press**.

69. Symonds, B.L., R.F. Cook, and B.R. Lawn, *Dynamic Fatigue of Brittle Materials Containing Indentation Line Flaws*. Journal of Materials Science, 1983. **18**(5): p. 1306-1314.
70. Lawn, B.R. and E.R. Fuller, *Equilibrium Penny-Like Cracks in Indentation Fracture*. Journal of Materials Science, 1975. **10**(12): p. 2016-2024.
71. Lawn, B., *Fracture of Brittle Solids*. 2nd ed. 1993, Cambridge: Cambridge University Press.
72. Rooke, D. and D. Cartright, *Compendium of Stress Intensity Factors*. 1976, Uxbridge, Middlesex: Hillingdon Press.
73. Chai, H., *Fracture mechanics analysis of thin coatings under plane-strain indentation*. International Journal of Solids and Structures, 2003. **40**(3): p. 591-610.
74. Fett, T. and D. Munz, *Stess Intensity Factors and Weight Functions*. 1997, Southampton UK: Computational Mechanics Publications.

CURRICULUM VITAE

James Jin-Wu Lee

Education

- | | |
|--------------------|---|
| 2002-2007
Ph.D. | University of Maryland, College Park, Maryland
Materials Science and Engineering |
| 1999-2001
M.S.E | Catholic University of America, Washington, DC
Biomedical Engineering |
| 1992-1996
B.S. | Johns Hopkins University, Baltimore, Maryland
Biomedical Engineering |

Publications

1. Lee, J.J.-W., Wang Y., Lloyd, I., Lawn, B., Joining Veneers to Ceramic Cores and Dentition with Adhesive Interlayers. *Journal of Dental Research*, 2007. In Press.
2. Lee, J.J.-W., Lloyd, I., Chai, H., Jung, Y. G., Lawn, B., Arrest, Deflection, Penetration and Reinitiation of Cracks in Brittle Layers Across Adhesive Interlayers. *Acta Materialia*, 2007. In Press.
3. Wang, Y., Lee, J.J.-W., Lloyd, I., Wilson, O.C., Rosenblum, M., Thompson, V., High modulus nanopowder reinforced dimethacrylate matrix composites for dental cement applications. *Journal of Biomedical Materials Research Part A*, 2007. In Press.
4. Schultheis, L., Lee J., Annand J, Gilka P, Schultheis, A. 1999 " High pass mechanical filtering of the forelimb in the hindquarter suspended rat" *Trans Ortho Res Society* 569.
5. Schultheis, L., Lee J., Annand J, Rajput, Z, Schultheis, A. "Bone strain in the hindquarter suspended rat model of weightless spaceflight" *Trans Ortho Res Society* 78,1999.
6. Schultheis L, Schultheis A, Inoue N, Lee J, Salameh K, Stepanoff I, Adams R, Chao EYS, Berkowitz D, 1998 "Frequency-domain analysis of ambulatory forces on the forelimbs of hindquarter suspended rats in a simulation of reduced gravity" *Trans Ortho Res Society*(23) 135.

Presentations

1. Lee JJW, Wang Y, Lloyd IK, Wilson Jr. OC, and Thompson V, 2006 “Layered Structures Joined with Novel Resin Composite”, American Association for Dental Research Meeting & Exhibition (March 8-11, 2006)
2. Wang Y, Lee JJW, Lloyd IK, Wilson Jr. OC, Rosenblum M, and Thompson V, 2005 “High Modulus Nanocomposites”, MS&T 05 Annual Meeting & Exhibition, Session: Nanocomposites, Pittsburgh, PA, September 27, 2005
3. Lee JJW, Wang Y, Lloyd IK, Wilson Jr. OC, Rosenblum M, and Thompson V, 2005 “Laminar Sandwich Dental Composites with High Elastic Modulus Adhesive Join Layers”, 30th Annual Biomaterials Conference Memphis Tennessee April 27-30 2005.
4. Wang Y, Lee JJW, Lloyd IK, Wilson Jr. OC, Rosenblum M, and Thompson V, 2005 “Processing of Dental Composites with a High Modulus using Nanosized Alumina Oxide”, 107th American Ceramic Society Annual Meeting & Exposition, Bioceramics session, Baltimore, Maryland, April 12, 2005
5. Wang Y, Lee JJW, Lloyd IK, Wilson Jr. OC, Rosenblum M, and Thompson V, 2005 “High Elastic Modulus Dental Composites”, 83rd International and American Association for Dental Research, Baltimore, Maryland, March 9, 2005
6. Daphtary MM, Ruff CB, Shapiro JR, Bauss F, Lee J, Schultheis LW. 2001 “Effects of ibandronate on bone properties under 50% and 100% weightbearing conditions.” Annual ASBMR (American Society of Bone and Mineral Research) Meeting 2001, Phoenix Arizona.
7. Daphtary MM, Ruff CB, Shapiro JR, Rastogi S, Lee J, Schultheis LW. 2001 “Effects of dynamic loading on bone structural properties under conditions of 50% weightbearing.” BMES (Biomedical Engineering Society) 2001 Meeting, North Carolina, USA.
8. Daphtary MM, Ruff CB, Shapiro JR, Rastogi S, Lee J, Schultheis LW. 2000 Inaugural Program of the Interdepartmental Program in Space Medicine, Uniformed Services University of the Health Sciences Bethesda Maryland.
9. Schultheis, L. Rastogi S., Lee J., Annand J., Ruiz J., Schultheis A 1999 “Bone Strain is Accentuated by Ground Reaction Forces With Higher Than Normal Frequency Spectra.” American Society of Biomechanics.